NASA CR-112159

INVESTIGATION OF BIOWASTE RESISTOJETS FOR SPACE STATION APPLICATION

By Carl R. Halbach, Russell J. Page, Owen J. McCaughey
and Robert A. Short

JULY 1972

Prepared under Contract No. NAS1-10934 by

ADVANCED ROCKET TECHNOLOGY (ARTCOR)

Irvine, California 92664

for

NATIONAL AERONAUTICS AND SPACE ADMINISTRATION

LANGLEY RESEARCH CENTER

INVESTIGATION OF BIOWASTE RESISTOJETS

FOR

SPACE STATION APPLICATION

By Carl R. Halbach, Russell J. Page, Owen J. McCaughey

and Robert A. Short

July 1972

Prepared under Contract No. NAS1-10934 by

ADVANCED ROCKET TECHNOLOGY (ARTCOR)

Irvine, California

for

LANGLEY RESEARCH CENTER

NATIONAL AERONAUTICS AND SPACE ADMINISTRATION

TABLE OF CONTENTS

LIST OF FIGURES

LIST OF FIGURES (Continued)

LIST OF FIGURES (Continued)

LIST OF FIGURES (Concluded)

LIST OF TABLES

INVESTIGATION OF BIOWASTE RESISTOJETS FOR SPACE STATION APPLICATION

By Carl R. Halbach, Russell J. Page, Owen J. McCaughey and Robert A. Short

Advanced Rocket Technology (ARTCOR)
Irvine, California

SUMMARY

The feasibility of using electrically conducting ceramics to heat biowaste propellants to 2000°K in resistojet thrustors has been demonstrated. These thrustors are being developed for use on the space station. Among the candidate ceramic heater materials, zirconia and thoria are chemically resistant to the biopropellants, and they are also sufficiently conductive at high temperatures to make them suitable for the heater elements in these thrustors. A Proof-of Concept thrustor design is presented, incorporating a multiple passage cylindrical heater made of zirconia ceramic which is capable of operating at 2000°K wall temperature with CO_2 and H_2O biopropellants. For the 25 mlb size thrustor, specific impulses of 200 seconds for CO_2 and 275 seconds for H_2O biopropellants are predicted.

A spiral-wound noble metal wire starter heater is used to preheat the ceramic heater to make it conductive. Once the ceramic heater starts conducting, the starter heater is turned off. A ballast resistor identical to the starter heater is used in series with the ceramic heater because of the latter's negative resistance characteristic; the ballast resistor provides current stability for the ceramic heater. Both the ballast resistance power (about 20% of the total input power) and heat losses from the ceramic heater are efficiently recovered by a propellant-cooled regenerator section of the thrustor. The ceramic heated thrustor design operates at high heater efficiency (approximately 90%), thereby minimizing power consumption.

Both heat transfer and mechanical considerations led to the selection of a cylindrical, multiple-passage configuration for the ceramic heater. For a given cylinder length, heat transfer is increased by increasing the number of axial passages or holes in the heater. Typically, 6 holes are used, resulting in a relatively short and rugged ceramic heater, 70 mm long by 4.1 mm in diameter, for an L/D ratio of 17. In the 25 millipound size thrustor, flow is laminar in the multiple passages. Flow instabilities, which can occur when heating gas under laminar flow conditions in multiple-parallel passages, is avoided in this design by proper thermal distributions to limit temperature ratios across the ceramic heater tube to within allowable values.

Five hundred hour tests at temperatures above 1900°K have been completed with zirconia ceramic heaters on both CO_2 and H_2O biopropellants.

The heaters showed no sign of chemical corrosion or change other than normal grain growth. These heaters operate equally well in air, a very oxidizing atmosphere. In addition, a 500 hour test in a 10^{-5} Torr vacuum was completed without harmful effects to the ceramic heater.

Compared to contempory biowaste resistojets which utilize noble metals for all heater elements, the advanced ceramic heater concept offers the following advantages:

1) High voltage (Order of 100 volts) - low current characteristic, requiring minimal power adaptation to the space station power supplies.

2) A 15 to 20 percent improvement in specific impulse, made possible by higher operating temperatures in the heater.

3) As a result of item 2), a minimization or possible elimination in the supplemental propellant required on space station.

4) Greater growth potential in view of the higher performance capability and greater compatibility with the biopropellant variations.

INTRODUCTION

Electrical resistance heated rockets, called resistojets, are being developed to operate on the biowaste propellants CO_2, H_2O and CH_4 for the Space Station/Space Base. These biowaste resistojets are intended to operate with electrical power inputs of up to several hundred watts. When supplied with such power levels, biowaste resistojets can be expected to meet the orbit-keeping and control moment gyro (CMG) desaturation requirements of the space station.

The resistojet is a conceptually simple device. The propellant is convectively heated by flowing the propellant in contact with the resistance heater. The heated gas is then accelerated through a nozzle to obtain thrust. Exothermic chemical reactions are not required to achieve high specific impulses. Instead, electrical power is used to raise the temperature of the biopropellants in order to obtain the high specific impulse.

The contemporary biowaste resistojets (references 1 through 4) utilize metallic materials for their resistance heater elements. These thrustors are of the evacuated-concentric tubes type, having a low voltage-high current power characteristic requiring power adaptation to the space vehicle power supply. Rhenium metal, which has a structural temperature capability in excess of 2400°K (references 1 and 2), is used for the reducing propellants H_2 and NH_3. The biowaste propellants CO_2 and H_2O are oxidizing at high temperatures, while CH_4 presents a carbon deposition problem. Performance on CH_4 is limited by the requirement to keep operating temperatures low enough to avoid carbon decomposition in the thrustor. A threshold heater

temperature of 950°K with pure CH_4 is indicated (references 3 and 4) in order to avoid the long-term changes in thrust output and the adverse effects on the resistance heater which would result from carbon deposition in the thrustor. With the addition of CO_2 and or H_2O to the CH_4, the threshold temperature can be increased slightly to 1000°K. Large percentages of CO_2 or H_2O do not prevent the decomposition of methane within the thrustor.

To maximize propellant performance, it is desirable to use the CH_4 propellant undiluted except for normal EC/LS contaminants at the 950°K temperature, and to use the CO_2 and H_2O separately from the CH_4 at higher chamber temperatures. In this mode, an overall higher specific impulse is possible. The contemporary biowaste resistojet (reference 3 and 4) is being developed for this high performance mode using noble metals for the heater elements to achieve resistance to the oxidizing environments of heated CO_2 and H_2O. Candidate noble metals (alloys) for the contemporary biowaste resistojet are platinum, platinum-rhodium, and platinum-iridium. Platinum alone has insufficient strength to be used in the evacuated-concentric tubes design (reference 4). Platinum-rhodium alloy has sufficient strength but was found to suffer extreme carbonyl corrosion with CO_2 at temperatures above 1300°K. Platinum-iridium alloy, having even greater strength than Pt-Rh alloy, performs well in CO_2 and H_2O and was used in the 10 mlb biowaste thrustor test reported in reference 3. However, trace additions of oxygen may occur in the biopropellants, causing an oxidation corrosion problem with the Pt-Ir alloy (reference 5). Reference 6 predicts a weight percent of oxygen of 0.3 in the molecular sieve waste output. (See table I taken from reference 6). This can be neutralized by the addition of 0.04 percent by weight of hydrogen which is caused to react with the oxygen to form water. Gaseous mass balances for the McDonnell Douglas 90 day manned test of a regenerative life support system (reference 7) showed slightly more than one percent oxygen for two CO_2 concentrators tested (solid amine and molecular sieve). Oxygen output was greatest for the solid amine concentrator at 1.3 weight percent; that level could be neutralized by 0.2 percent of hydrogen.

An alternate material being considered is thoria dispersion strengthened platinum (TD Pt). Strength is lower than for the alloys, particularly if the material is annealed prior to launching the rocket into space, as in a thrustor qualification test firing, for example. The launch imposes the most severe structural load on a resistojet thrustor. The annealed yield strength is not sufficiently improved over pure Pt for direct adaptation of TD Pt to the contemporary biowaste resistojet. A significant advantage, however, with the dispersion strengthened material is grain growth stabilization, which greatly improves creep strength and which should significantly improve grain boundary corrosion. In view of the low yield strength of TD Pt, however, the contemporary design would most likely have to be compromised to an even lower voltage-higher current power characteristic. For example, the 10 mlb biowaste resistojet described in reference 3 (Pt-Ir alloy heater) operates at 2.5 volts at 40 amperes for 100 watts of power. With TD Pt heater material, even lower voltage-higher current seems inevitable if the structure is to be capable of withstanding the launch vibration environment.

Table I

PROPELLANT DESCRIPTIONS

Propellant	Source	Composition		
		Species	Mole Fraction	Mass Fraction
CO_2	Molecular sieve waste output (scrubbed from spacecraft atmosphere)	CO_2 N_2 O_2	0.984 0.012 0.004	0.989 0.008 0.003
CH_4	Sabatier waste output	CH_4 CO_2 N_2 H_2O	0.917 0.054 0.014 0.015	0.832 0.133 0.020 0.015
H_2O	Water recovery	H_2O	1.000	1.000

Normally, sufficient biopropellant is available to accomplish the orbit-keeping and CMG desaturation tasks with a resistojet using metal heater technology. Peak demands occur during increased solar activity periods, for example, and supplemental propellant is then required. Water has been selected as the supplemental propellant because it is easy to resupply and is compatible with the thrustors (reference 6).

While resistojets are conceptually simple, development has been paced by heater material limitations and the drive for maximum specific impulse and long, reliable lifetimes. Higher specific impulses than those possible with the noble metal heater technology in the biowaste environment is desirable from the following two points of view:

1. Supplemental propellant requirements can be reduced or eliminated.

2. Advanced performance thrustors offer greater growth potential for the Space/Base application.

This report presents the technological status of a continuing program to develop an advanced performance biowaste resistojet. Ceramic materials are being used for the heater and offer substantial increases in chamber temperatures with the biowaste propellants. Increased performance is possible with certain ceramic oxides because of their excellent corrosion resistance in oxidation environments and their high melting point temperature (above 3000° K).

LIST OF SYMBOLS

a	thermal diffusivity, m^2/s
A	area, m^2
C_p	specific heat at constant pressure, J/kg - °K
D	diameter, m
d	diameter, m
E	Young's Modulus, N/m^2; or voltage, volts
F	thrust, N
f	defined as R x S; or Darcy friction factor
G	evaporation rate, kg/m^2-s
h	specific enthalpy, J/kg; or heat transfer film coefficient, W/m^2 - °K
I	current, amperes
I_{sp}	specific impulse, sec
k	thermal conductivity, W/m - °K
L	length, m
$\dot{m}$	mass flow rate, kg/sec
M	molecular weight; or Mach number
n	number of channels; or temperature exponent of viscosity
Nu	Nusselt number
P	static pressure, N/m^2; or power, watts
P_T	total (stagnation) pressure, N/m^2
Q	heat flux rate, W
R	gas constant, J/kg - °K; or electrical resistance, ohms
R_1	thermal stress resistance parameter, °K

LIST OF SYMBOLS (Concluded)

R_2	thermal stress resistance parameter, W/m
R_3	thermal stress resistance parameter, m^2-°K/s
Re	Reynolds number
t	time, sec
T	static temperature, °K
T_T	total (stagnation) temperature, °K
$\overline{T}$	absolute temperature ratio = T_{out}/T_{in}
V	velocity, m/s
x	parameter defined as $\pi nLkNu/\dot{m}C_p$
α	coefficient of linear thermal expansion
$\dot{\delta}$	surface recession rate, m/s
γ	specific heat ratio, C_p/C_v
ε	radiant emissivity
μ	Poisson's ratio; or viscosity, N-s/m^2
ρ	density, kg/m^3; or electrical resistivity, Ω-m
σ	stress, N/m^2
ϕ	surface temperature change rate °K/s

THRUSTOR DESIGN

Ceramic Heater Concept

Metal oxide ceramics offer the potential for structural temperatures above the melting points of the noble metals. Significant improvements in thrusting performance become possible with ceramic heater material but not without mechanical design anomalies relative to the ductile metals. Brittleness of the ceramic oxides manifests itself in thermal shock and brittle fracture problems aggravated by the mode of operation required of a biowaste resistojet. The resistojet must be capable of many starts from a cold-quiescent condition. It is neither efficient nor practical to maintain a hot heater during non-thrusting periods. The resistojet must respond to a start-up command in a reasonable period of time. Response time is not critical for the biowaste resistojet application; however, it should not be excessive. Pulsing is not a requirement. On the other hand, no more than a few minutes should be required to reach steady-state operating conditions. Thousands of hours of thrusting are required along with thousands of cycles if the biowaste resistojet is to be suitable for space station applications.

To heat a ceramic, which in turn can heat the biowaste propellant, various alternative methods can be employed, including:

(1) Direct resistive heating of a conducting ceramic.
(2) Indirect heating by arc discharge.
(3) Inductive heating using a ceramic as a susceptor.
(4) Indirect heating by a metal resistance heater.

The first of these is being studied intensively for the advanced biowaste resistojet. The conducting ceramics can be used for arc discharge electrodes as a second possible approach. An arc discharge-ceramic heater concept offers a potential for much higher temperatures relative to ohmic heating alone. This concept may have application for pulsing type applications, for example.

Inductive heating has been used with zirconia ceramic, with the ceramic serving as a susceptor to the radio frequency energy field. A thrustor based upon this principle might be referred to as an Inductojet. Reference 7 discusses the use of yttria stabilized zirconia susceptor rings for a high temperature furnace with temperature capability in excess of 2000°K. Nickel-chrome alloy wire preheater wires are retracted. This mode of heating is not being studied at this time, primarily because induction coupling losses would result in a lower efficiency than with an ohmic heated device. Also, the radio frequency field of a induction heater requires RF shielding attention relative to space station applications.

Several factors enter into a decision whether or not to choose an indirect metal heater concept with respect to ceramic heaters as well as all metal thrustors. An indirect heater in this case is one which transfers heat by radiation or conduction to another body which in turn heats the

propellant by convective heat transfer. This might be a wire wound resistance heater radiating to a closed metal passage containing the propellant. Other than being able to accommodate a higher voltage-lower current, no advantage is gained here by using a noble wire heater since it must be operated hotter than a directly exposed heater. Such a heater would suffer increased vaporization losses, particularly if exposed to vacuum. A rhenium wire heater in a vacuum could be considered for the biowaste resistojet, however, since it has a higher temperature capability (sublimation recession rate is 5 orders of magnitude lower for Re compared to Pt, and the melting point of Re is significantly higher than for Pt, 3440 versus 2045°K). While such a thrustor, all metal or ceramic, would operate well at first, premature failure could occur due to grain growth induced leakage in which the propellant could attack the rhenium. Such leakage does occur in time, but otherwise is generally insignificant relative to thrusting performance.

Compared to all of the indirectly heated configurations, the excessive temperatures required for radiant heat transfer tend to result in significant metal evaporation rates which result in near-term electrical shorting problems. The vaporized metal tends to condense on colder insulator surfaces resulting in short circuit effects. A distinct advantage, on the other hand, of a wire-wound heater is that it can be tailored to have electrical characteristics which adapt simply to the spacecraft power system.

The advanced biowaste resistojet concept currently being studied utilizes ohmic heating of ceramic materials to transfer thermal energy to the biowaste propellants to achieve chamber gas temperatures of 1800 to 2000°K. Melting temperatures of the ceramics being considered exceed 3000°K for a large operational temperature margin. A composite heater material approach (hybrid) is being considered which utilizes metal technology for regenerative cooling passages and the starter heater. Ceramic heater material is used for the final highest temperature stage. The hybrid is attractive using the best properties of both the ductile metals and high temperature ceramics. Electrically, the thrustor can be tailored to adapt directly to the spacecraft electrical power system, to a 120 volt AC power supply, for example.

Both zirconium dioxide and thorium dioxide can be used as conducting ceramics. These materials are solid electrolytes having a defect structure (oxygen deficient lattice) which permits oxygen ions to pass through the crystal lattice. Such a mechanism results in ionic conduction as compared to electronic conduction in the usual case of electrical current flow. Some electronic conduction may occur; however, current flow is predominately the result of the ionic conduction in these materials.

Ionic conduction in ceramic materials has been used for decades, having had a commercial beginning in Germany. Originally, stabilized zirconia was used as a light bulb referred to as the Nernst glower or illuminator. Presently, this lamp is used as an infrared source for spectroscopy. The material's ability to transfer oxygen ions has been used to develop oxygen sensors and as electrolyte for fuel cells and electrolysis devices (to convert H_2O into its basic elements H_2 and O_2,

for example). It is important to note that the ceramic can be impervious to all gases and pass only oxygen ions. Reference 9 presents a summary review of the applications for ZrO_2. Reference 10 presents a detailed technical discussion on conduction in ceramic oxides.

Pure zirconia undergoes a destructive crystal phase change when cycled to high temperature. Additives are used, generally yttria (Y_2O_3), calcia (CaO), or magnesia (MgO) to effect a stabilization of the mixed oxide crystal to a face-centered cubic fluorite structure. For electrically conducting ceramic applications, the first two additives are generally used. For the advanced resistojet application Y_2O_3 is preferred as a stabilizer since CaO has a greater tendency to evaporate at very high temperatures.

The advanced biowaste resistojet concept is shown schematically in figure 1. Variations are possible in the arrangement of the various components, and the figure 1 schematic is presented as a typical case to indicate the function of the components of the thrustor. In the order of the propellant flow path direction, the advanced resistojet includes the following:

1. An evaporator heat exchanger to vaporize liquid water propellant.

2. A resistance-type heater to supply energy for preheating the evaporator and meeting the enthalpy rise requirements for vaporization of the water.

3. A regenerative propellant pass to recover radial heat losses and increase the thermal efficiency of the thrustor.

4. A ballast resistor to provide stabilization of the ceramic heater.

5. A starter heater coil to preheat the ceramic heater to its conducting (ignition) temperature.

6. The ceramic heater, operated in series with the ballast resistor, with two electrodes for making electrical connections.

7. An exhaust nozzle to accelerate the heated propellant for producing thrust.

8. An insulation system, not shown in figure 1, to maintain a high thermal efficiency.

The starter heater and ballast resistance coils are physically one common coil electrically divided as depicted in figure 1.

The ionically conducting ceramics have a negative resistance characteristic (resistance decreases with increasing temperature). If connected directly to a constant voltage supply, such a resistor would continue to increase in temperature, drawing increasing amounts of power until destruction occurred. A current controlling device, called a ballast, is required in this case, as it is with an arc lamp. During normal operation of the ceramic heater, the ballast resistor depicted in figure 1 operates in series with the

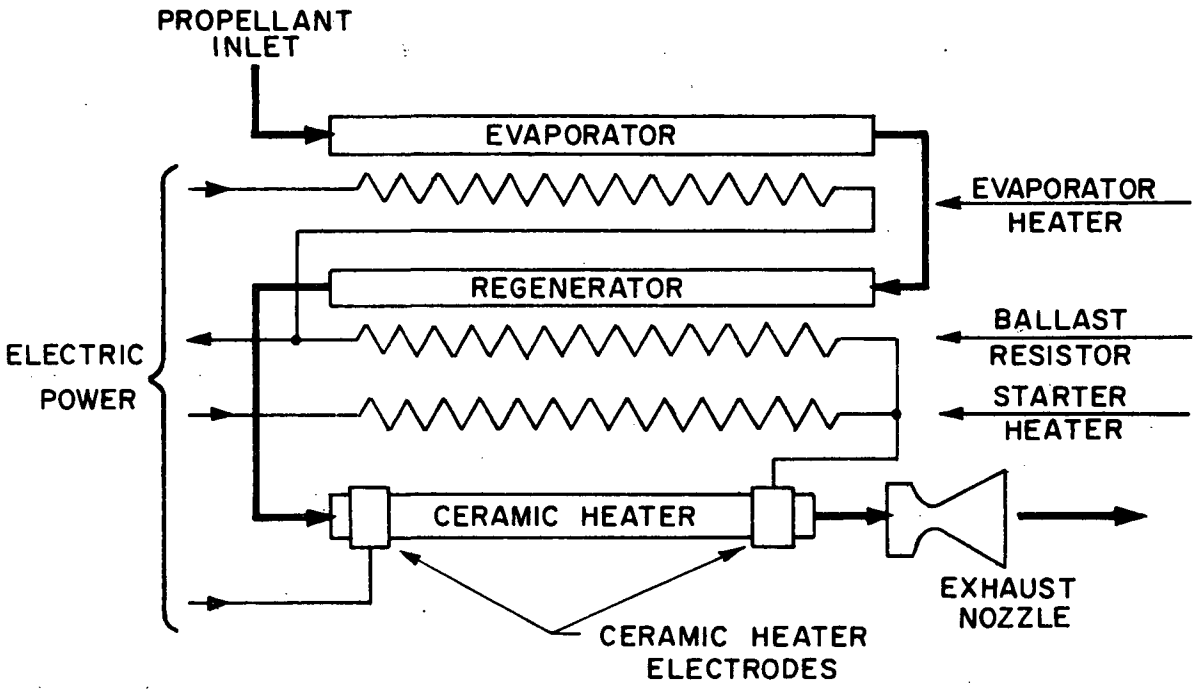

Figure 1.- Advanced biowaste resistojet concept.

ceramic heater. Any increase in current in the series circuit results in an increased voltage drop across the ballast resistor. With an adequate ballast resistance, stable operation is achieved.

Referring to figure 1, the propellant is heated to about 400°K in the evaporator and to about 800-900°K in the regenerator. The final stage ceramic heater raises the propellant temperature to about 1800 to 2000°K. The final temperature depends on the power input to the ceramic heater. During steady state operation with water propellant for example, about 300 watts of electrical power would be required for a 25 mlb thrustor. This power would typically be proportioned as follows:

Heater Component	Electrical Power, watts
Evaporator	125
Ballast Resistor	35
Ceramic Element	140
Total	300

Of the total of 300 watts, approximately 270 watts go into the propellant and 30 watts are attributed to thermal losses. In this case, the overall heater thermal efficiency is 90 percent. Note that the ballast dissipates only 20% of the combined ballast-ceramic heater power and, therefore, does not compromise the thrustor thermally. Most of the ballast power goes into the regenerator.

Figure 2 indicates a control concept for the advanced biowaste resistojet. When the thrustor is cold, the ceramic heater element appears to the electrical circuit as an insulator having a resistance measured in megohms. To start the thrustor, the starter heater is turned on. As shown in figure 2, the starter operates in series with the ballast resistance coil, both supplying ohmic heating at about 1300°K. In the event water propellant is being used, the evaporator is first preheated to a steaming condition (400°K). The figure 2 schematic indicates a start up override signal which would prevent propellant flow initiation until the evaporator is preheated. The evaporator heater is controlled to maintain a set temperature of about 400°K at the evaporator outlet.

Once the ignition temperature (about 1000°K) is reached on the ceramic heater, and provided that propellant pressure is adequate as sensed by a pressure switch, the start up control removes the starter heater from the circuit. The ceramic heater is then powered up to full operating temperature in series with the ballast resistor and controlled, for example, by a resistance signal. The resistance of the ceramic heater provides a high resolution signal of the mean temperature of the heater. Resistance is easily measured by dividing the voltage drop across the ceramic heater by its current flow.

The figures 1 and 2 thrustor concept is readily adaptable to an all-metal thrustor. The present exploratory design can be assembled with a metal tube replacing the ceramic heater element. This thrustor would be

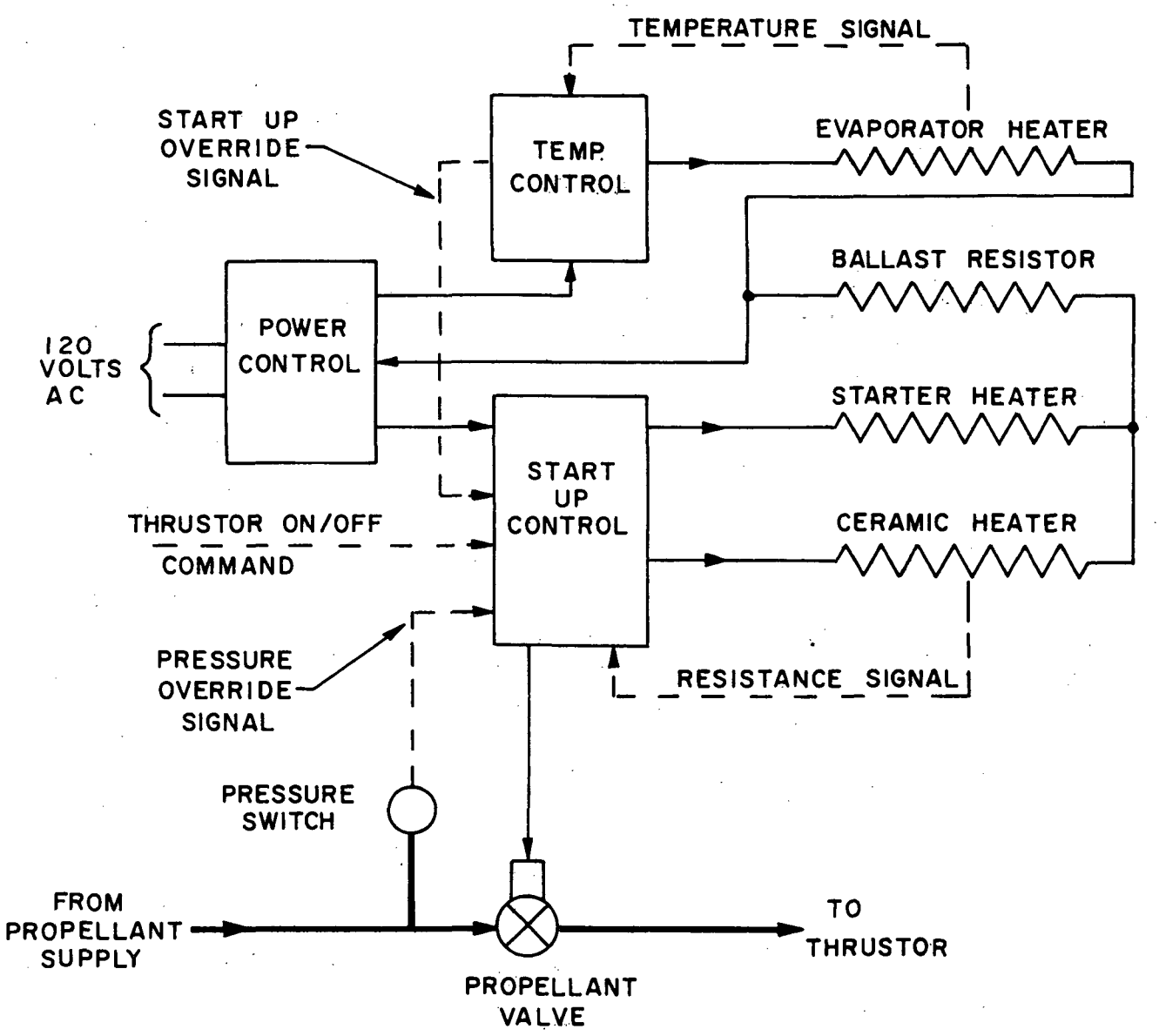

Figure 2. Advanced biowaste resistojet control concept.

operated with the starter and ballast coils serving as a heater at a conservative gas temperature of 1200°K. Thrusting performance would be sufficiently high to consider using this thrustor as a demonstration unit for EC/LS/RCS ground tests. The all-metal version would be relatively inexpensive while offering moderate thrusting performance.

The thrustor design philosophy adopted for the ceramic heater biowaste resistojet offers a near-term interim thrustor while further development activities continue on an advanced high performance ceramic heater thrustor. Performance goals for the ceramic heater thrustor and the all-metal adaptation can be summarized as follows for a 25 mlb thrust size:

TABLE II

BIOWASTE RESISTOJET THRUSTOR PERFORMANCE GOALS

Thrustor Gas Temperature, °K	All-Metal 1200	Advanced-Ceramic Heater 1800	2000
Propellant	Predicted Specific Impulse, seconds		
CO_2	145	185	200
H_2O	200	260	275

For comparison, the long-lifetime specific impulse possible with the noble metal-concentric tubes resistojet, according to reference 3, is 170 seconds for CO_2 and 240 seconds for H_2O.

Thermal Analysis

Introduction.- After selection of the basic concept and the configuration of the ceramic heater thrustor, as described in the Ceramic Heater Concept section, it was necessary to perform a preliminary thermal and gas dynamic analysis of the design concept for the purpose of predicting performance and operating parameters and of sizing elements in order to design a Proof-of-Concept thrustor in sufficient detail to permit fabrication and test. The thermal analysis effort was tailored to those objectives; simplifying assumptions were liberally employed whenever it was judged that the simplifications would not significantly affect the validity of the end result, i.e., the Proof-of-Concept designs. The judgments were based on previous experience of ARTCOR staff members in designing electro-thermal thrustors. Analytical rigor was not an objective in this phase.

Thrustor thermal design philosophy and concepts.- The thrustor concept which was selected, analyzed and sized for the Proof-of-Concept (POC) design is shown schematically in figure 3. It is essentially identical to the

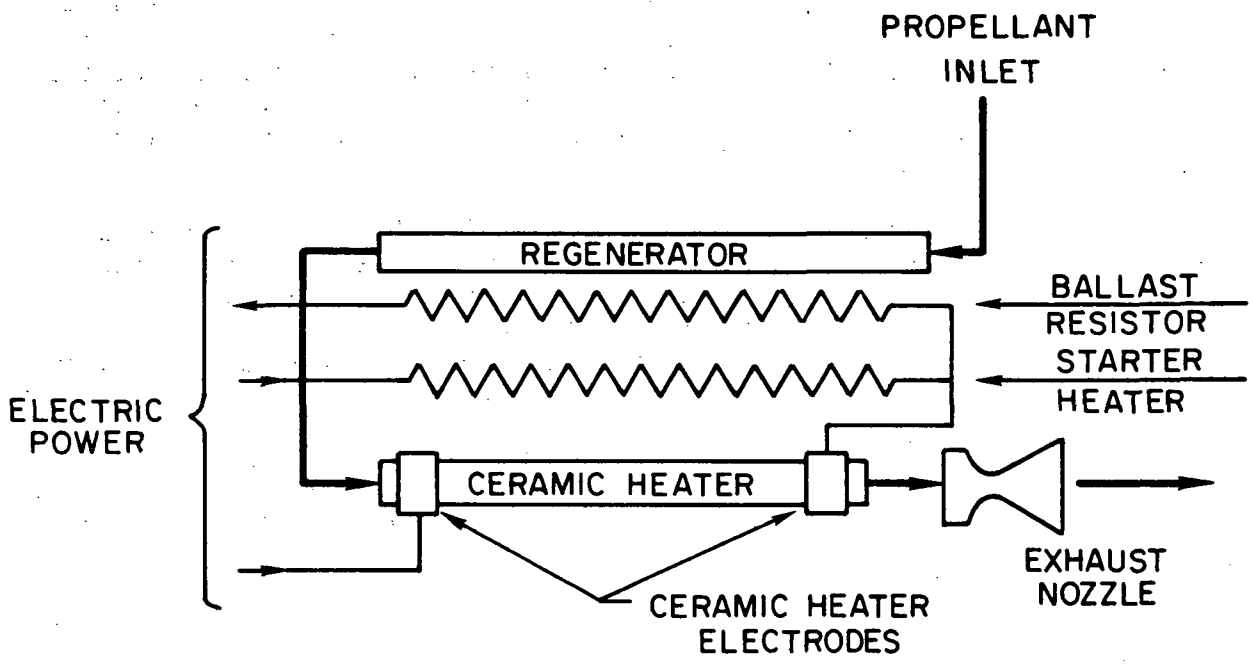

Figure 3.- Schematic diagram of proof-of-concept thrustor configuration.

concept shown schematically in figure 1 in the Ceramic Heater Concept section, except for deletion of the evaporator and evaporator heater. The evaporator section was not included in the POC thrustor design in order to provide better accessibility to the regenerator stage and the ceramic heater during development testing. This facet of the POC design is discussed in the Mechanical Design section.

The power control schematic selected for the POC design is a simplified version of the advanced biowaste resistojet control concept shown in figure 2, in which the evaporator heater and evaporator temperature controller are deleted.

The general configuration selected for analysis, sizing and detailed design is shown in figure 4. This selected configuration evolved from a series of trial configurations which were studied during the course of the first part of the program. The reasons for adopting this particular configuration for the POC thrustor are discussed in the Mechanical Design Section.

A specific cross-sectional configuration for the ceramic heater was also selected for the POC thrustor after a series of trial cross-sections had been examined analytically and, to some extent, experimentally. From structural and thermal efficiency points of view, it is desirable to have a relatively short ceramic heater. For a given heater length, a higher gas temperature can be achieved by using multiple parallel flow passages through the ceramic heater tube.

That concept can be demonstrated in the following manner. Consider a simplified case of heat transfer in a set of n parallel channels at constant wall temperature

$$Q = hA\Delta T_{LMTD} \tag{1}$$

where Q is the rate of energy transfer to the gas, h the convective film coefficient, A the surface area of the channels, and ΔT the log mean temperature difference (LMTD). Relating Q to the product of mass flow rate $\dot{m}$ and the enthalpy change of the gas, expressing h in terms of the Nusselt number Nu, thermal conductivity k and channel diameter d, and expressing the area as πdnL, where L is the length of the channels, the final tube wall to gas temperature difference can be shown to be

$$T_{wall} - T_{gas\ final} = \frac{T_{wall} - T_{gas\ initial}}{e^{x}} \tag{2}$$

where

$$x = \frac{\pi nLkNu}{\dot{m}\ Cp} \tag{3}$$

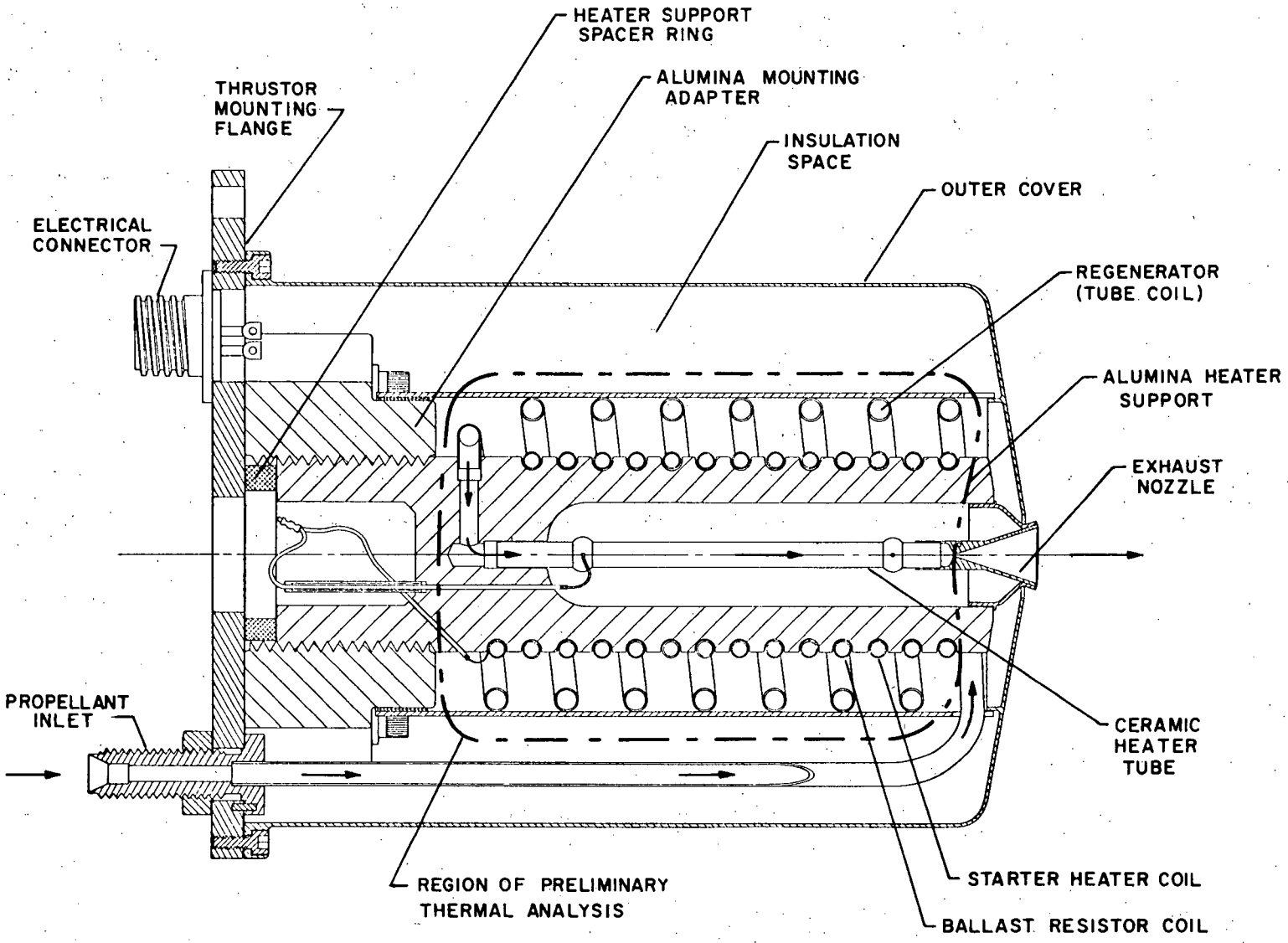

Figure 4.- Proof-of-Concept thrustor configuration, showing region included in preliminary thermal analysis.

In this simplified case, Nusselt number and the property values k and C_p are considered constant at average values. Note that the final gas temperature is independent of channel diameter, and is affected geometrically only by the channel length and the number of channels. Channel diameter is, of course, a major factor in determining the pressure drop across a multi-passage heater tube.

The selected ceramic heater cross-sectional configuration is shown in figure 5. It consists of 6 parallel passages through a ceramic heater of cylindrical form. The use of multiple passages greatly improved the heat transfer effectiveness of the heater for a given length over that of a single-passage configuration. The number, size and arrangement of the passages, and the outside diameter of the cylinder, were all arrived at by optimizing qualitatively with balanced regard for heat transfer effectiveness, fluid velocity, pressure drop, electrical conduction, and structural, size, and manufacturing considerations. When the heater cross-section shown in figure 5 evolved from those considerations and calculations, that design was frozen for the POC thrustor configuration and an extrusion die was fabricated to produce a number of ceramic heaters of that design for experimental evaluation.

For the regenerator (see figure 4) the selected design involved indirect heating of the propellant in a spiral-wound regenerator tube, with the outside of the tube being heated predominately by radiation from

(1) The ohmically-heated ballast resistor and starter heater coils, and the radiantly-heated alumina heater support during starting, and

(2) The ohmically-heated ballast resistor coil, and the radiantly-heated alumina heater support during cruising.

The regenerator tube itself is not ohmically heated in this biowaste resistojet.

The thrustor energy flow paths are discussed further under the Preliminary Thermal Analysis heading.

Thermal design parameters.- The POC thrustor is designed to operate on either CO_2 (carbon dioxide) or vaporized H_2O (steam) as a propellant at the thrustor maximum operating temperature. A separate evaporator will be required with the POC thrustor for operation on liquid water as a propellant, for the reasons previously given. With the maximum operating temperature fixed by materials considerations, the power input to the thrustor will be less when operating on CO_2 as the propellant, compared with steam, because of the higher heat capacity of steam.

A series of design parameters and constraints were established and specified for the POC thrustor, based on previously selected performance goals, material operating temperature limits (both short duration and continuous), and similar factors. These parameters and constraints are tabulated in table III. In general, they are considered to be relatively conservative values for a ceramic heater thrustor, allowing some margin for subsequent performance improvement. Specifically, the POC thrustor was

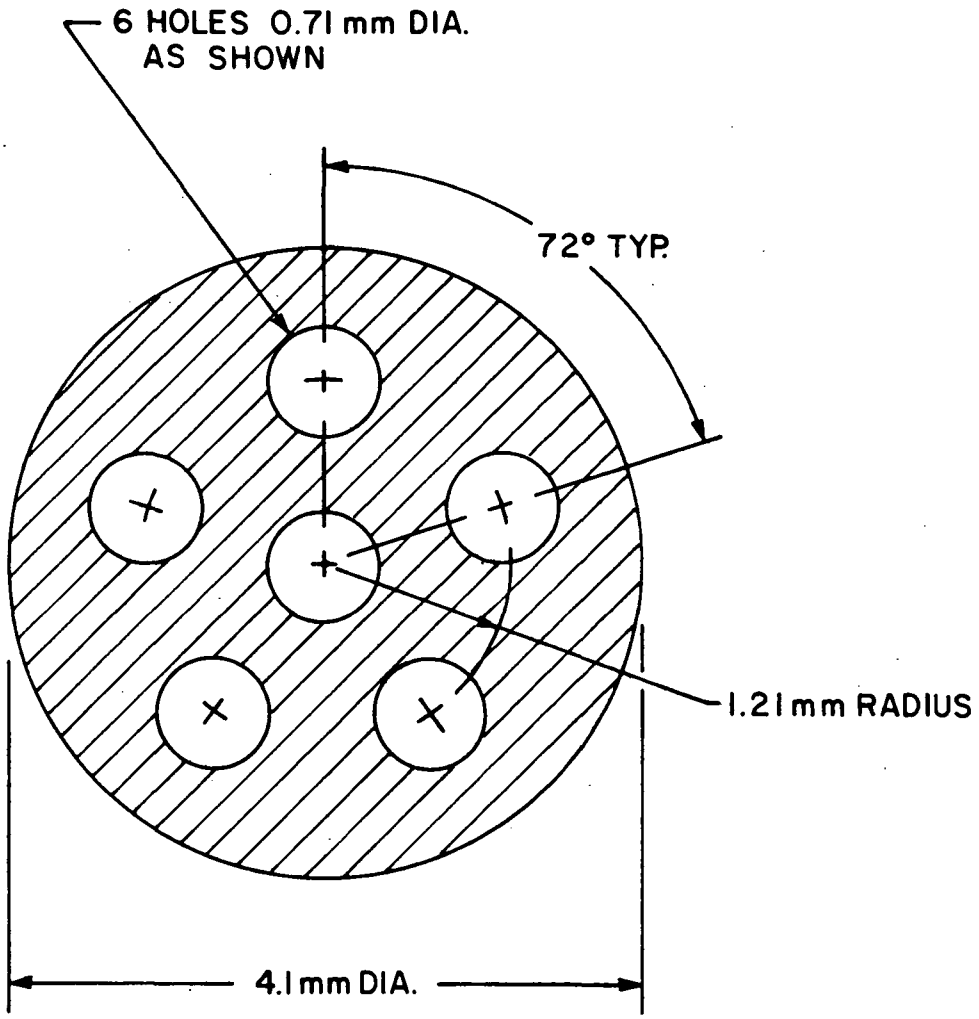

Figure 5.- Selected ceramic heater cross-section.

Table III

FIXED DESIGN PARAMETERS AND CONSTRAINTS
FOR PROOF-OF-CONCEPT THRUSTOR ANALYSIS

Design Parameter	Symbol	Units	H_2O Vapor		CO_2	
			Cruise	Starting	Cruise	Starting
Thrust	F	N	0.1112	--	0.1112	--
Specific impulse	I_{sp}	sec	256	--	183	--
Propellant mass flow rate	$\dot{m}$	kg/sec	4.34×10^{-5}	TBD	6.08×10^{-5}	TBD
Nozzle inlet gas pressure	P_{T_7}	N/m^2	1.013×10^5	TBD	1.013×10^5	TBD
Regenerator inlet gas temperature	T_{T_2}	°K	417	417	298	298
Intermediate gas temperature	$T_{T_3}=T_{T_4}$	°K	TBD	TBD	TBD	TBD
Nozzle inlet gas temperature	T_{T_7}	°K	1800	--	1800	--
Ceramic heater wall temperature	T_4	°K	<2000	>1100	<2000	>1100
Ballast/starter heater wire temp.	T_1	°K	<1200	<1400	<1200	<1400
Time to start	t	sec	--	<60	--	<60
No. of starts	--	--	--	>10,000	--	>10,000

TBD = To be determined

designed for an exit gas stagnation temperature of 1800°K, corresponding to a maximum wall temperature of the ceramic heater of about 1860°K (i.e., exit gas temperature approaches to within about 60°K of wall temperature), whereas it is expected that the ceramic heater will eventually be capable of operating at a maximum wall temperature of at least 2000°K. The ballast resistor and starter heater operating temperatures were set at 1180°K for cruise and 1300°K for starting, based on the evaporation characteristics of the selected material (Pt-20 Rh) relative to the desired operating life.

The POC thrustor was designed to the values listed in table III. Most of the actual detailed calculations for component sizing were made for steam as the propellant rather than CO_2, since the requirements for steam were generally controlling in the sizing of elements. Material operating temperature limits were chosen from a combination of published data and experimental data obtained in the Advanced Rocket Technology (ARTCOR) laboratory on this and related programs (see particularly reference 20).

A nominal chamber (nozzle inlet) pressure of 1 atmosphere was selected for the thrustor design after a review of the effects of chamber pressure on thrustor design.

Thermal properties of biowaste propellant gases.- The two biowaste propellants given primary consideration in this program were carbon dioxide gas and vaporized water (steam). Although methane gas (CH_4) is also a possible biowaste propellant, it cannot be heated above about 950°K in a thrustor because of its tendency to deposit carbon at higher temperatures, and it is therefore not an attractive individual propellant for an advanced high temperature thrustor.

A set of values of the thermodynamic and transport properties of both propellants were required for the thermal analysis. All key properties were collected and correlated for both propellants for the range of temperatures from 300 to 2000°K, at a pressure of 1 atmosphere. The key thermodynamic properties include: gas constant, specific heat, specific heat ratio, enthalpy, entropy and sound velocity; the key transport properties include: viscosity, thermal conductivity, and Prandtl number.

A number of reliable data sources were used in preparing the property data correlations as functions of temperature. In those cases where discrepencies existed between references for a particular property, judgment was exercised in the weighting factor to be applied to any particular set of properties, based on the estimated reliability of the original set of data. Sources of data included references 11 through 19.

The key thermodynamic and transport properties used in the thermal analysis are listed in table IV for several temperatures, at a pressure of 1 atmosphere.

Physical and thermal properties of materials of construction.- The selected POC thrustor concept shown in figure 4 is a hybrid configuration based on the use of noble metal (platinum alloy) components in the regenerator section of the thrustor, and ceramics in the final heater stage and

Table IV

THERMODYNAMIC AND TRANSPORT PROPERTIES
OF PROPELLANT GASES

P = 1 atmosphere

Gas Property	Symbol	Units	Gas	Temperature - °K 500	1000	1500	2000
Gas constant	R	J/kg - °K	CO_2	188.9	188.9	188.9	188.9
			H_2O	461.5	461.5	461.5	461.5
Specific heat at const. pressure	C_p	J/kg - °K	CO_2	1015	1234	1326	1372
			H_2O	1980	2265	2600	2835
Specific heat ratio	γ	--	CO_2	1.230	1.181	1.166	1.159
			H_2O	1.309	1.252	1.214	1.194
Viscosity	μ	$N\text{-}s/m^2$	CO_2	2.33×10^{-5}	3.89×10^{-5}	5.12×10^{-5}	6.22×10^{-5}
			H_2O	1.70×10^{-5}	3.59×10^{-5}	5.17×10^{-5}	6.08×10^{-5}
Thermal Conductivity	k	W/m - °K	CO_2	0.0330	0.0660	0.0940	0.117
			H_2O	0.0346	0.0874	0.148	0.206
Specific enthalpy	h	J/kg	CO_2	4.01×10^5	9.72×10^5	16.2×10^5	22.9×10^5
			H_2O	9.30×10^5	19.9×10^5	32.2×10^5	45.9×10^5

for support and insulation of the metal heater coils. The basis for selecting the various materials of construction of the POC thrustor is given in the Mechanical Design section.

The key physical and thermal properties of the materials of construction required for the thermal analysis were: thermal conductivity, specific heat, density, radiant hemispherical total emittance, and electrical resistivity. The significant materials of construction, with their physical and thermal properties, are shown in table V. These property values were correlated from a number of reliable reference sources, including references 20 through 31.

Preliminary thermal analysis of thrustor.- One-dimensional steady state radial heat flow model: The first and simplest thermal model used for designing and sizing the POC thrustor was the one-dimensional radial heat flow model. This model employs the assumption of no axial variation in temperature in the components of the thrustor; only radial temperature variations and radial heat flow are assumed. Although this is a relatively crude assumption, past experience has shown that it has proved satisfactory for initial design work. The one-dimensional radial heat flow thermal model used in the preliminary analysis is shown as a network diagram in figure 6(a), and as an energy flow arrow diagram in figure 6(b).

Parametric design calculations and optimizations: The preliminary analysis was made with water vapor as the propellant, since a thrustor sized and designed to operate on water vapor will also operate on carbon dioxide at reduced voltage and power input for the same maximum temperatures. Connection to a 120 V. a.c. power source was assumed for the design.

A regenerator inlet temperature T_{T_2} of 417°K was assumed, corresponding to slightly superheated steam out of the evaporator at about 1.5 atmospheres pressure (allowing about 0.5 atmospheres pressure loss through the thrustor). The ceramic heater exit gas temperature T_{T_7} for the cruising condition was conservatively set at 1800°K in order to limit the ceramic heater maximum wall temperature T_1 (assumed to be uniform throughout for the one-dimensional phase of the analysis only) to approximately 1850°K, as previously discussed. This left the cruising condition intermediate gas temperature T_{T_4} at the inlet to the ceramic heater as unspecified and a direct function of the unspecified power split between the ceramic heater and the ballast resistor. The intermediate gas temperature T_{T_4} was treated as the principal independent variable and was assigned a series of values between 700 and 1000°K in order to determine the optimal thrustor design. For each assigned value of the parameter T_{T_4}, a complete steady-state power balance was calculated for the thrustor for the cruise condition. This power balance involved the balancing of electrical power input, to both the ballast resistor and the ceramic heater, with internal heat power transferred between components by various combinations of radiation, convection and conduction heat transfer processes, and with external power output in the form of both enthalpy rise in the propellant and external heat loss.

TABLE V

PHYSICAL AND THERMAL PROPERTIES OF THRUSTOR MATERIALS OF CONSTRUCTION

Material	Temp. T °K	Density, ρ kg/m^3	Specific heat, C J/kg °K	Electrical resistivity, ρ ohm-m	Thermal conductivity k W/m °K	Hemispherical total emittance ε -
Platinum 20% rhodium alloy	800	1.874×10^4	168	3.25×10^{-7}	70	0.10
	1000	↓	176	3.72×10^{-7}	75	0.125
	1200		185	4.18×10^{-7}	80	0.15
	1400		197	4.62×10^{-7}	85	0.175
TD nickel						(polished) (oxidized)
	800	8.9×10^3	500	2.8×10^{-7}	45	.10 - .45
	1200	↓	550	3.9×10^{-7}	49	.15 - .60
	1600		615	-	68	.20 - .70
Yttria-stabilized zirconia *	800	5.60×10^3	560	1.1×10^1	1.82	-
	1200	↓	670	2.5×10^{-1}	1.88	0.4
	1600		775	3.0×10^{-2}	2.00	0.4
	2000		858	9.0×10^{-3}	-	0.5
Type ZYF zirconia felt insulation **	800	3.21×10^2	590	-	0.135	.54
	1200	↓	630	-	0.224	.40
	1600		670	-	0.340	.40
	2000		750	-	0.492	.51
96% alumina	400	3.72×10^3	940	1.5×10^{11}	13.7	.75
	800	↓	1080	3.2×10^7	5.7	.61
	1200		1160	3.2×10^4	4.0	.46
	1600		1230	2.5×10^2	-	.41

* (ZrO_2 + 10 mole % Y_2O_3)

** (6% theoretical density, steam atmosphere)

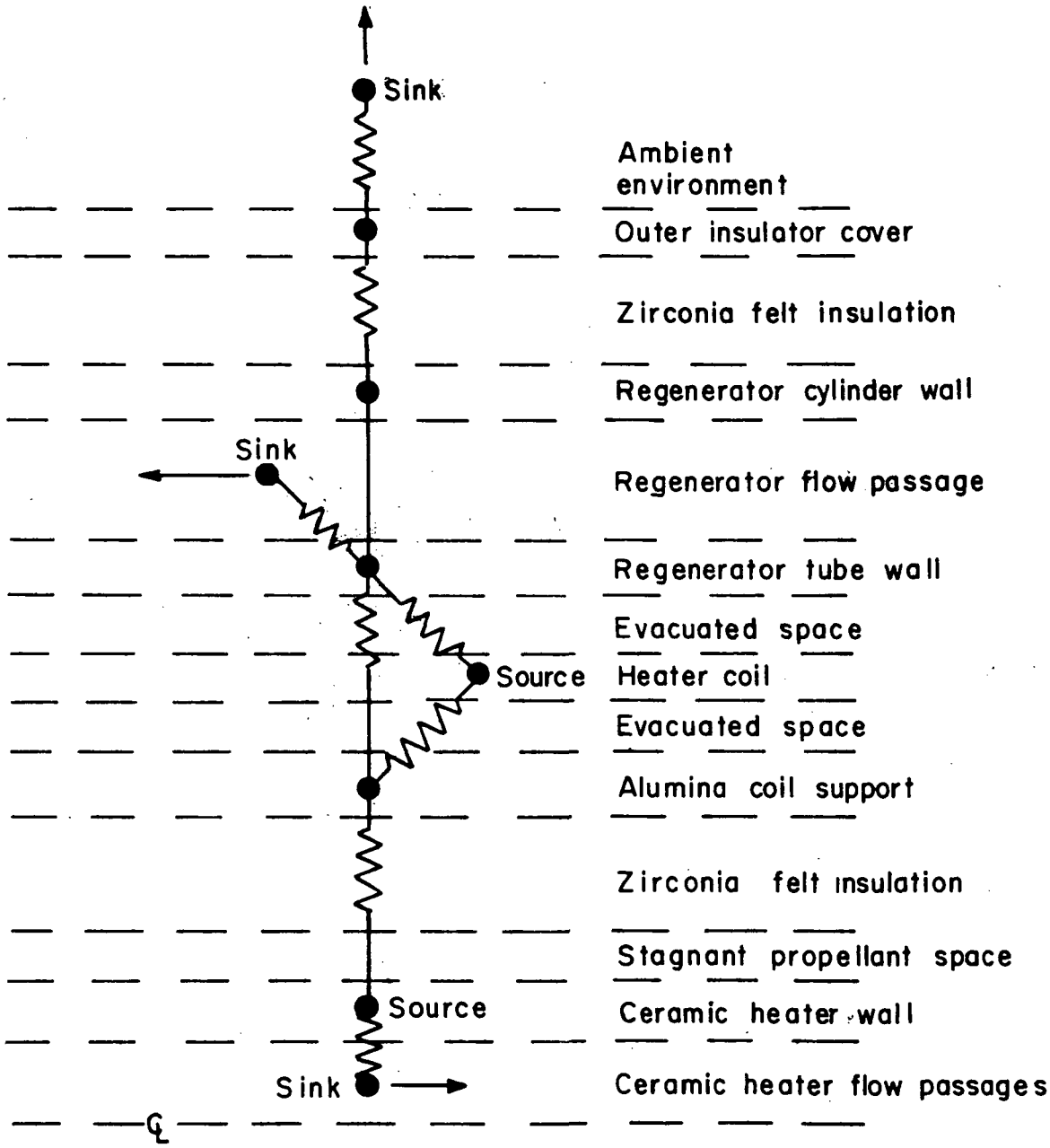

(a) One-dimensional radial heat flow model - thermal resistance network

Figure 6.- Thermal analysis model of POC thrustor (cruise)

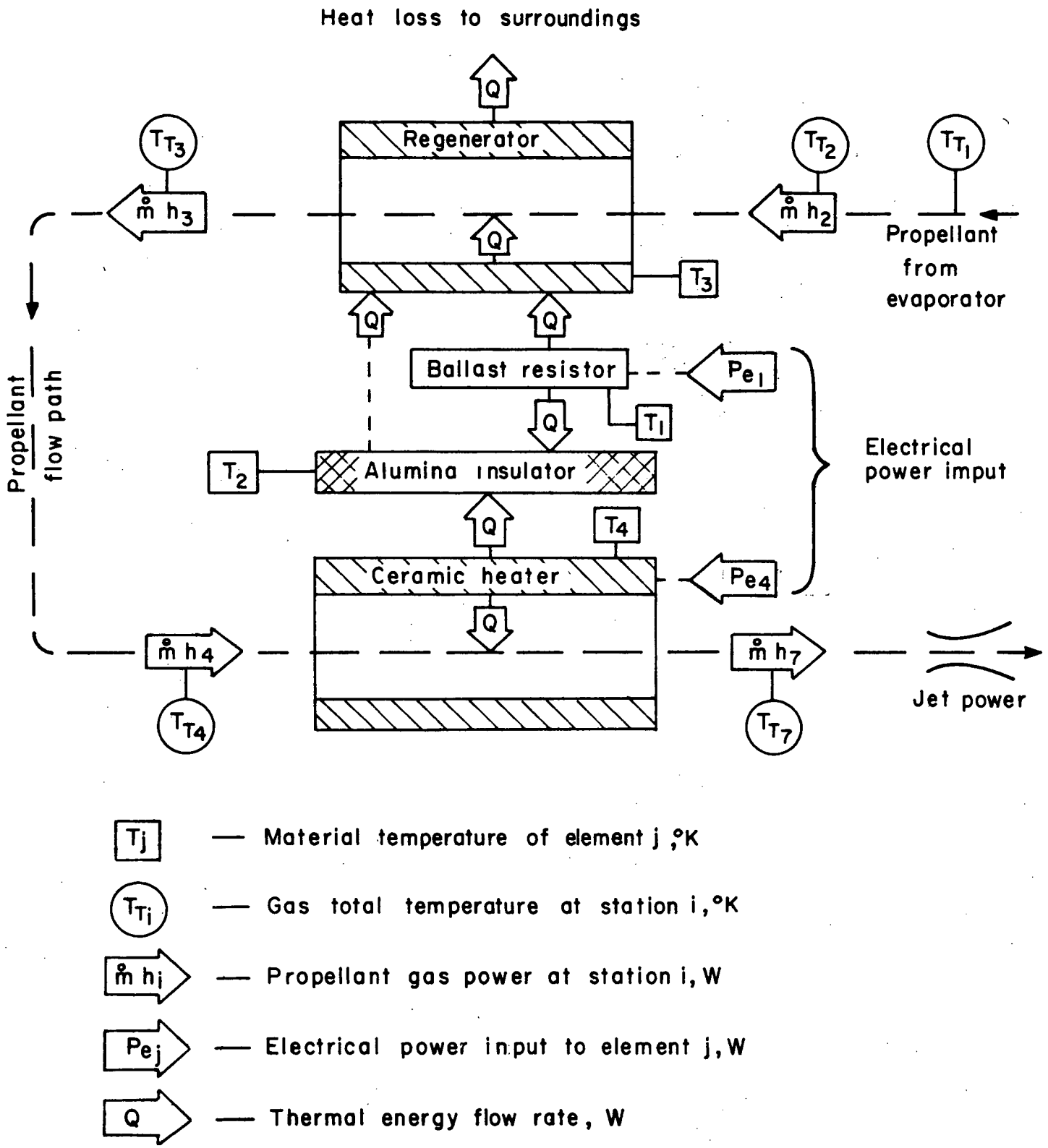

(b) Energy flow diagram - simplified model

Figure 6.- Concluded

For each value of the principal parameter T_{T_4} the design and size of each of the key thermal elements of the thrustor was calculated and sub-optimized, taking into account the variations with temperature of the physical, thermodynamic and transport properties of the component material and the propellant gas. This required successive approximations and iterative calculations, at both the single thermal zone and overall thrustor levels, for each value of T_{T_4}, in order to find solutions which satisfied both the power balance requirements and the various physical constraints.

These constraints included the need to maintain compatibility of:

(1) Component sizes relative to each other and to the thrustor assembly,

(2) Overall electrical resistance of the thrustor to a 120 V. a.c. power supply at the required power input, and

(3) Maximum operating temperatures of individual components within the long-lifetime limitations of their materials of construction,

and other similar constraints.

For computational purposes, the overall thermal analysis was broken down into a number of sub-problems which could be solved and optimized semi-independently of each other, with the results of the various sub-solutions then being used to complete the total thrustor power balance and design computations.

The sub-problems which were analyzed as part of the overall solution included:

(1) Three-way radiative energy interchange between the ballast resistor heater coil, the alumina coil support, and the regenerator tube coil plus coil support cylinder.

(2) Convective heat transfer between the propellant gas and the regenerator tube coil.

(3) Convective heat transfer between the propellant gas and a ceramic heater with an internal distributed heat source and conductive heat transfer in the ceramic material.

(4) Radiative-convective heat transfer from the ceramic heater surface through the zirconia felt insulation to the alumina coil support.

(5) The required ballast resistor heater coil wire length, diameter, and coil configuration as a function of required radiative surface area and coil electrical resistance.

and several other sub-problems of a similar nature.

References 21 through 39 were consulted for specialized thermal analysis methods and thermal properties data during the course of analyzing and solving the various phases of the overall thermal problem. The method of analysis and solution of one of the sub-problems--the idealized three-way radiative energy interchange between the ballast resistor heater coil, the alumina coil support insulator and the regenerator--is described in detail in the Appendix. Excessive space would be required to show the methods of analysis of all of the phases of the thermal analysis. Therefore, only the results will be presented for the other phases.

The principal results of all of the cruise condition thermal analyses were a series of calculated sets of values of component dimensions, operating temperatures, and energy flow rates within a family of POC-type thrustors, each set computed for a different value of the intermediate gas temperature T_{T4} (defined as the ceramic heater inlet, or regenerator outlet, gas temperature) for operation on steam. All results were required to conform to the initial design parameters and constraints listed in table III. The results of the computations were then plotted against the intermediate gas temperature T_{T4} (or its approximate numerical equal, the regenerator wall temperature T_3) for the purpose of selecting the optimal design value of the intermediate gas temperature for the cruise condition. The principal plots are shown in figures 7 through 12.

Selection of cruise condition thrustor design values: The curves of figures 7 through 12 collectively define the design dimensions of the POC thrustor within fairly narrow limits, based on the general configuration of the hybrid thrustor adopted at the beginning of the analysis. The key plots in establishing the design limits are figures 7, 11 and 12. Figure 7 establishes an effective lower limit of about 720°K on the cruise condition intermediate gas temperature T_{T4}, below which the percentage of total power dissipated in the ballast resistor is too small to satisfactorily stabilize the current in the ceramic heater over its full range of possible operating temperatures. Figures 11 and 12, on the other hand, establish an effective upper limit of about 950°K on the intermediate gas temperature T_{T4}, above which the ballast resistor heater wire becomes so long that it cannot be fitted into the adopted configuration without compressing the coil solidly, thereby shorting it out.

It was concluded that the average ballast resistor coil spacing/wire diameter ratio should actually not be less than about 2.0, in order to eliminate the possibility of localized shorting-out which might result from any non-uniform spacing of the coil turns. From figure 12 it can be seen that this requirement implies that the intermediate gas temperature T_{T4} must be about 850°K or less. The value of T_{T4} = 850°K was then selected as a trial design value, and all of the other computed results, principally those shown in figures 7 through 11, were checked for feasibility and suitability at the 850°K value. All conditions were found to be both feasible and suitable for the 850°K temperature, and that value of the intermediate gas (steam) temperature was therefore chosen as the design point value for the cruise condition of the POC thrustor.

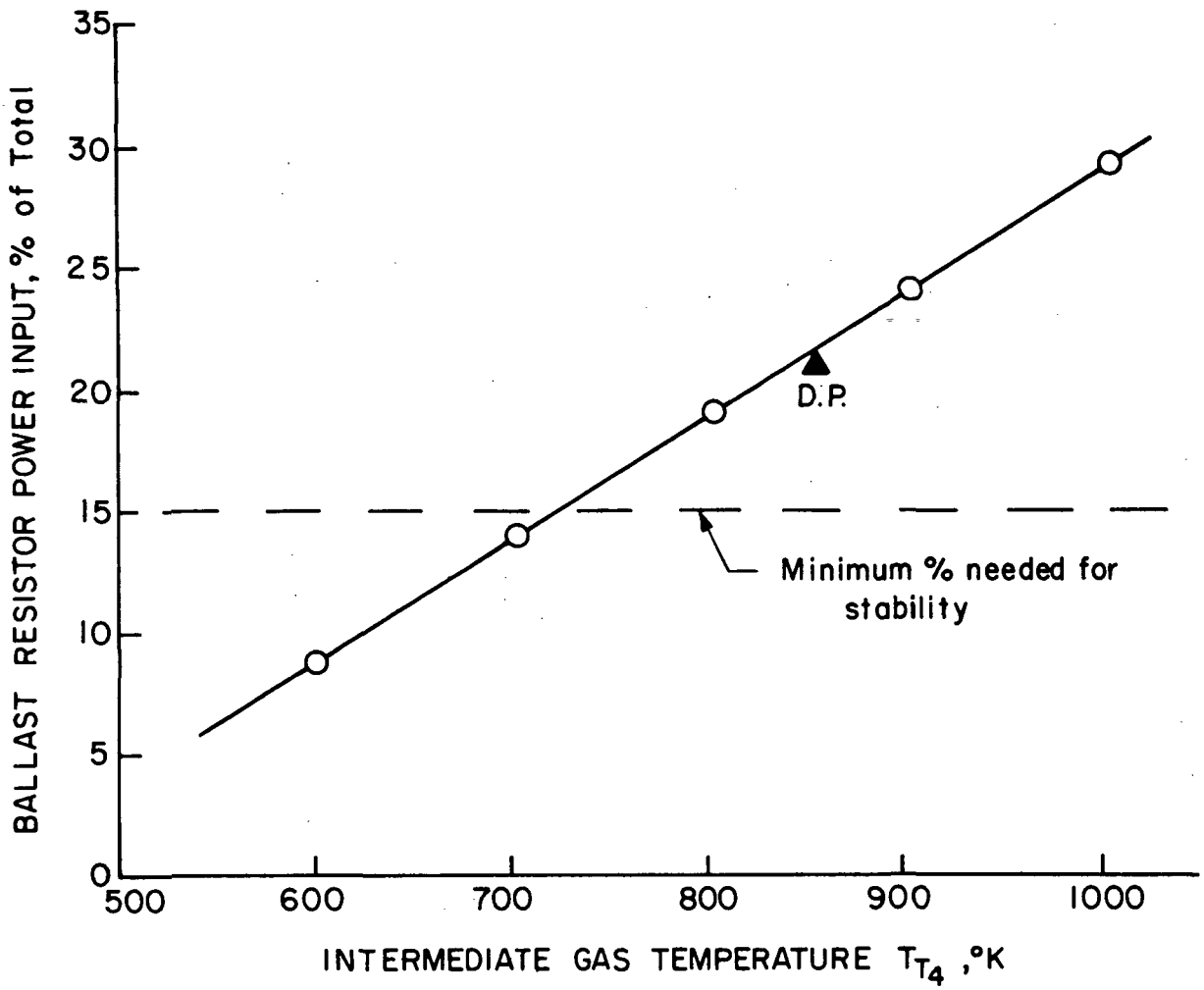

Figure 7.- Ballast resistor power input as a fraction of total power input.

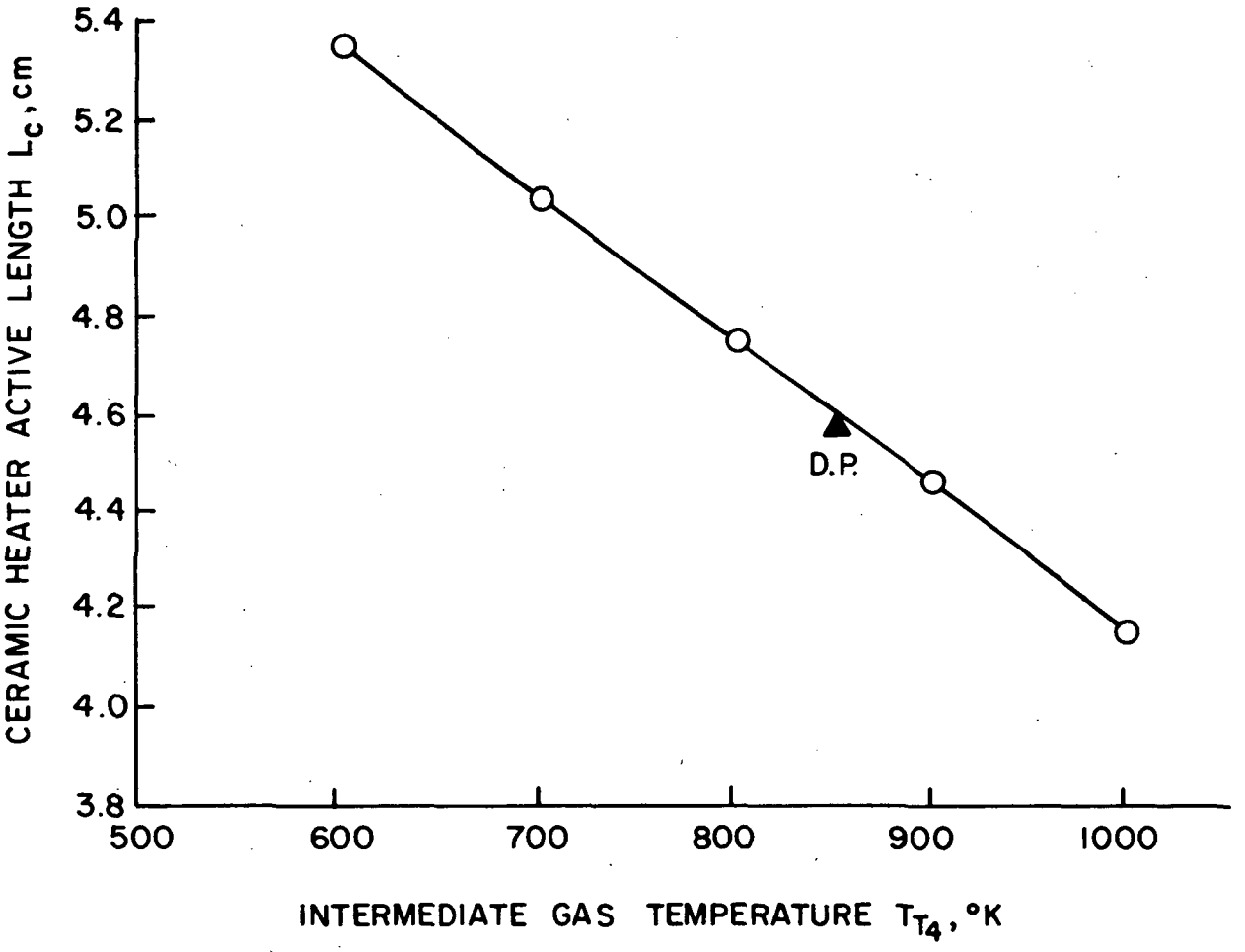

Figure 8.- Active length of ceramic heater as a function of intermediate gas temperature.

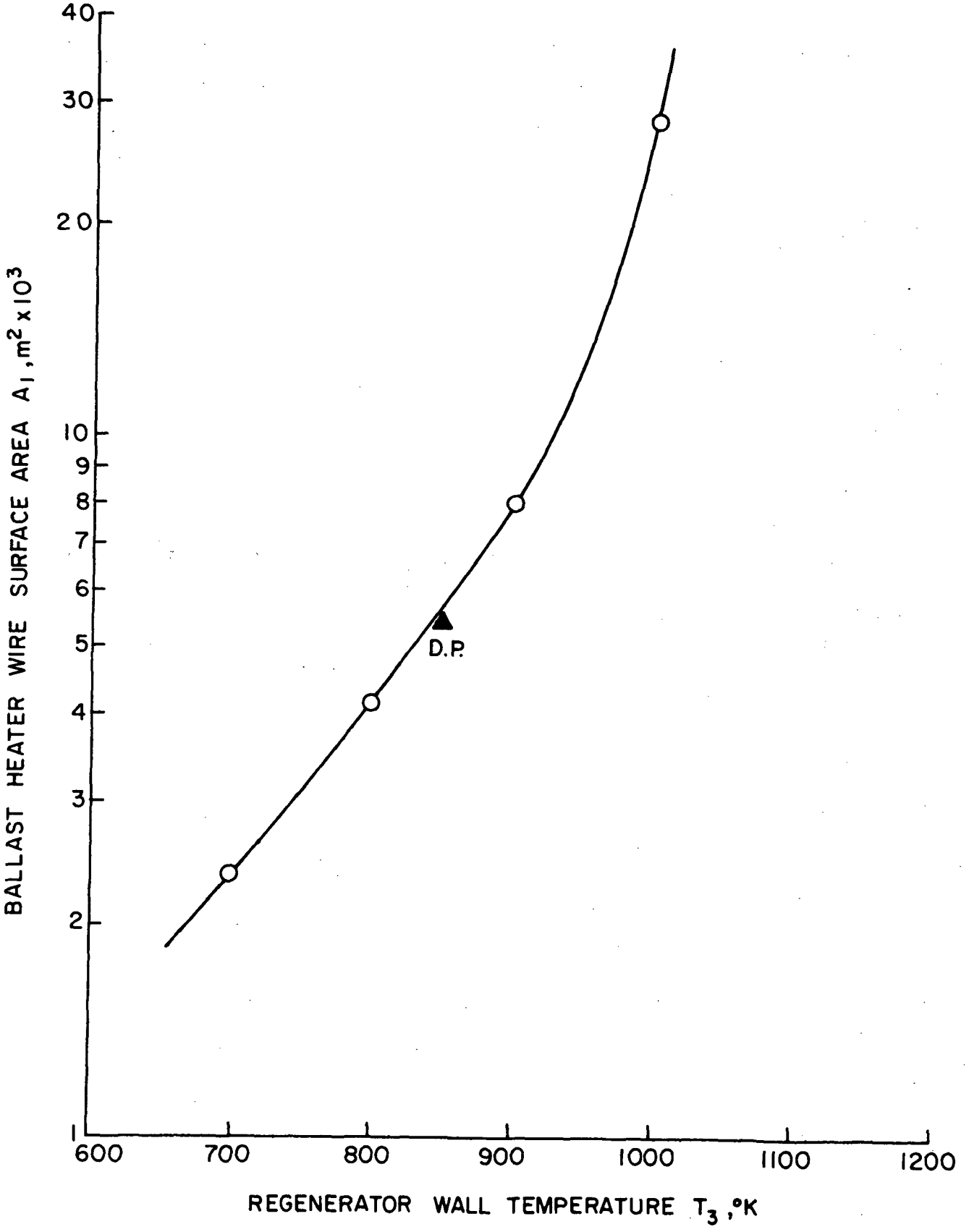

Figure 9.- Ballast resistor heater surface area as a function of regenerator wall temperature.

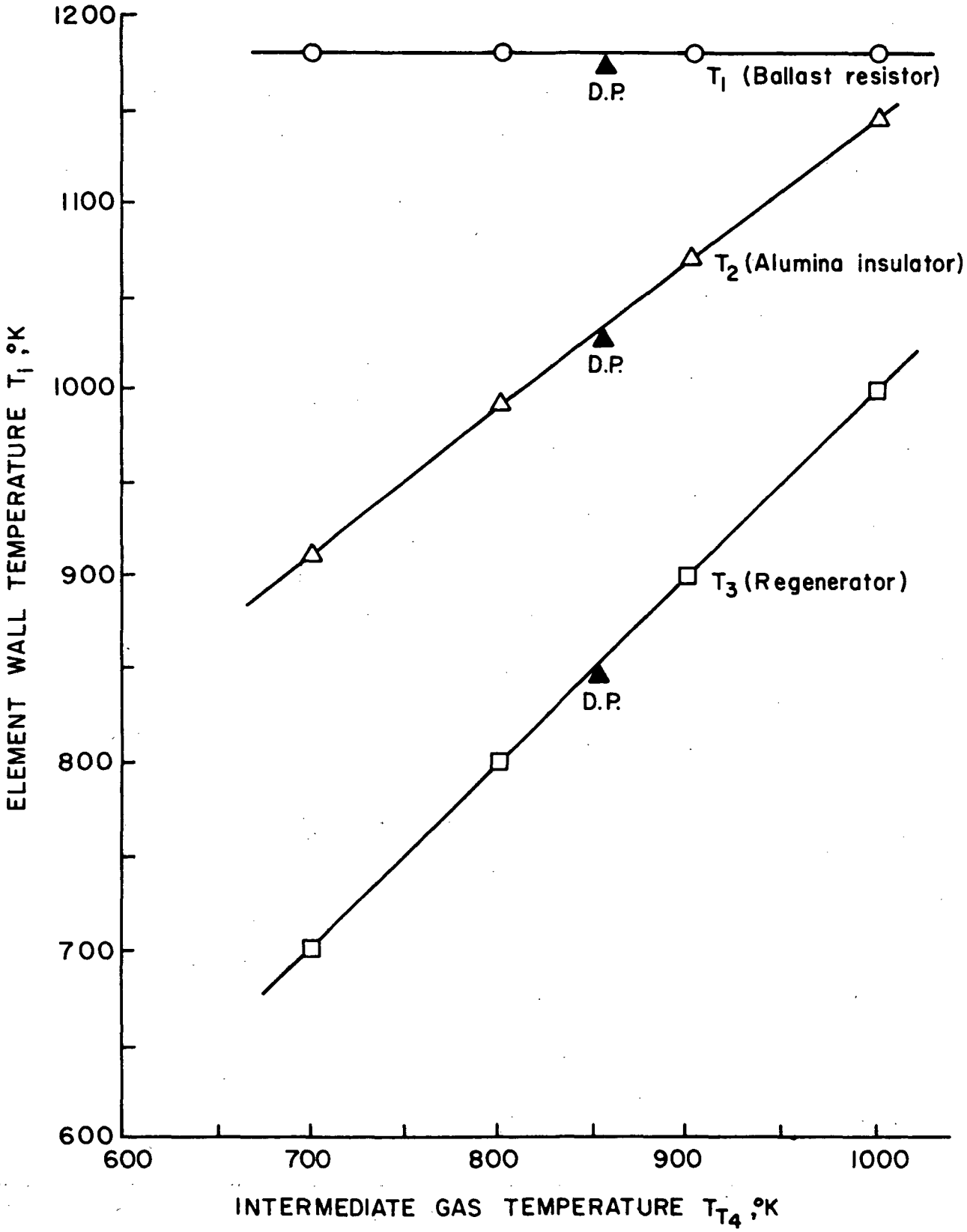

Figure 10.- Regenerator zone wall temperatures as functions of intermediate gas temperature.

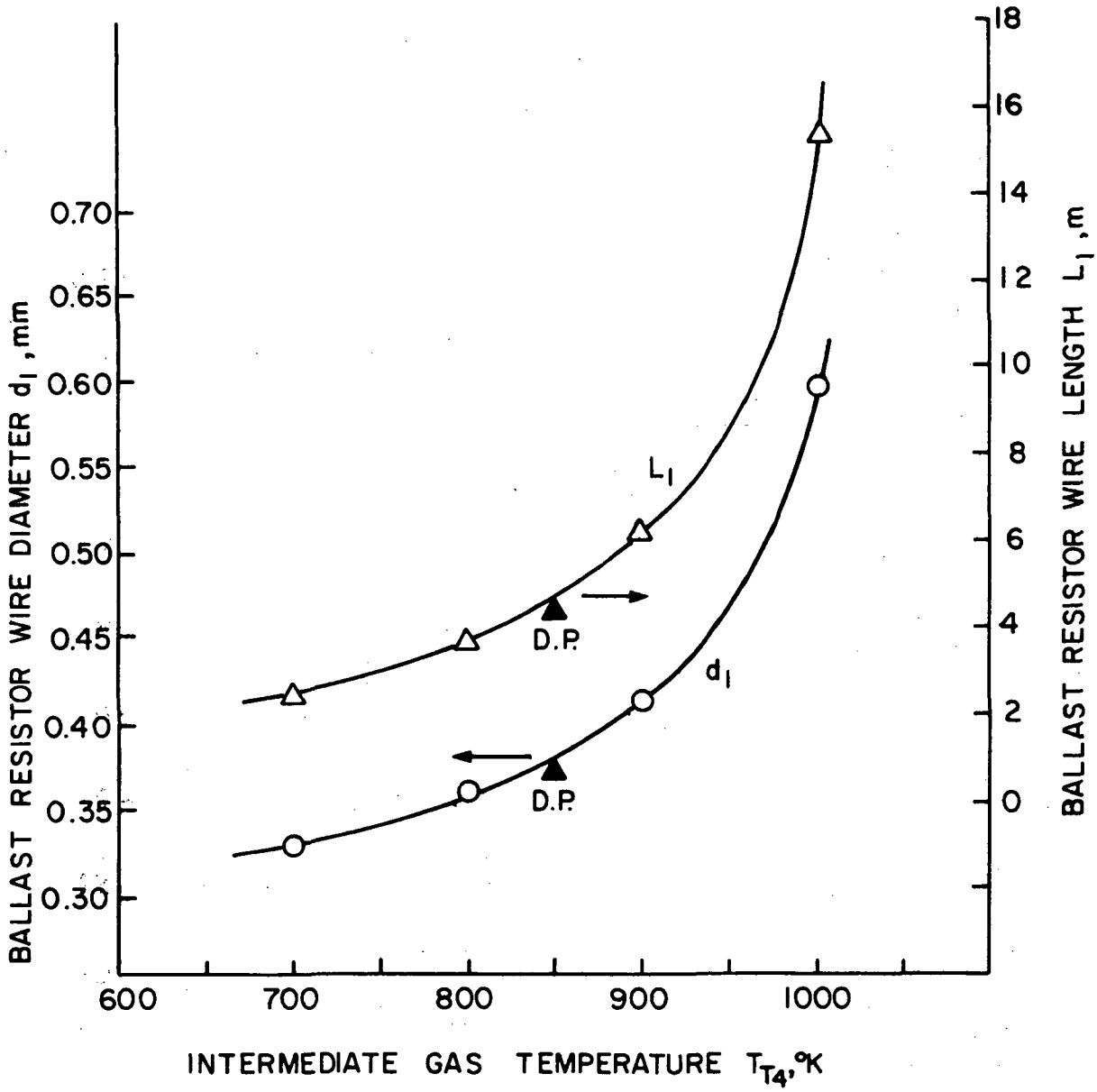

Figure 11.- Ballast resistor wire diameter and wire length as a function of intermediate gas temperature.

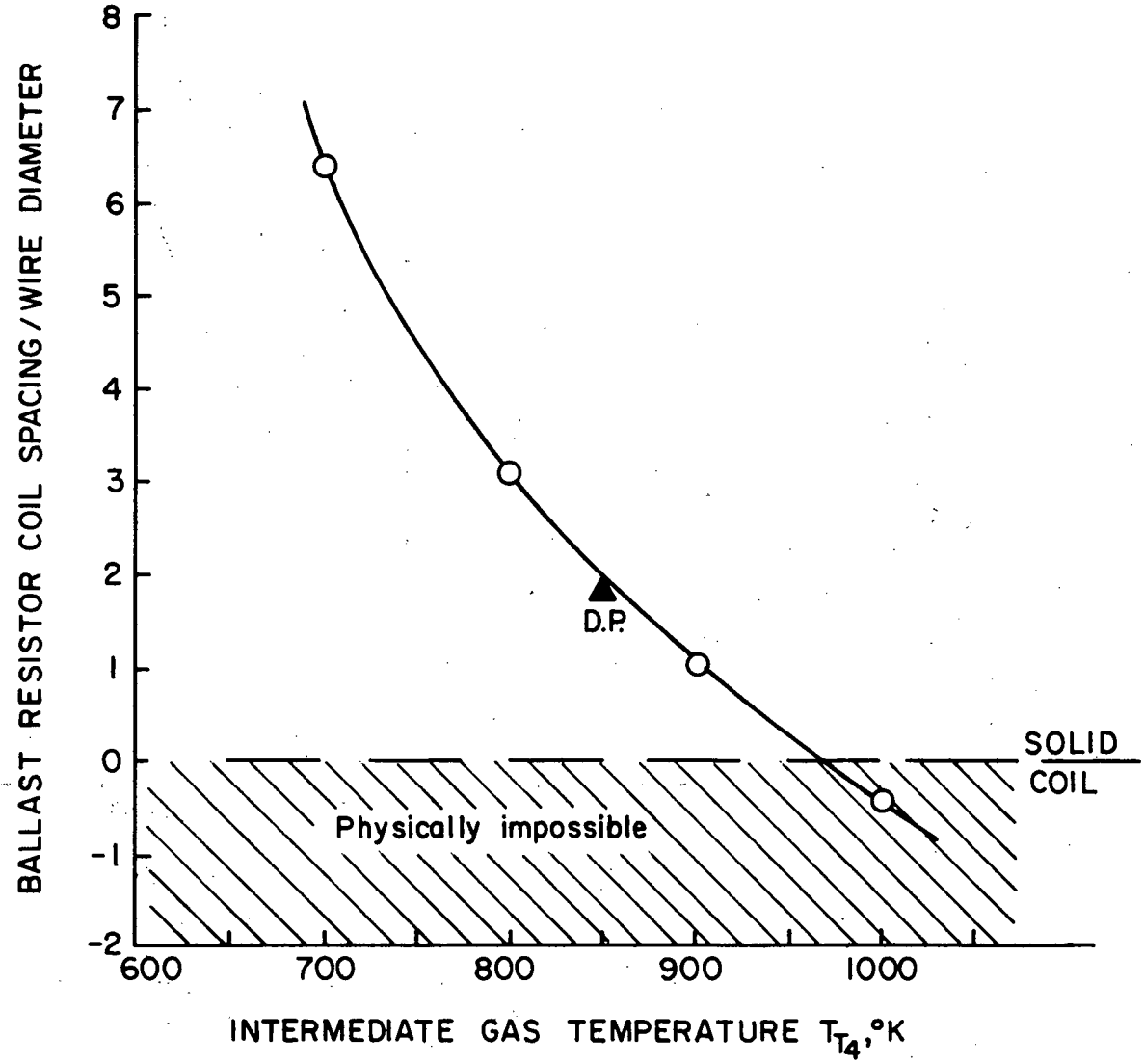

Figure 12.- Ballast resistor coil spacing/wire diameter ratio as a function of intermediate gas temperature.

From figure 7 it can be seen that the ballast resistor dissipates 22% of the total power input (excluding the H_2O evaporator power) at the selected design point, a condition which should result in more than adequate current stability over the full operating range of the ceramic heater. From figure 11 it is found that the ballast heater wire diameter for the design condition is 15 mils (0.381 mm), a suitable size for forming a heater coil from Pt-20Rh wire. From the same figure it is found that the required wire length is 4.70 m, also a suitable value. It should be noted in Figure 11 how rapidly the required wire length increases when the intermediate gas temperature is increased above about 925°K, thereby creating the space limitation problem which shows up clearly in Figure 12 as a coil which does not fit within the available space.

Thermal design for the start-up condition: The analysis and design computations for the thrustor start-up condition involved two parts:

(1) A pseudo steady-state thermal analysis made for the purpose of defining the dimensions of a Pt-20 Rh wire starter heater required to bring the ceramic heater up to ignition temperature in order to start the thrustor, and

(2) A transient thermal analysis made for the purpose of estimating the time required to start the thrustor and bring it to a steady state cruise condition.

In calculating the dimensions of the starter heater (Item 1 above), the starting configurations shown schematically in Figures 2 and 3 was used; that is, the start-up power was applied across the ballast resistor and starter heater in series, with the ceramic heater switched out of the circuit. Thus, starting is actually accomplished with both coils operating in series, not with just the starter coil alone. Physically, the two coils are installed side by side in a two-start set of spiral channels in the alumina coil support insulator, with the coils connected together at one end.

Since the same starting current flows through both coils, and since they are both made of Pt-20 Rh wire, with the same operating temperature limits, it is clearly logical that they should be the same wire diameter, that is, 15 mils (0.381 mm), the previously calculated diameter of the ballast resistor wire. The maximum allowable temperature for both wire coils was set at 1300°K for the short duration starting operation, compared with the 1180°K temperature which was previously specified for the ballast coil for long duration cruise conditions. Both temperature levels were based on evaporation data for the Pt-20 Rh alloy, and were specified in such a way as to limit the total amount of evaporation from the coils to tolerable levels over the full projected life of the thrustor.

In a first attempt at calculating the required length of the starter heater wire it was assumed that the full line voltage (~120 V.a.c.) was applied across the two coils in series. It was quickly found that, for that assumption, the required length of the starter heater was too great (about 20 m. wire length), and the coil could not be fitted into the available space even when solidly compressed. The assumption of full line voltage was then abandoned in favor of using a reduced voltage for starting.

In the second set of calculations, it was assumed that the starter heater coil is physically identical to the ballast resistor coil, with a wire length of 4.70 m, since a wire of that length forms a coil which fits almost perfectly in the available space. Assuming that configuration (i.e., two identical 4.70 m wire coils in series), the starting voltage required to heat the coils to 1300°K wire temperature in the regenerator zone was calculated and was found to be 44.4 volts. The method of analysis used (references 30 through 33) was that of radiative interchange between three isothermal surfaces; it was essentially identical to the analysis discussed earlier and described in detail in the Appendix for the radiative interchange in the regenerator zone for the cruise condition.

The primary mode by which the POC thrustor is started involves turning on the thrustor electrically to preheat the thrustor structure prior to commanding propellant flow. An alternate mode also being considered is as follows: Starting power is applied to the starter heater and ballast resistor in series, causing them to heat to 1300°K; heat is transferred radiatively from the heater coils to the regenerator walls (with the alumina insulator serving as an intermediate radiative surface); heat is transferred convectively from the regenerator walls to a reduced flow of propellant, heating the propellant to 1150°K; the heated propellant then convectively heats the cold ceramic heater, bringing the wall temperature up to about 1100°K; when the ceramic reaches the 1000-1100°K range of wall temperatures, it begins conducting; and the start of conduction in the ceramic causes the starting control to switch from the starting to the cruise mode, thus allowing the ceramic to heat itself up to the 1850-1900°K operating temperature.

In order for this process to work properly, it is necessary to limit the propellant flow rate during starting to a value which will permit the reduced input power for starting to heat the propellant in the regenerator to an exit temperature of approximately 1150°K. In addition, the regenerator must be sized so that the propellant exit temperature is within a few degrees of the maximum wall temperature.

For the selected two-coil configuration, with its associated resistance of 36.3Ω, and the calculated starting voltage of 44.4 volts, the power dissipated in the two coils in series during starting is

$$Q_1 = \frac{E^2}{R} = \frac{(44.4)^2}{36.3} = 54.3 \text{ W.} \tag{4}$$

An upper limit on the allowable propellant flow rate during starting can be computed by temporarily assuming that all of the thermal power from the coils is transferred through the regenerator into the propellant (steam) to heat it to an exit temperature of 1150°K. On that basis, the upper limit on the starting flow rate is

$$\dot{m} = \frac{Q_1}{h_3 - h_2} = 3.46 \times 10^{-2} \text{ g/s} \tag{5}$$

where $h_3 - h_2 = 15.69 \times 10^2$ W-s/g is the enthalpy rise of steam when heated from $T_{T2} = 417°K$ to $T_{T3} = 1150°K$.

The propellant flow rate during starting should actually be limited to about 3.0×10^{-2} g/s to allow for heat leakage from the coils via other paths. Regulation of the propellant flow rate during starting would be accomplished by a flow-limiting device of one of the types described in reference 60.

For a regenerator tube inside diameter of 0.125 in. (3.05 mm.), the length of the tube required to convectively heat the propellant to within 5°K degrees of the wall temperature was computed for both the starting and the cruise conditions. The calculations were based on laminar flow in a tube with constant wall temperature (reference 39), a consequence of the original one-dimensional assumption. The results were

	Starting	Cruise
Minimum regenerator tube length, m	0.508	0.865

In this case the cruise condition was controlling, and the regenerator tube length was set at 0.865 m. = 865 mm.

An order-of-magnitude analysis was made to determine the time required to heat the ceramic heater up to ignition temperature by using the previously described reduced flow of heated propellant as the heat transfer mechanism. The methods and charts of reference 34 were used to approximate a solution to this transient problem. It was found that the ceramic element could be convectively heated to ignition temperature in about 12 seconds after propellant flow is started, provided that the regenerator is heated to operating temperature before starting the flow. A more thorough and accurate analysis of this transient problem is planned for the following phase.

Summary of calculated POC thrustor dimensions: The methods by which the thermally-determined design dimensions and operating temperatures of the POC thrustor were computed and selected have been outlined in the preceding paragraphs. All of those results were summarized in table VI for use in the mechanical design phase of the program, as described in a following section of the report.

Analyses of stability, temperature distribution, and other thermal/gas-dynamic problems.- In the preceding section on the preliminary thermal analysis of the thrustor a one-dimensional radial heat flow model of the thrustor was employed in the analysis; that is, it was assumed that there was no axial variation in the temperature of any of the solid elements of the thrustor. That type of model is generally adequate for the initial analysis and design of a complete resistojet thrustor. There are, however, certain design problems for which the one-dimensional radial heat flow model does not produce adequate or useful results. Some of those problems and methods for their solution are discussed in this section.

Stability considerations for the multiple-passage ceramic heater: An ohmically-heated multiple-passage ceramic heater, with a laminar flow of gas through parallel passages, has the potential for developing unstable operating modes for any one of several reasons if proper care is not exercised in the design of the thrustor. The potential for unstable operation of the ceramic

Table VI

DESIGN DIMENSIONS, MATERIALS AND MAXIMUM OPERATING TEMPERATURES OF KEY ELEMENTS OF THE POC THRUSTOR

Calculated results of thermal analysis
(subject to modification during mechanical design)

Dimensions	Material	Max. Operating Temp. °K	
		Starting	Cruise
Ceramic heater element			
Active length . . . . . 46.0 mm Outer diameter. . . . . 4.1 mm No. of passages . . . . . 6 Diameter of passages. . . 0.71 mm	Yttria-stabilized zirconia	--	1860
Ballast resistor heater coil			
Wire length . . . . . 4700 mm Wire diameter . . . . . 0.38 mm Coil diameter . . . . . 2.67 mm No. of turns. 560	Platinum-20% rhodium alloy	1300	1180
Starter heater coil			
Wire length . . . . . 4700 mm Wire diameter . . . . . 0.38 mm Coil diameter . . . . . 2.67 mm No. of turns. 560	Platinum-20% rhodium alloy	1300	<1000
Coil support insulator			
Outside diameter. . . . . 30.5 mm Inside diameter . . . . . 16.0 mm Axial length ("active" grooved section). . . . 71.0 mm	96% Alumina	1240	1030
Regenerator Coil			
Tube inside diameter. . . 3.05 mm Tube length . . . . . 865 mm Coil pitch diameter . . . 45.0 mm No. of coil turns . . . . 6 Coil pitch. . . . . 10.9 mm Axial length of coil. . . 71.0 mm	Platinum-20% rhodium alloy	1160	855
Regenerator coil support cylinder			
Cylinder inside diameter.. 49 mm Wall thickness. . . . . 0.75 mm	TD nickel	1160	855

heater basically arises from the fact that conducting ceramics have negative electrical resistance characteristics; that is, their resistivity decreases with increasing temperature, opposite to the characteristic of metals. Because of this, geometry limitations exist beyond which thermal instabilities could possibly occur. For example, for a too large a diameter - too thin a tube wall - hot spots in the form of stria could theoretically form. If that should occur, the ceramic would become more conductive along the stria and could locally overheat to destruction.

In addition to negative resistance characteristic as a potential source of instability, there is a potential flow instability which can occur under certain circumstances when there is heat addition to a laminar flow of gas in parallel passages between inlet and outlet plenum chambers. This type of instability has been a matter of some concern in nuclear rocket engines, and is discussed in reference 40, for example.

Thus, the question of stability of operation of the ceramic heater is a multi-faceted problem in which one must consider all possible sources of instability and any possible interactions between sources. For example, it is conceivable that if laminar flow instability were to occur, it might possibly be capable of inducing localized current instability, or striation, in the conducting ceramic, because of variations of conductive heat transfer rate (cooling) from one passage to another.

It would be theoretically possible to develop a comprehensive analytical model of the ceramic heater, one which would take into account and balance all possible energy flow paths simultaneously, permitting a determination of the transient behavior of the heater. If such a comprehensive model were available, it would be possible to determine with reasonable certainty whether or not the heater would be unconditionally stable under all possible operating conditions. However, such a model would be very complex, since it would have to incorporate provisions for treating all of the following energy transfer mechanisms, and their mutual interactions, simultaneously:

(1) Three-dimensional time-dependent heat conduction in a non-analytic geometric shape, with time- and space-dependent temperature distribution, thermal conductivity, and internal heat generation.

(2) Three-dimensional time-dependent electrical current conduction in a non-analytic geometric shape, with a time- and space-dependent temperature distribution and a negative temperature coefficient of electrical conductivity.

(3) Three-dimensional thermal radiation heat transfer within each of six parallel passages through a radiatively participating gas, with time- and space-dependent wall temperatures and material thermal properties.

(4) Three-dimensional thermal radiation heat transfer between the exterior cylindrical surface of the heater and its insulation surroundings, with time- and space-dependent wall temperatures and material thermal properties.

(5) One-dimensional time-dependent laminar flow of a compressible fluid in six parallel capillary passages, with friction and heat addition.

(6) Two-dimensional convective and radiative heat transfer between a radiatively participating gas and the walls of heater passages, with time- and space-dependent wall temperatures and flow velocities.

While it is obvious that not all of the above listed factors would be of equal importance in determining the operating stability of the heater, it is also apparent that a comprehensive analysis of the complete problem would be a very difficult undertaking, since it would involve solution of a set of simultaneous non-linear partial differential equations in three-dimensional space. Computer-based numerical methods would be required because of the non-analytic cross-sectional shape of the conducting solid, and the probable intractability of the equations in any event. Caution would have to be exercised in making any simplifying assumptions because the question of stability hinges to a great extent on the influences of the kinds of second-order effects which are usually simplified out of an analytical model.

For this phase it was only feasible to consider isolated parts of the overall problem. It is a necessary, but not sufficient, condition for proof of overall stability to prove that some of the various individual sources of potential instability are not actually destabilizing in this specific situation. That has been accomplished to some extent in this phase, as exemplified in the following paragraphs.

The sub-problem of gross stability of the electric current in the conducting ceramic is dealt with elsewhere in this report, where it is shown that the use of a metallic ballast resistor (positive resistance) in series with the conducting ceramic makes the ohmically-heated system stable on a gross basis, provided that about 15% or more of the total power is dissipated in the ballast resistor. The use of the ballast resistor does not in itself, however, ensure localized stability (absence of current striation) within the ceramic body. That type of localized stability remains to be fully demonstrated, either analytically or experimentally, in the next phase of the program. Thus far in the experimental part of this program there has been no evidence to suggest that any such instabilities actually exist; all available evidence is to the contrary.

The sub-problem of the stability of the laminar compressible flow with friction and heat addition in parallel passages with equal pressure drops (the so-called nuclear rocket problem) has been investigated in this phase. Flow stability of this type is also a necessary, but not sufficient, condition for overall stability. The methods of reference 40 (pp. 142-148) were used in the analysis of this sub-problem. In that reference a criterion for flow stability in a parallel-path laminar flow system is derived; the stability criterion is (in the notation of the reference)

$$(1 + \overline{T})^{n+1} (2 - n\overline{T}) > 2 \qquad (6)$$

where

$\overline{T} = \frac{T_{out}}{T_{in}}$ = absolute temperature ratio across heater

n = temperature exponent of viscosity of propellant gas at mean temperature, defined by $\frac{\mu_{m+a}}{\mu_{m-a}} = \left(\frac{T_{m+a}}{T_{m-a}}\right)^n$

This type of flow stability problem can be thought of as one arising from the negative flow resistance characteristics of such a system under certain combinations of conditions. The stability criterion depends only on the temperature exponent of viscosity of the propellant gas in question and the temperature ratio across the heater. Since the propellant gases are specified, thereby fixing the values of n, the flow stability criterion for the ceramic heater can be expressed in terms of a maximum permissible temperature ratio $\overline{T}$ for each propellant. The following results were obtained:

Propellant	CO_2	Steam	H_2 (ref.)
n (at T_m)	0.46	0.69	0.50
$\overline{T}_{max} = (T_{out}/T_{in})_{max}$	3.92	2.56	3.60

For the ceramic heater in the POC thrustor the value of the actual $\overline{T}$ is given by

$$\overline{T}_{act} = \frac{T_{T_7}}{T_{T_4}} = \frac{1800}{850} = 2.118 \qquad (7)$$

Thus, it is seen that one potential source of instability in the ceramic heater, the parallel-path laminar-flow-with-heat-addition source, is not operative in this thrustor, since both of the biopropellants exhibit an adequate stability margin, that is, $\overline{T}_a < \overline{T}_{max}$ for both CO_2 and steam. One more necessary, but not sufficient, condition for complete heater stability has been demonstrated.

Temperature distribution along gas flow path: In the Preliminary Thermal Analysis section, axial variations in temperatures of components were necessarily neglected in favor of the one-dimensional heat transfer analysis, in the interest of calculating initial component design dimensions as early as possible. However, it was found during the stability investigation that some knowledge was needed of the axial distribution of wall and gas temperatures along the ceramic heater.

If the possibility of asymmetric temperature distributions in the ceramic resulting from striation of the current is temporarily neglected, and if the configuration is simplified for analysis to that of a central passage surrounded by a cylindrical ceramic tube equal in solid cross-sectional area to 1/6 of the area of the actual 6-passage heater, one can set up a simplified two-dimensional analytical model of the principal energy transfer mechanism within the heater, involving two-dimensional thermal conduction, internal heat generation, and convective heating of the flowing propellant, in order to accurately solve for the axial distributions of gas and ceramic temperatures. A finite difference numerical analysis technique for solving this problem is described in reference 35, and similar or related techniques are discussed in references 37 and 38.

Finite difference calculations were made to estimate the temperature distributions in the POC thrustor ceramic heater. The results of these calculations have been combined with simple estimates of the axial temperature distributions in the regenerator, and all of those results have been plotted as an overall estimate of temperature distributions along the gas path, in figure 13. Figure 13(a) shows the estimated temperature distribution which occurs near the end of the starting cycle, just before ignition of the ceramic; figure 13(b) shows the estimated temperature distribution which occurs during the steady-state cruise condition. (It should be noted in figure 13 that the gas path axis does not represent a uniform distance scale; the part of the path which represents the ceramic heater has been expanded on the gas path axis for clarity.)

Calculated flow velocities and pressure drops in the ceramic heater and regenerator passages: It was necessary to calculate the variations in exit Mach number from the ceramic heater capillary passages as a function of operating parameters (total mass flow rate and exit temperature) in order to determine whether the choked flow condition is approached at any time in either the operation of the complete thrustor or in component tests on the ceramic heater assembly. The calculated value of the heater passage exit Mach number for the POC thrustor was found to be $M_e = 0.17$ for the design flow rate of 0.06 g/s of CO_2, and the Mach number did not exceed 0.20 in any of the component tests run during the program. Thus, the flow in the heater passages did not approach the choking condition.

The propellant pressure losses in the regenerator and in the ceramic heater were calculated in order to determine the required supply pressure for a given chamber pressure, and also to determine the axial and radial pressure loadings on the ceramic heater for mechanical design purposes. Analytically, the problem is one of calculating stagnation and static pressure changes in pipe flow with combined friction and heat transfer (plus the tube curvature effect in the regenerator). As pointed out on pp. 414-417 of reference 41, this problem cannot be solved exactly in closed form, but it can be solved approximately by iterative techniques if (1) either a constant wall temperature or a constant heat flux can be assumed, and (2) the Mach number in the passages is less than about 0.3. Since both of those conditions can be satisfied for the purposes of the initial thrustor design, the outlet

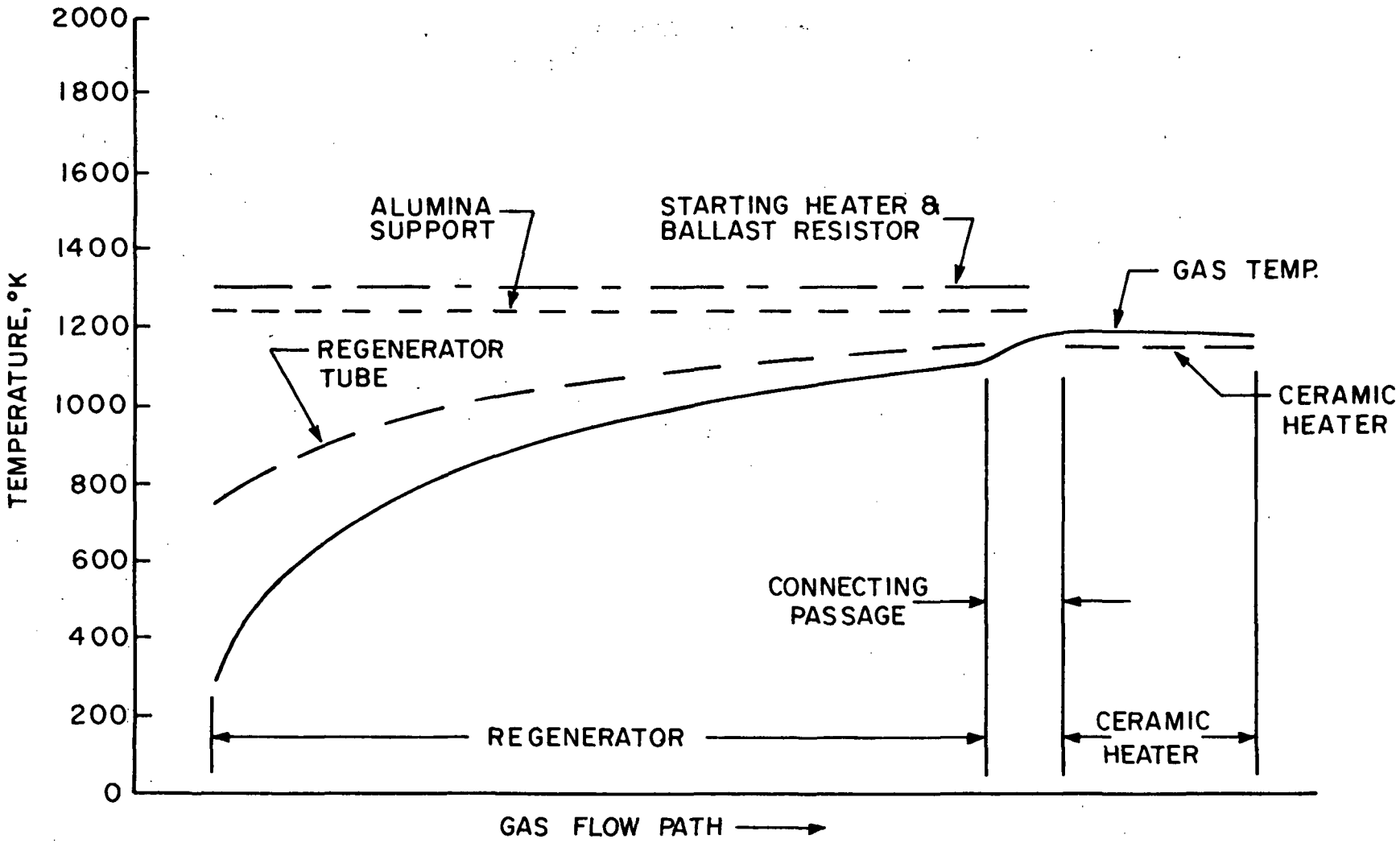

(a) Starting condition

Figure 13.- Estimated temperature variations along gas path

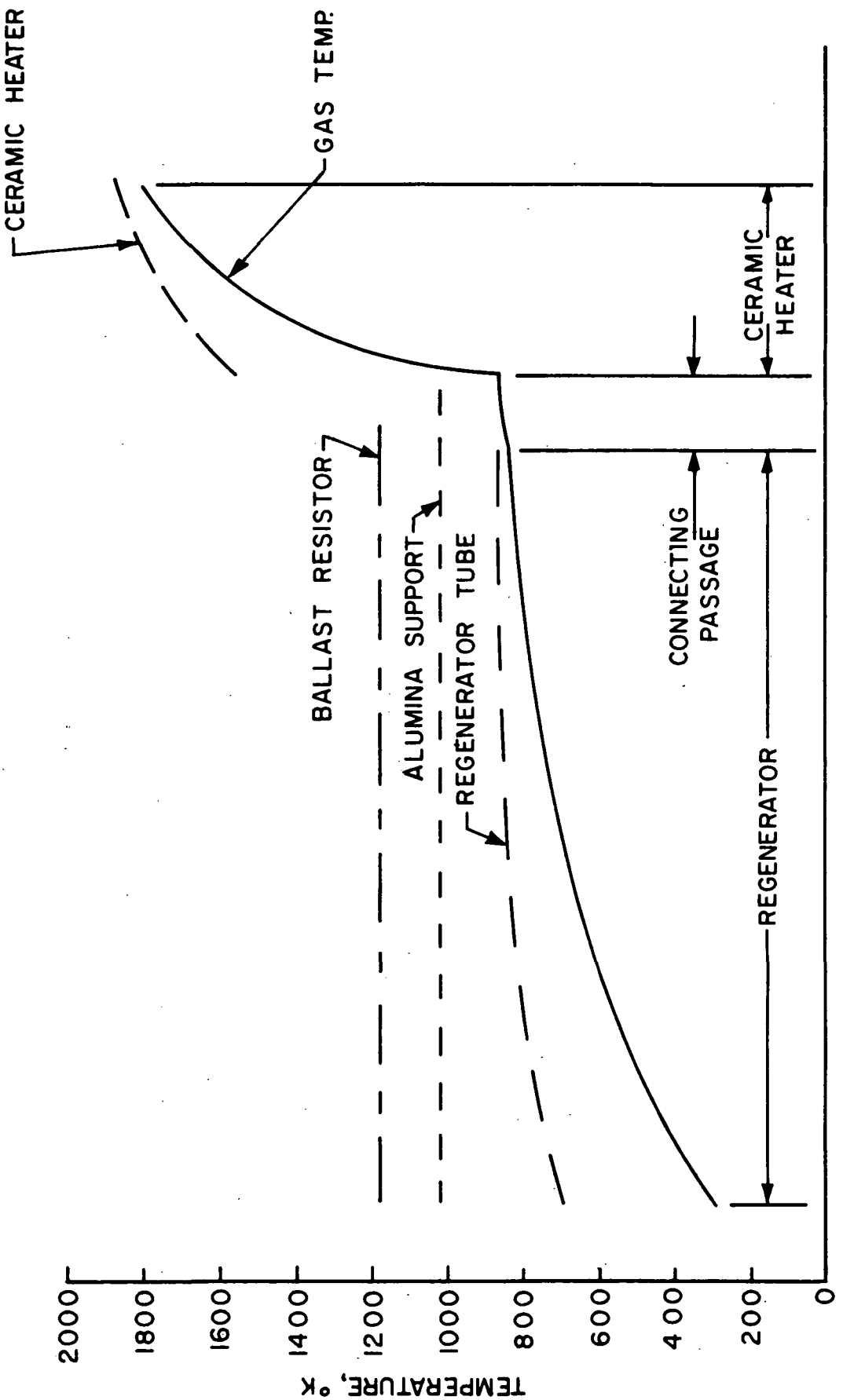

(b) Cruise condition

Figure 13.- Concluded

to inlet stagnation pressure ratio through each of the two components can be computed from equation [9.61]* of reference 41, which is (in the notation of the reference)

$$\left(\frac{P_{02}}{P_{01}}\right)^2 = 1 - \left(\frac{k}{2}\right) M_1^2 \left[1 + \left(\frac{P_{02}}{P_{01}}\right)^2 \left(\frac{T_{01}}{T_{02}}\right) \left(\frac{M_2}{M_1}\right)^2\right] \times \left\{\left[f\left(\frac{L_2}{D}\right)\right]\left(\frac{T_w}{T_{01}}\right) + \left(\frac{T_w}{T_{01}} - 1\right)\left(e^{-fL_2/2D} - 1\right)\right\} \qquad (8)$$

For calculating pressure loading on the ceramic heater, the inlet static pressure can be taken as approximately equal to P_{01}, while the exit static pressure can be taken as the static pressure at station 2, calculated from P_{02} and M_2 by the isentropic relationships. The friction factor f is an average value for laminar flow calculated from

$$f = \frac{64}{(Re)_{avg}} \qquad (9)$$

Detailed stagnation pressure loss and static pressure loading computations, based on iterative solutions of equation (8), have not yet been completed for the POC thrustor. Interim pressure loss calculations were made for the initial mechanical design, using a simple pipe flow equation based on frictional effects only, with the friction factor for the laminar flow defined by equation (9). These calculations provided the following calculated pressure losses:

Propellant	CO_2	Steam
Regenerator pr. loss, kN/m^2	--	1.7
Ceramic heater pr. loss, kN/m^2	29	49

These results of simplified calculations are somewhat non-conservative, and that fact was taken into account in the design.

*A more accurate result could be expected by averaging the values calculated from equations [9.61] and [9.66] of reference 41.

Mechanical Design

Ceramic heater materials.- The design of the thrustor presented here began with a previous program (NAS1-10353, reference 20) in which a large number of high temperature materials were surveyed to determine the best candidates for use in advanced biowaste resistojet heat exchangers.

The following criteria were applied in the screening of materials. The first two alone leave less than ten potential candidates, excluding composites, out of more than 100 high temperature materials originally considered.

(1) The material should melt above 2500°K. The material should also be chemically stable to this temperature and not undergo any crystal structure changes.

(2) The material should resist oxidation in flowing biowaste gases to a temperature of at least 2100°K.

(3) Electrical resistivity should be of the order of 10^{-6} to 10^{-2} ohm-m in the temperature region of interest, or a concept must be possible employing an auxiliary heater.

(4) No reaction, or at least only slight reactions to the extent of acceptable weight losses ($\sim 10^{-8}$kg/m^{2}s), should take place between the material and flowing gases of H_2O, CO_2, CH_4, H_2, NH_3 and other species, such as CO, N_2 and some free radicals in very low concentrations.

Neither detrimental reactions nor formation of eutectics with solid carbon should take place. Solid carbon deposits would be expected largely from decomposition of CH_4 and partly from decomposition of CO_2.

(5) The material should resist surface evaporation losses (corresponding to surface recession rates of 10^{-10}m/s) in flowing gases to 2100°K and in vacuum to 1800°K.

(6) The material should have an acceptable high temperature endurance strength of at least 100 kN/m^2 (15 psi) and have minimal creep behavior in 10^4 hours.

(7) The material should have a high thermal stress/thermal shock resistance which takes into account thermal cycling conditions. High thermal conductivity, low thermal expansion, and relatively low Young's modulus are important in this respect.

(8) Joining capability to itself or other materials, such as the platinum metals, is important. This means a close match in linear thermal expansion.

(9) With regard to availability, if the material is not available in desired shapes commercially, sufficient data on its high temperature properties should be known, and fabrication technology for the development of suitable shapes should be a state-of-the-art at least on related materials. If new materials not available nor easily fabricated offer promise based upon the other criteria, a materials research and development effort, whose primary objective would be to establish feasibility for resistojet application should be identifiable.

(10) Because of the small quantity of material involved, material costs of up to $10,000 per kilogram are allowed if the properties warrant further consideration.

Table VII summarizes the materials surveyed and gives the primary basis for decision. As shown in the table, six candidates passed the above tests. Of these, stabilized ZrO_2, ThO_2, and ZrB_2 with additives were selected for further study and experimental evaluation. ZrB_2 was later abandoned for several reasons, the most important being its relatively low resistance to propellant attack and its poorer electrical properties compared to the oxides. The properties of ZrO_2 and ThO_2 are discussed briefly below. A more detailed treatment can be found in reference 20.

In pure ZrO_2 a reversible monoclinic to tetragonal transformation at atmospheric pressure occurs at about 1425°K. The monoclinic-to-tetragonal inversion is accompanied by a 3.2% length reduction on heating and an associated length increase (at about 1275°K) on cooling (reference 42). Rapid cooling expansion occurs within a 10°K temperature interval and this would fragment (a phenomenon called ratcheting) a part made of pure ZrO_2. To permit its use in solid parts usable at high temperature, ZrO_2 must be stabilized by adding cubic oxides with cations of similar radius to Zr^{4+}. Such mixtures convert ZrO_2 irreversibly to the cubic form when heated beyond 1825°K. Many oxides have been used for stabilization, but the most commonly used are CaO, Y_2O_3, and MgO. MgO-stabilized zirconia partially reverts to the monoclinic form when cycled through the 1175-1625°K temperature zone (reference 42). The following discussion, is therefore, limited to the CaO and Y_2O_3 stabilized forms.

Zirconia is fully stabilized by the addition (typically) of 5 weight percent (10.4 mole percent) CaO or 15 weight percent (8.8 mole percent) Y_2O_3. Purity has an important effect on some of the thermophysical properties of zirconia. There are many impurities which can be found accompanying zirconia in its natural state or unintentionally added in processing in addition to those deliberately added for stabilizing crystalline structure, enhancing electrical conductivity, etc. For instance, comparing the two important stabilizers Y_2O_3 and CaO on the basis of full stabilization, zirconia stabilized with the former is more refractory than the latter, having a melting point approximately 100°K higher. Of the various impurities, Al_2O_3 has a strong influence on electrical conductivity, acting as a poison in percentages around 2%, an undesirable feature in conducting ceramic resistojets.

TABLE VII

RESULTS OF HIGH TEMPERATURE MATERIALS STUDY - SELECTION AND REJECTION

Material class	Materials with acceptable melting points [a]	Selection or primary basis for rejection
Elements	C, graphite, B	Oxidize <<2000°K
Refractory metals	W, Re, Ta, Os, Mo, Nb, Hf, Ru Ir	Oxidize <<2000°K Oxidation rate high
Carbides	HfC, TaC, NbC, Ta_2C, ZrC, TiC, WC, W_2C, UC, Al_4C_3, MoC, ThC_2, ThC, Mo_2C, SiC, CeC_2, B_4C, UC_2	Oxidize <2000°K
Nitrides	TaN, ZrN, TiN, BN, UN, ThN	Oxidize <<2000°K
Inter-metallics	$TaSi_2$, $MoSi_2$, Mo_3Si, Mo_5Si_3 NbSi, Nb_5Si_3, Ta_5Si_3, Ta_9Si_2 Ti_5Si_3, V_5Si_3, W_3Si_2 Zr_2Si, Zr_3Si_2, Zr_4Si_3, Zr_5Si_3 Zr_6Si_5, Cr-Al, Mo_3Al WSi_2 Re_3W_2 Ba_3P_2 CeS	Oxidize <2000°K Too brittle Little information available Too volatile
Oxides	ThO_2, HfO_2, ZrO_2, CaO UO_2 OsO_4, CeO_2 MgO BeO $ZrSiO_4$ (zircon) $SrZrO_3$, $BaZrO_3$ $Be_3Zr_2O_7$, $CaArO_3$	Acceptable Easily oxidized Too volatile Reacts with CO, H_2O at elevated temperature Volatilzes in H_2O at 1475°K Max. cont. service:1775-2050°K Little information available
Borides	HfB_2 + SiC and/or C ZrB_2 + SiC and/or C HfB_2, ZrB_2, WB, TiB_2, ThB_4 MoB, Mo_2B	Acceptable Acceptable Oxidize <2000°K

[a] Materials not listed have melting points below 2500°K or their melting points are not known.

One form of yttria-stabilized zirconia of great interest has been developed at the Air Force Materials Laboratory (reference 43). Extremely fine particle size zirconia powders, average size 50A, are produced by simultaneous thermal and hydrolytic decomposition of zirconium and yttrium alcoholates such as those of isopropyl alcohol. The vapor decomposition of the alkoxides to oxides produces purity in excess of 99.95%, a level hitherto not available from commercial sources. This high purity apparently has a definite bearing on the properties of the material. For example, while coarse grain grades of commercial zirconia have higher thermal shock resistance than fine grain grades, the finer grade has improved thermal properties (reference 44).

Cold pressing, followed by sintering at 1725°K of this powder, produced translucent, fully dense cylindrical and bar-shaped bodies with grain size 35-50μ (reference 43) and it is possible that yttria acts as a grain growth inhibitor in this case. It was possible to achieve full stabilization at a sintering temperature as low as 1075°K and with an yttria content of only 5 weight percent. Hot pressing might reduce forming temperature further.

A bar of this form of zirconia showed no change in an air atmosphere up to 2475°K for 262 hours with numerous cyclings. The material could be useful to 2775°K; the major limitation being loss of the stabilizer Y_2O_3 at the higher temperatures.

An example of the high purity is the hafnium content which is 0.5-2% in commercial grade and less than 0.05% in alkoxide-produced zirconia. Hafnia undergoes a monoclinic to tetragonal inversion at about 2000°K. A high purity form of stabilized zirconia might well be the best for resistojet applications.

Thoria, ThO_2, has the highest melting point of any oxide and is for that reason alone of considerable interest for high temperature applications. Its melting point is listed in the range of 3200-3600°K by various sources; the most probably figure is 3540°K according to volume 4 of reference 21. It is very inert in its chemical properties.

Thoria is stable under most conditions. It requires no stabilizers. Thoria, like stabilized zirconia, is an electrical conductor at elevated temperatures. The resistivities of these oxides are compared with those of other materials in figure 14. Their thermal expansion characteristics are compared with other materials in figure 15. Table VIII summarizes the important physical and mechanical properties of ThO_2 and ZrO_2.

The authors' experience in resistojet design has shown that the most important material property considerations are those that occur over long time periods (thousands of hours) to limit thrustor life. The study of reference 20 presents a detailed discussion of the following effects for many materials.

Physical-chemical considerations.- A number of physical-chemical interactions between the biowaste gases and the materials ZrO_2 and ThO_2 must be taken into account for resistojet design temperatures to about

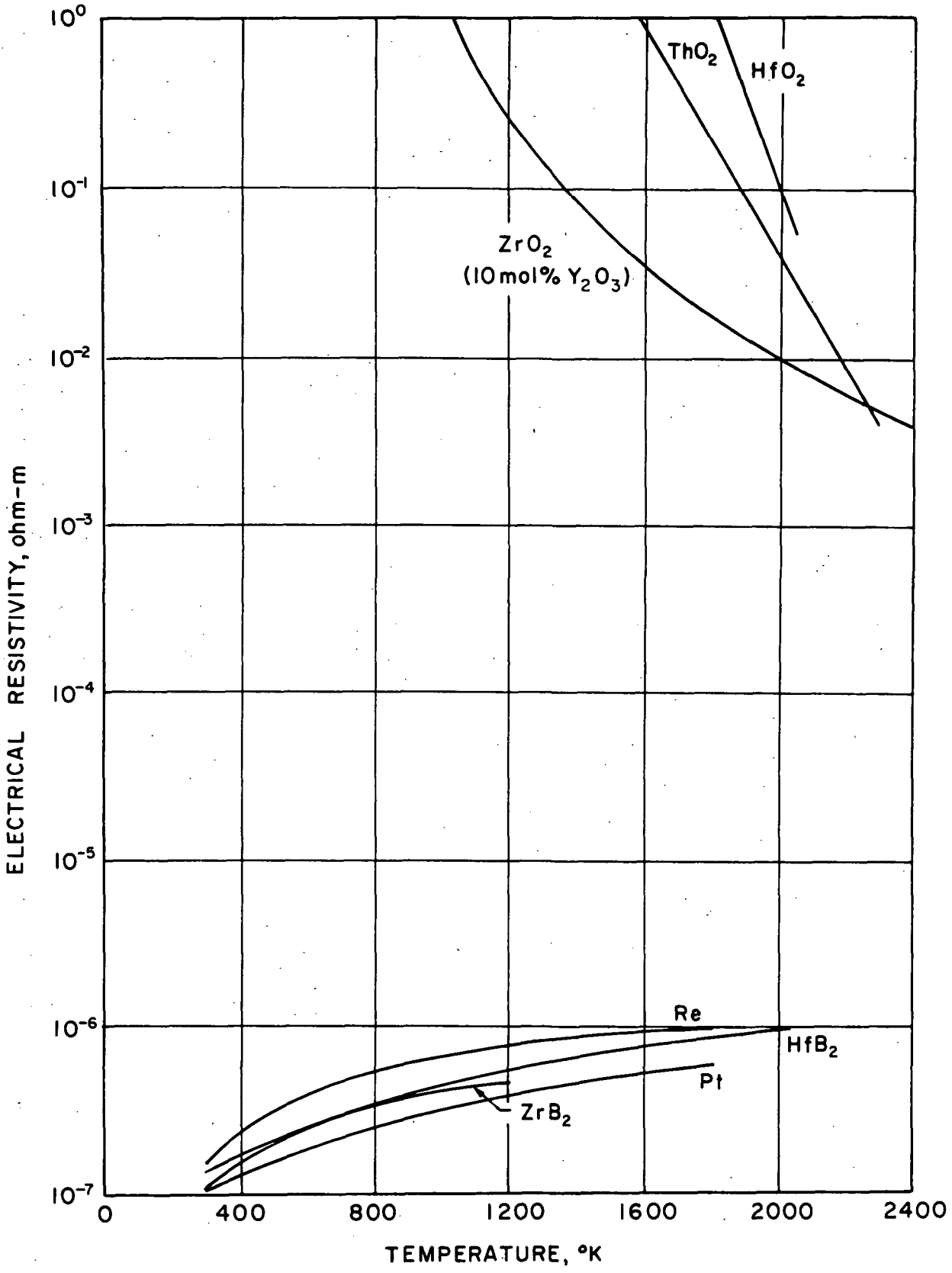

Figure 14.- Electrical resistivity of candidate materials compared with Re and Pt.

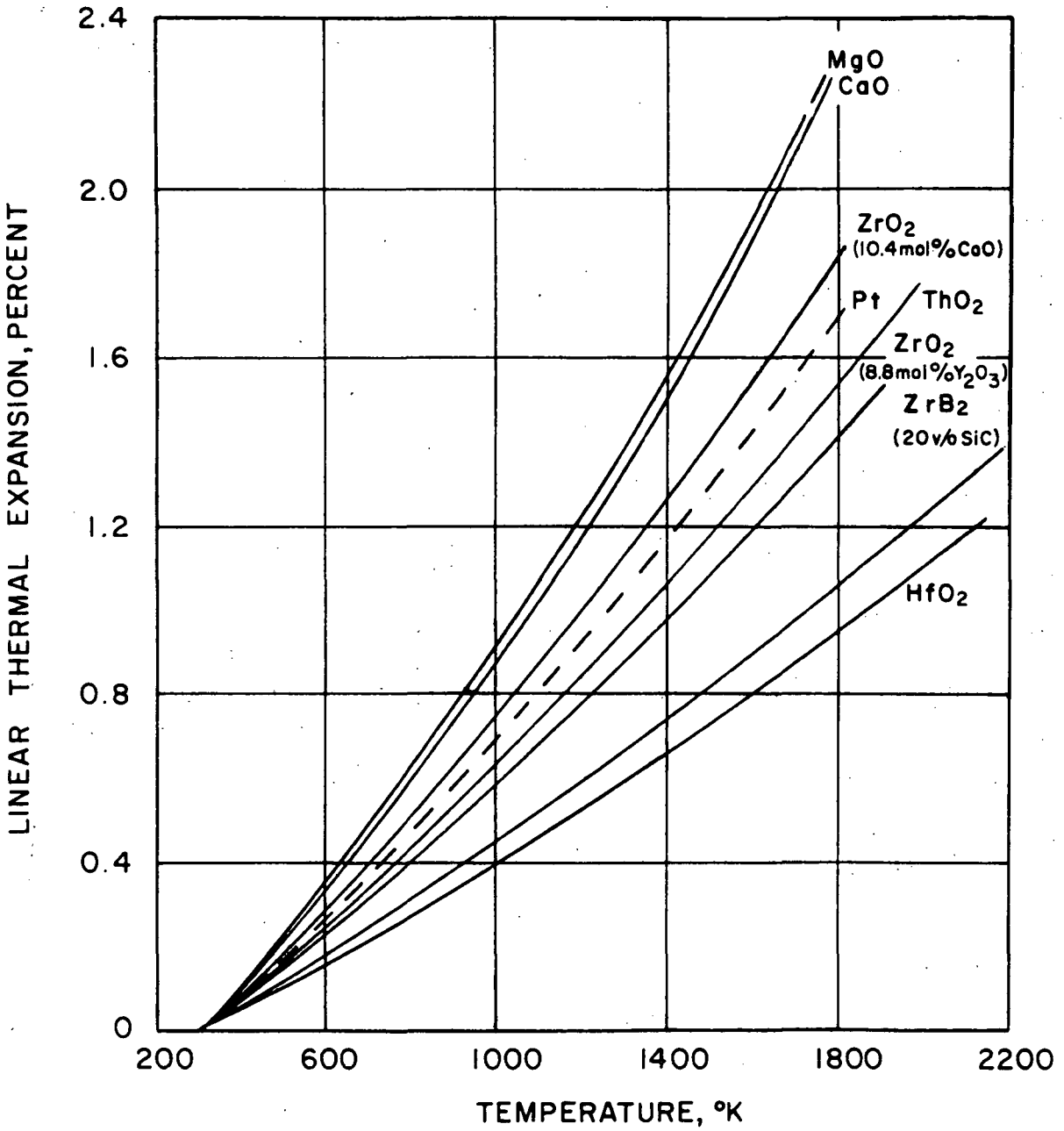

Figure 15- Linear thermal expansion of candidate materials compared with platinum.

TABLE VIII

PHYSICAL, THERMAL AND MECHANICAL

PROPERTIES OF CANDIDATE HIGH TEMPERATURE MATERIALS

Property	Thoria ThO_2	Zirconia ZrO_2	Platinum (for reference)
Additives	None	10 mole % Y_2O_3	None
Melting point, °K	3540	2998	2047
Specific gravity	9.86	5.60	21.45
Specific heat, J/kg °K			
@ 288°K	235	460	133
1200°K	304	670	158
2000°K	331	858	180
Thermal conductivity W/m °K			
373°K	11.3	1.76	70.3
1200°K	3.0	1.88	90.4
1600°K	2.5	2.00	108.8
2000°K	2.4	-	-
Thermal diffusivity, m^2/s			
1200°K	9.8×10^{-7}	4.9×10^{-7}	2.6×10^{-5}
2000°K	7.0×10^{-7}	-	-
Thermal linear expansion, % (298-1800°K)	1.54	1.42	1.68
Electrical resistivity, ρ, Ω-m			
298°K	-	-	1.05×10^{-7}
1200°K	4×10	2.5×10^{-1}	3.95×10^{-7}
1600°K	1	3×10^{-2}	4.95×10^{-7}
2000°K	4×10^{-2}	9×10^{-3}	-
Total normal emissivity, ε_n			
1200°K	0.29	0.4	0.12
1600°K	0.27	0.4	0.17
2000°K	0.30 - 0.55	0.5	-
Modulus of elasticity, $KN/m^2 \times 10^{-7}$			
298°K	14.6	(15.5)*	17.1
1200°K	12.4	(13.2)*	-
Estimated working stress (creep) 10,000 hrs @ 1800°K, kN/m^2	300	1000	Nil
Sublimation recession at 1800°K, kg/sm^2	1.7×10^{-8}	10^{-8}	5×10^{-7}

* 8.8 mole %

2000°K. The most important is high temperature chemical reaction and corrosion. Any reaction between a hot gas and resistojet material is, of course, detrimental to the operation of the resistojet. Any gaseous reaction products would result in mass change of the material, resulting in ultimate consumption of the material or that portion of it subject to reaction with time, to the point that the operating characteristics would change. Solid reaction products in the form of particles could be swept away by the flow of gasses and similarly result in mass losses or result in possible nozzle throat blockage should deposition of the reactants occur. The mass losses are a function of reaction rate kinetics and perhaps whether scales are formed through which gaseous reaction products must penetrate. The reaction rate kinetics between the ceramics and gas species in question are not well known and design criteria involving factors such as wall thickness requirements depend on the completion of an endurance-type experimental program. The stability of scales depends on their adherence to the tube wall. It is likely, however, that even scales would be eroded away by the high-velocity flowing gases, exposing the wall to new attack. Materials which form scales are to be avoided since subsequent spalling of scales presents a nozzle blockage problem.

It is well to bear in mind that reaction and corrosive attack of the tube wall is a strong function of temperature and, therefore, any mass loss, scale formation, etc., will vary locally along the tube. Increased partial pressure of the gas will also tend to increase reaction rate. Flow velocity is another parameter to consider. Increased axial flow velocity of the gas does not necessarily mean increased mass flow of gas to the surface. In fact, increased gas flow means less residence time and possible less likelihood for reaction. The erosive effect of the gas increases, however, with increased axial flow velocity. Design criteria, must therefore, be based on the situation at the critical (generally the hottest) section of the tube where the attack is most severe.

Preliminary test results indicate that stabilized zirconia is compatible with the biopropellants CO_2 and H_2O. These results are discussed in the COMPONENT TESTS section which follows. With respect to compatibility with these various propellants, ZrO_2 has been rated higher than ThO_2 on the basis of more information available in the literature; however, the literature recognizes ThO_2 to be chemically more stable than ZrO_2. From the data available, it appears reasonable to expect ZrO_2 and ThO_2 to be useful for extended periods at high temperature with the flowing biopropellants.

Sublimation.- The process of sublimation or evaporation of material from a surface can be an important factor in determining the service life of a device operating at high temperature. The surface recession rate is greatest in a vacuum; it can be suppressed by several orders of magnitude by adding an inert atmosphere.

The surface recession rate due to sublimation is determined from:

$$\overset{\circ}{\delta} = \frac{G}{\rho} \tag{10}$$

where $\dot{\delta}$ is the surface recession rate, m/s, G is the mass loss rate in Kg/m^2s, and ρ is the density. G may be determined from experimental data, or may be found from the vapor pressure.

$$G = \frac{P_v}{\sqrt{2\pi RT/M}} \tag{11}$$

The recession rates for ZrO_2, ThO_2, Pt, Ir and Re in a vacuum are given in figure 16. Platinum and iridium were used extensively in earlier biowaste resistojets (reference 45). Rhenium was used for resistojets using H_2 and NH_3 propellants and life tested at high temperature for 8000 hours (reference 46).

Under conditions of a flowing gas the recession rate is influenced by the properties of the gas and its pressure and velocity. Zima, reference 47, treats erosion rates of metal tubes for vacuum and for helium at one atmosphere and 100 ft/sec. (30.48 m/s). Conversion factors for other gases are given. Recession rates in flowing gas are proportional to the square root of the velocity and inversely proportional to the square root of the pressure. Therefore, knowing the rate at one atmosphere and 100 ft/sec, $\dot{\delta}_{1,100}$, then:

$$\dot{\delta}_{P,V} = \dot{\delta}_{1,100} \left[\left(\frac{P_1}{P} \right) \left(\frac{V}{V_{100}} \right) \right]^{0.5} \tag{12}$$

As an example of the suppressing effect of pressure even under conditions of 100 ft/sec. flow velocities, for the tubular geometries of Zima, the recession rate for rhenium at 2500°K is reduced by a factor of 100 over that in a vacuum.

Creep deformation.- Creep, the deformation of a material with time under compressive or tensile loading due to pressure or restrained differential thermal expansion, is an important consideration in the design of resistojets that must have long service lives with many parts operating at high temperature. Creep can cause two effects which cannot be compensated for and must be accommodated in the design. First, the parts may change shape to the extent that surfaces of a different electrical potential may touch causing short-circuiting. Second, they may creep to failure. The design must be suitable to withstand these effects during the thrustor lifetime.

An extensive survey of available creep data for ZrO_2 and ThO_2 was conducted under Contract NAS1-10353 (reference 20). Unfortunately, few data are available on low stress, long-term creep at temperatures above 1600°K. No tensile creep data are available at all. From the available data, it is apparent that resistojets employing ceramics must be carefully designed so that parts operating at temperatures in excess of about 1300°K must be in compression or, if in tension, must have a stress well below 10^5 N/m^2 (15 psi). This can be achieved by employing chamber pressures of no more than one or two atmospheres, or by pressure balancing the ceramic heater element, and by the avoidance of restrained differential thermal expansion.

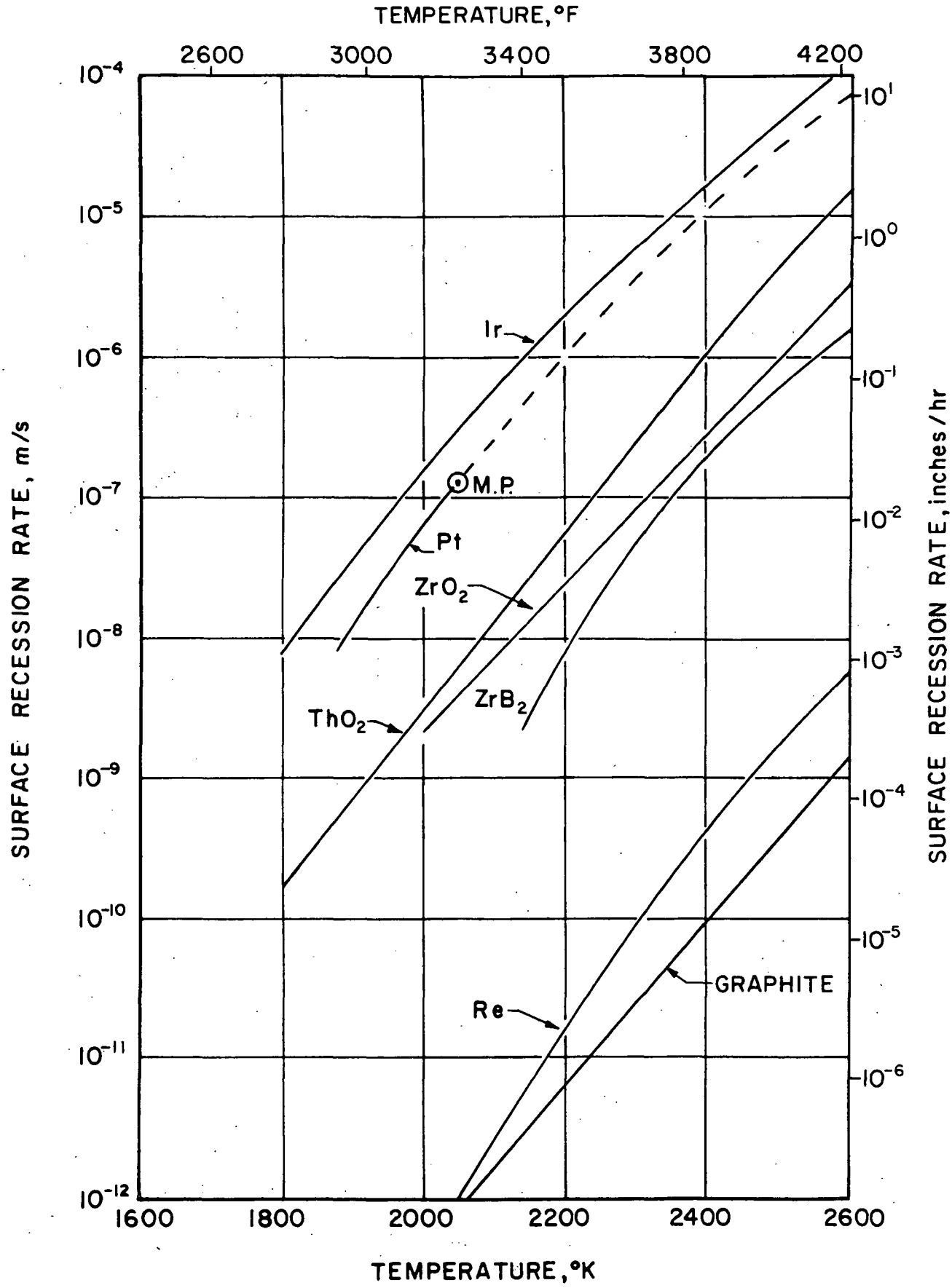

Figure 16 - Surface recession rates due to sublimation of high temperature materials in a vacuum.

Thermal Stress Resistance.- If a body is uniformly heated, thermal stresses do not occur provided that the body is homogeneous, isotropic and unrestrained. Thermal stresses arise from temperature gradients, differential thermal expansion and variations in material properties in the body of interest. The susceptibility of ceramic materials to thermal stresses has long been recognized and studied. It is an important consideration with regard to their potential for use in resistojet thrustors where high heat flux rates and temperature gradients can exist in some designs.

Kingery (reference 48) shows the various analytical descriptions which have been developed for the conditions to initiate fracture of a brittle material considering simple shapes in a variety of thermal stressing situations. Based upon these analyses, no single parameter or test value is a suitable index to rate a material's resistance for all conditions of thermal stressing. The material properties which affect thermal stress resistance are elastic strength, coefficient of thermal expansion, Poisson's ratio, and in some cases, thermal conductivity, diffusivity or emissivity.

Analyses for different conditions result in the following three parameters that can be used to rate the thermal stress resistance of material under conditions where plastic strain is insignificant:

$$R_1 = \frac{\sigma_f (1 - \mu)}{E\alpha} \tag{13}$$

$$R_2 = \frac{\sigma_f k(1 - \mu)}{E\alpha} \tag{14}$$

$$R_3 = \frac{\sigma_f a(1 - \mu)}{E\alpha} \tag{15}$$

where σ_f is either the tensile or shear fracture stress of the material whichever is significant to the problem, E is Young's modulus, α is the coefficient of linear thermal expansion, k is the thermal conductivity, a is the thermal diffusivity, and μ is Poisson's ratio. For ceramics, the most serious thermal stresses are tensile. Since the compressive strength is generally four to eight times the tensile strength, failure from compressive stresses is relatively unimportant. Shear strengths for ceramics are always greater than or equal to the tensile strengths.

Conceptually, the critical condition for fracture, f, is defined by the product

$$f = R \times S$$

where R is the appropriate material parameter (R_1, R_2, or R_3), and S is a corresponding parameter dependent only on specimen geometry and size. R_1 can apply when fracture results from an extreme thermal shock, in which case f is the instantaneous surface temperature change, ΔT_f, of an object,

initially at one temperature and then suddenly heated or cooled, a situation which is generally referred to as thermal shock. R_2 can apply under conditions of a steady-state heat flux, Q_{max}, that will cause a sufficient temperature gradient to induce fracture. R_3 can apply to the minimum constant rate of surface temperature change, ϕ_f, that will cause fracture. The three corresponding equations are

$$\Delta T_f = R_1 S \tag{16}$$

$$Q_{max} = R_2 S \tag{17}$$

$$\phi_f = R_3 S \tag{18}$$

In summary, it should be emphasized that the use of these factors would be exact only to a homogeneous isotropic body whose physical properties are substantially independent of temperature. These relations do not cover all possible conditions but are representative of the factors comprising thermal stress resistance.

The size and shape of a ceramic part greatly influences its resistance to thermal stresses. In particular, for moderate rates of temperature change, the thermal stress resistance of a part is inversely proportional to specimen dimensions. For very high rates of change, this size effect is only important for small dimensions. In general, shapes having sharp corners or edges are to be avoided, as are parts having both thick and thin sections together. For complex shapes, or materials which are subject to plastic flow, experimental measurements are the only reliable method for measuring thermal stress resistance of the specific system.

Table IX presents the calculated values of the thermal stress resistance factors for ZrO_2 and ThO_2 on the basis of properties at the temperatures noted. The higher the resistance factor, the more resistant is the material to weakening or thermal fracture from thermal stress. The resistance factors at the higher temperature condition (1600°K) would appear to be highest for ZrO_2 on the basis of the trends indicated in table IX. These factors should be taken only as relative.

Materials tests conducted under NAS1-10353 (reference 20) employed Y_2O_3 stabilized ZrO_2 tubes made by slip casting (tubes produced by Zircoa) and cold pressing (tubes produced by Coors). Other tests employed extruded and slip cast thoria samples, both supplied by Zircoa.

Tube samples were coated on both ends with metal by various processes and brazed to Kovar end fittings which were attached to inlet and outlet tubes. These were connected to a gas supply system. The tubes were heated by radiation from a resistance-heated graphite cylinder surrounding the sample and exposed on the inside to flowing CO_2, N_2, H_2 and steam. In these tests none of the samples exhibited any degradation caused by reaction with the gas at temperature. All of the tests were terminated either voluntarily or by heater failures or leaky end fittings.

TABLE IX

CALCULATED THERMAL STRESS RESISTANCE FACTORS

Factor	Temperature °K	ThO_2	ZrO_2
R_1 (°K)	298	50.4	69.7
	1200	37.5	56.7
	1600	-	66.2
R_2 (W/m)	298	726	122
	1200	112	107
	1600	-	132
R_2 (m^2°K/s) x 10^6	298	313	47.5
	1200	37.5	28.4
	1600	-	31.1

The conclusions of that program were that both ZrO_2 and ThO_2 showed great promise for use in biowaste resistojets but that they required careful design to avoid their weaknesses in the areas of creep, tensile strength, and thermal shock. Tests of conducting ceramic heaters, reported in detail in the COMPONENT TESTS section, showed that zirconia is resistant to biowaste propellant attack, and with proper material formulation, can resist thermal cycling for at least thousands of cycles. The greatest weakness, demonstrated in cyclic tests, is sensitivity to steep gradients at the electrode interface. This is felt to be an engineering problem to be solved by proper geometric design.

Details of the design.- The results of the work done under contract NAS1-10353 (reference 20) and the early tests of the present program resulted in the following design guidelines for an advanced ceramic biowaste resistojet:

(1) In order to take advantage of the superior temperature capabilities of the ceramic materials, they must be used as resistance heaters. If an auxiliary metal heater were to be used to indirectly heat a ceramic heat exchanger, it would have to operate at a higher temperature than the ceramic in order to transfer heat to the ceramic and thence to the propellant. This produces the danger of the heater touching the ceramic, which would result in thermal shock failure of the ceramic. Also, there are no metals suitable for direct exposure to the propellants at the high temperatures

at which the ceramics can operate in biowaste propellant atmospheres. The use of metal radiant heaters in a vacuum results in metal sublimation with consequent plating of adjacent surfaces and ultimate electric shorts.

(2) Because of the high resistivities of conducting ceramics at room temperature, an auxilliary "starter" heater must be used to bring the ceramic to an intermediate level of the order of 1000°K, where the resistance of the ceramic becomes low enough so that selfheating can then take over and raise the temperature to its design operating level of about 1800 to 2000°K.

(3) Conducting ceramics have negative resistance characteristics with temperature and therefore require a series resistor, or ballast, for stable operation from a constant voltage supply. This ballast resistor must be used as a propellant preheater as well in order to obtain good overall electrical power efficiency.

(4) The design should carefully avoid tensile stresses in the ceramic materials and should limit compressive stresses to the order of 100 kN/m^2 (15 psi), in regions where the temperature approaches 2000°K, to produce a one-year service life as governed by creep. Tensile stresses, if unavoidable, should be limited to the order of 10 kN/m^2.

(5) Ceramic structural parts having a vacuum on one side and pressure on the other should be limited to temperatures below 1700°K to prevent life-limiting sublimation losses and creep due to pressure-induced tensile stresses.

(6) The chamber pressure should be limited to about one atmosphere to minimize stresses tending to produce creep in the cases where the ceramic heater element is not pressure balanced.

In accordance with the above guidelines, the development thrustor shown in figure 17 was designed. This thrustor concept requires no new technology for its success, but relies only upon available materials and processes. The adaptation of the electrically conductive ceramic as a direct gas heat exchanger is believed to be new or uncommon and may involve gas flow- electrical current instabilities as discussed in the preceeding Thermal Analysis section.

Referring to the part numbers in figure 17, it can be seen that the base of the thrustor is the stainless steel mounting plate, part no. (13), to which all of the other parts are attached. This plate is a disc with three triangular "ears" for external attachment. Propellant and electrical connections are through this plate via parts (15) and (19), respectively.

Part no. (3), the alumina mounting flange, is attached to (13) by four stainless steel screws (17) and insulating transite washers (21.)

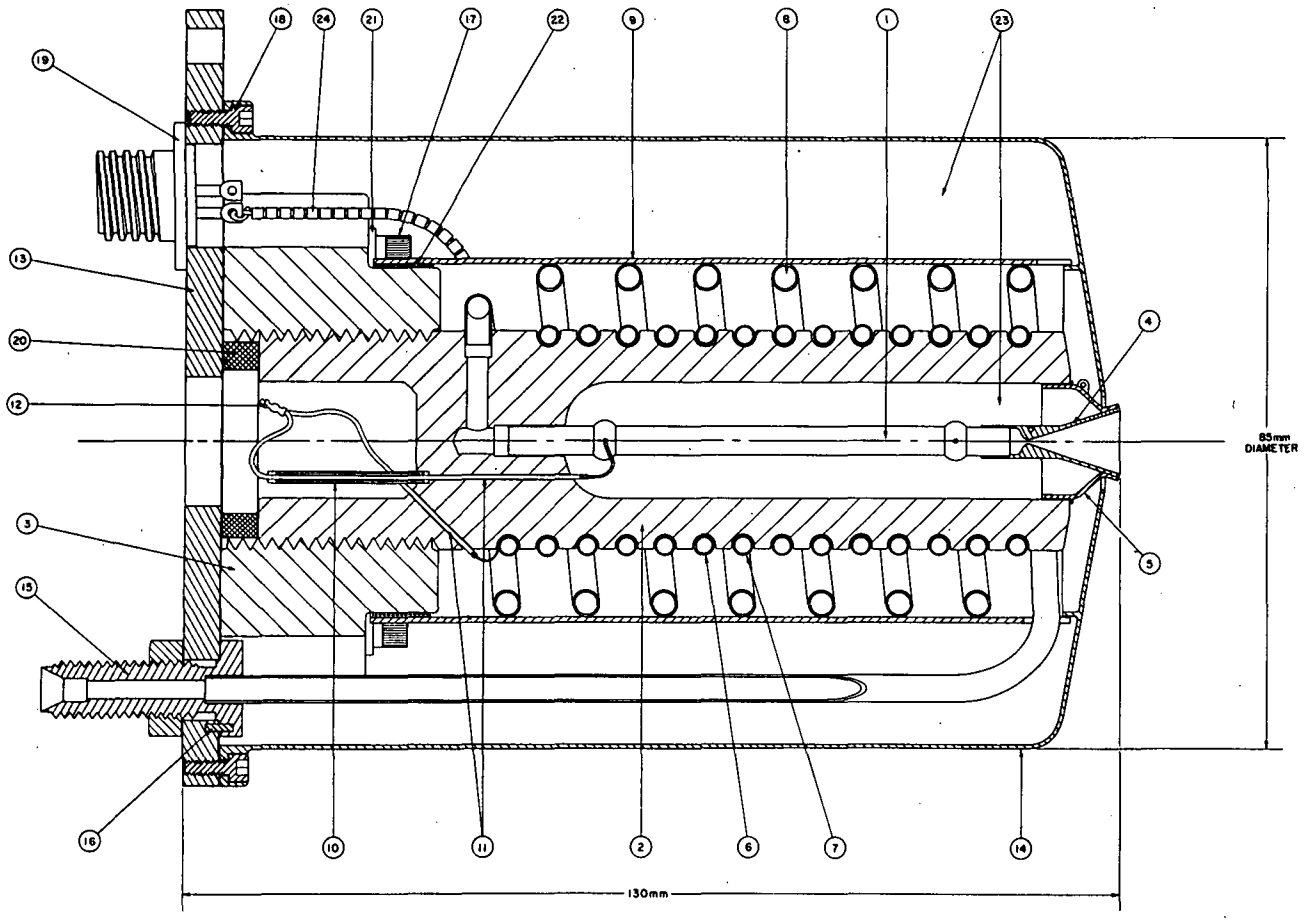

ITEM	QTY	DESCRIPTION	MATERIAL
24	–	INSULATING BEADS	96% ALUMINA
23	–	INSULATION	ZIRCAR FELT
22	–	INSULATING TAPE	ZIRCAR TAPE
21	4	WASHER	TRANSITE
20	1	SPACER	TRANSITE
19	1	POWER RECEPTACLE	PSC-T102PM-8-3P-F1
18	4	2-56 CAP SCREW	304 CRES
17	4	10-32 CAP SCREW	304 CRES
16	1	DOWEL PIN	304 CRES
15	1	INLET FITTING	304 CRES
14	1	INSULATION COVER	304 CRES
13	1	MOUNTING PLATE	304 CRES
12	1	CRIMP CONNECTOR	PLATINUM
11	–	ELECTRODE WIRE	PLATINUM
10	1	ELECTRODE TUBE	PLATINUM
9	1	COIL SUPPORT	TD NICKEL
8	1	REGENERATOR COIL	Pt-20Rh ALLOY
7	1	BALLAST HEATER	Pt-20Rh ALLOY
6	1	STARTER HEATER	Pt-20Rh ALLOY
5	1	NOZZLE FLANGE	TD PLATINUM
4	1	NOZZLE	TD PLATINUM
3	1	MOUNTING FLANGE	96% ALUMINA
2	1	HEATER SUPPORT	96% ALUMINA
1	1	CERCON HEATER	STABILIZED ZIRCONIA

ARTCOR

ADVANCED RESEARCH AND TECHNOLOGY CORP. IRVINE CALIFORNIA

DRAWN: [illegible] DATE: 4-9-72

CHECKED: [illegible] 4-13-72

APPROVED:

TITLE:

25MLB
CONDUCTING CERAMIC
BIOWASTE RESISTOJET

CONTRACT NO NASI-10934

DWG NO 72100

SIZE: 750mm x 1100mm SCALE: 4X SHEET: 1 OF

A Zircar cloth gasket (not shown) separates (3) and (13) for better thermal isolation and mechanical cushioning. Part no. (2), the alumina heater support, is attached to (3) by means of a threaded joint having the dual purposes of minimizing conductive heat loss and facilitating assembly and disassembly. The transite (asbestos and cement) spacer, part no. (20), adjusts the clearance between (2) and (13) to help align the propellant inlet tube and maintain proper clearance between the nozzle (4) and insulation cover (14) at the other end. Part no. (2), shown separately in figure 18, is the principal structural part of the thrustor. It supports the conducting ceramic heater and the starter and ballast heaters, and, with the nozzle assembly, forms the thrustor's pressure vessel.

In the surface of this part are a pair of parallel grooves (A) that begin on opposite sides of the part at one end and wind in a double helix to terminate on opposite sides at the other end. In the assembled thrustor, each groove contains a heater coil of 3.05 mm diameter and 560 mm length made of 0.38 mm (0.15 inch) diameter Pt-20 Rh wire. These are the starter and ballast heaters, parts (6) and (7), respectively. At one end these wire coils are joined to larger platinum leads and passed through holes in the alumina (B) to an interior cavity where both are attached to one lead from the ceramic heater, part no. (1), by means of a short piece of crimped tubing (12). The lead from the heater passes through a hole in the alumina and through a platinum tube, part no. (10), to which it is silver-brazed. The tube is brazed to a metallic coating applied to the ceramic by the Moly-manganese process. This process is also used to metalize the surfaces of part no. (2) to which the nozzle flange (5) and the regenerator coil (8) will be brazed. At the other end of part no. (2), the heater coil wires pass through two short holes (C) and are attached to larger platinum leads which are terminated at two of the pins on the power receptable, part no. (19). The third terminal of (19) is attached to the lug on nozzle flange (5) and thence, through the nozzle, to the second ceramic heater electrode wire. All three of the lead wires are strung with alumina beads as shown in the drawing. The electrical circuit is discussed in more detail later.

Part no. (1), the conducting ceramic heater, shown in cross-section in figure 5, has six longitudinal flow passages for better heat transfer than with a single passage. The heater is 70 mm long by 4.1 mm in diameter. It is presently specified as stabilized zirconia but may eventually be made from thoria. At present it has two wrapped platinum wire electrodes covered with ZrO_2 cement. Other electrode geometries are under investigation, however, and the final configuration is not yet known. One possible electrode configuration would join the heater to the nozzle by diffusion bonding, or a similar process, and eliminate the separate electrode wire presently employed.

The ceramic heater rests at one end in the alumina part no. (2) with a sliding fit to permit unrestrained expansion during operation of the thrustor. The other end rests in the nozzle, part no. (4). With the sliding joint between the no. (2) part and the heater, gas leakage will occur, maintaining the cavity in the alumina part at a pressure equal to the inlet

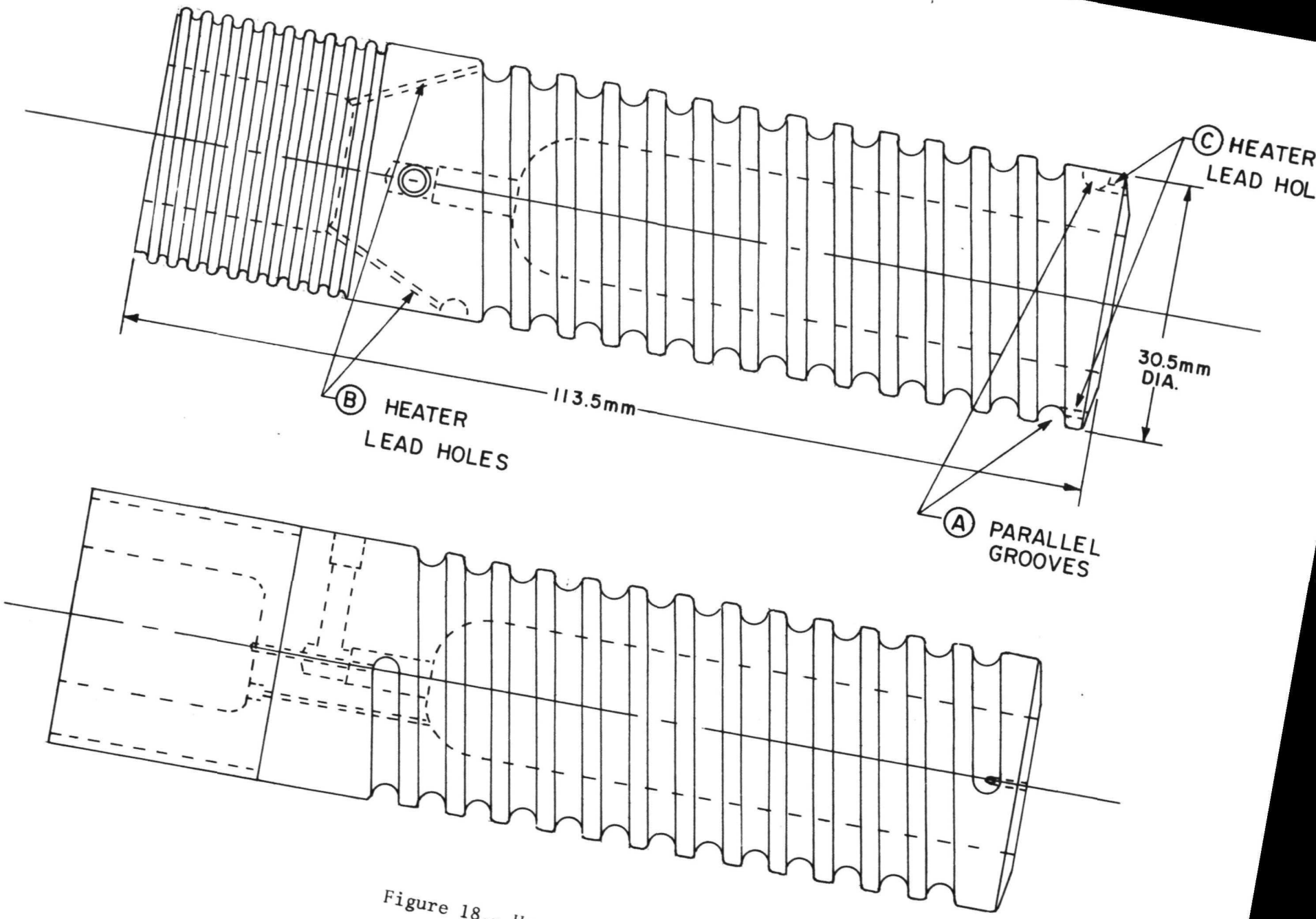

Figure 18.- Heater support detail.

pressure of the heater tube thus minimizing stresses tending to cause creep. A small pressure differential occurs as a result of friction plus heat addition pressure losses within the tube. This loading causes an insignificant compressive stress at the downstream end of the heater tube. The walls of this cavity in part no. (2) will be lined with Zircar felt insulation to minimize thermal losses.

The nozzle (4) and nozzle flange (5) have been designed to permit separate assembly of the flange to the alumina part (2) and the nozzle to the heater (1), the two mating cones then being joined by welding. These cones have been extended longer than necessary on the development model to permit cutting and reassembly if required. The nozzle itself has a throat diameter of 0.76 mm and an exit diameter of 8.8 mm, giving a geometric area ratio of 116. The nozzle is a straight cone with a half angle of 18°. The throat diameter of 0.76 mm corresponds to 25 mlb of thrust with an effective chamber pressure of about 1.4 atmospheres, depending on the propellant used.

Propellant enters the thrustor through the stainless steel inlet fitting (15) which is fastened to the mounting plate with a hex nut (prevented from turning on the other side by a small dowel, part no.16). This fitting is silver brazed to the Pt-20 Rh regenerator coil (8). The propellant flows to the nozzle end of the thrustor and into the regenerator coil where it spirals toward the opposite end where the coil joins the alumina part (2). It continues through the alumina part and then through the six parallel passages of the ceramic heater to the nozzle. The regenerator coil and its support (9) intercept most of the heat lost from the starter-ballast heaters and the alumina part (2) and transfer it to the incoming gas. In the start-up mode, the starter-ballast heat warms the ceramic heater by multiple heat transfer paths to the point where its resistance is low enough for current flow and self-heating. In the normal operating mode, the regenerator simply intercepts the heat that would otherwise be lost. The regenerator coil and its support will be brazed together for better heat transfer with a high temperature brazing alloy that has not yet been selected. The coil support material was originally to be Pt-20 Rh but has been changed, most probably to TD nickel or some nickel alloy, for reasons of economy. At one end the support fits over the end of the alumina flange part (3) which has first been wrapped with Zircar tape (22). Its other end is centered and supported by the stainless steel insulation cover (14). The external insulation filling the space between parts (9) and (14) will probably be Min K-2000 or Zircar depending on preliminary compatibility tests. The insulation cover (14) is held in place by four stainless steel screws (18). The surface of this cover is polished, given a coating of electroless nickel, gold plated and polished again for low emissivity.

The mass of the thrustor shown in figure 17 is about 1.67 Kg (3.67 LB) in the 25 mlb thrust size. The thrustor is 130 mm (5.1 inches) long with an insulation cover diameter of 85 mm (3.4 inches).

The key parts in this design are:

1. The ceramic heater
2. The nozzle assembly
3. The heater support
4. The regenerator coil
5. The ballast and starter heaters

The materials which are candidates for use in the ceramic heater have been discussed in some detail earlier, along with design principles which must be applied to avoid their weaknesses. These materials all seem able to withstand operation at high temperature in the presence of biowaste propellant gasses, and the thrustor has been designed to avoid undue stresses in the ceramic heater. The principal design problems here are to avoid steep gradients at the electrodes which would cause thermal stresses and to avoid excessive temperatures in the electrode wires at their junction with the ceramics.

The nozzle assembly has been subjected to a careful stress analysis. The maximum stress, at a pressure of 2 atmospheres, of about 4.2×10^6 N/m^2 (600 psi) occurs at the cooler outer diameter of the flange part (5). The nozzle cone is subjected to a maximum stress of about 1.7×10^6 N/m^2 (250 psi) again at the cooler larger diameter. The hotter smaller diameter region (throat) faces a stress of only 0.9×10^6 N/m^2 (130 psi). The stresses are well within the capabilities of the TD Platinum material. The nozzle is thermally sized to operate at about 1400°K at its upstream end and less than 1300°K at its throat to avoid a sublimation loss problem. Creep is not a problem up to 1800°K with the TD Platinum material. Pt-Rh alloy is not being considered for the nozzle because of its corrosion problem with CO_2 having a trace of O_2 as discussed in the COMPONENT TEST section. An alternate material for the nozzle is a ceramic like that of the heater tube.

The alumina heater support is a relatively massive part and the steady-state stresses in it are quite low. During heat-up, however, it is subjected to a rather steep gradient in the region of the heater coils. A rigorous analysis of the thermal stresses in this part is quite difficult due to its complex geometry. A simplified calculation yields a maximum tensile stress in the part of 7.3×10^8 N/m^2 (10^4 psi) at the inner surface initially while that surface is cold. This is within the capability of the material and, of course, decreases as the part is heated. Experimental verification of the actual part's ability to withstand the transient condition is required. The part has been designed with generous radii on the edges and in the grooves to prevent unnecessary stress raisers.

The regenerator coil is made from Pt-20 Rh tubing with a 3 mm inside diameter and a 0.25 mm wall. An internal pressure of 2 atmospheres would produce a stress of only 1.4×10^6 N/m^2 (200 psi), well within the capabilities of the material. The coil, if free standing, would be subject to bourdon tube forces, but brazing it to the support prevents this. Loss of material from the coil by evaporation was considered but found to be

inconsequential at the temperature level required. The regenerator operates below 1000°K, for which no corrosion problems are to be expected.

The ballast and starter heater coils are not subjected to any appreciable stresses because of the nature of their configuration. They were, however, examined with regard to sublimation losses.

The possible evaporation losses for several key high temperature parts were examined to determine thrustor life expectancy if sublimation is the determining factor. These parts are listed in table X with their maximum operating temperatures, surface recession rates and time required for 10% thickness loss (or decrease in cross-sectional area where noted). It should be noted that the temperature of 1300°K listed for the ballast/starter heater coil occurs only during start up, which represents a small portion of a typical thrusting cycle. The "life" listed in table X is, therefore, an extremely conservative number. During normal operation the ballast heater operates at not over 1200°K, corresponding to a sublimation lifetime in excess of 10^4 hours. A possible consequence of evaporation loss from the starter and ballast heaters might be due to redeposition of the evaporated material in the heater support grooves. This build-up could result in continuous coating thick enough to cause shorting of the coils. If all of the material vaporized is presumed to redeposit in the grooves (a conservative estimate), then after one year of operation the maximum coating thickness could be 5×10^{-6} meter which should not be serious.

Another potential life determining mechanism that has been considered is the oxidation of Pt-Rh and platinum surfaces exposed to the flow of propellant. The principal areas of concern for this mechanism are the ceramic heater electrode wires and the nozzle throat. Using the oxidation rates in still air (very conservative), and defining life as in table X, the life expectancies with oxidation as a determining factor are:

Electrode wires	1.7×10^4 hours
Nozzle throat	5.6×10^4 hours

The effects of the high velocity gas on erosion of material at the throat, however, will require experimental evaluation. Removal of material could be increased. A significant increase is not anticipated since the thrustor heater passage and nozzle throat flow is laminar in which the gas velocities at the surfaces themselves are extremely low.

TABLE X

THRUSTOR LIFE EXPECTANCY AS DETERMINED BY

SUBLIMATION LOSSES

Part	Max. Temp. °K	Surface Recession Rate m/s	Life Hours
Ceramic Heater	2000	2×10^{-12}	$\sim 1.5 \times 10^{4}$ (a)
Ceramic Heater Electrode Wire	<1400	4×10^{-15}	$\sim 8 \times 10^{5}$ (a)
Nozzle Throat	<1300	6×10^{-13}	$\sim 10^{4}$ (b)
Heater Support	1100	Negligible	*
Ballast/Starter Heater Coil	1300	6×10^{-13}	5×10^{3} (a) (c)

(a) 10% reduction in cross-sectional area.

(b) 10% in flow area.

(c) 1300°K temperature actually represents only a small fraction of the total thrustor on time. 5×10^{3} hours is, therefore, an extremely conservative number.

* Not a limiting factor.

COMPONENT TESTS

Component tests were conducted to determine the compatibility of zirconia ceramic at high temperatures with the biopropellants and to evaluate its performance as a biowaste heater. Platinum-rhodium alloy was also tested with CO_2, and with CO_2 plus a trace of O_2 to determine if the O_2 addition would suppress carbonyl corrosion at high temperature. Of the two candidate ceramic materials, stabilized zirconia and thoria, only stabilized ZrO_2 was tested with biopropellants. Stabilized ZrO_2 has higher electrical conductivity in the temperature range of interest than does ThO_2. Zirconia is considered to have better mechanical properties relative to thermal stress resistance at high temperature and has a lower sublimation rate than ThO_2. Thoria, on the other hand, is considered to be generally more stable chemically than ZrO_2 and has a higher melting point (3500°K) than does ZrO_2 (3000°K). A decided advantage with ThO_2 over ZrO_2 is that ThO_2 is a stable material not requiring the addition of stabilizers. Yttria and calcia are generally used to effect a stable cubic structure in ZrO_2.

All tests in which ceramic heater samples were heated resistively by passing electrical current were conducted with alternating current. It is not certain what effect, if any, direct current would have on the ceramic with the biowaste propellants. It is known that direct current in an oxygen free environment will reduce zirconia. This phenonenon has been suggested (reference 49) as a means of increasing the electrical conductivity of the zirconia. Zirconia can, in this way, be made sufficiently conductive at ambient temperature so as not to need a starter heater.

Zirconia and thoria are solid electrolytes and conduct electricity by ionic conduction. Zirconia stabilized with CaO, for example, has a large fraction of oxygen vacancies. The calcium ions substitute for the zirconium ions in the zirconium lattice sites. With calcium ions having a charge of plus 2 rather than plus 4, electroneutrality occurs as the result of missing oxygen ions. Oxygen ions can move through the crystal lattice of these ceramics because of the oxygen deficient lattice. That is, these compounds have defects consisting of the oxygen ion vacancies and oxygen ions can exchange with the vacancies in the crystal lattice.

The movement of the oxygen negatively charge ions is anionic (toward the anode) conduction. There can be cationic conduction due to the movement of positively charged ions. However, this is negligible in stabilized zirconia and thoria relative to the anionic conduction. This can be explained in terms of the gaps within the crystal lattice relative to the size of the ions. Gaps between cations through which anions pass are about as large as the anions because of the small radii of the Zr^{4+} ions. Cations, on the other hand, must move through gaps only half their own size. These oxides are poor electronic conductors. Connected in an electrical circuit with metal electrodes interfacing the oxide, a current can be made to flow in the heated oxide. For the case of the oxide in an environment containing oxygen molecules and a direct current, electrons flow in the metal circuit to one electrode. An oxygen molecule enters at the metal electrode-to-ceramic interface (the cathode) and acquires four electrons in converting

to two oxygen ions. These anions diffuse through the ceramic toward the anode from vacancy to vacancy. At the opposite electrode (the anode), the reverse occurs, oxygen ions revert to molecules, giving up electrons which continue to flow in the metallic circuit to close the circuit loop. The equation for the oxygen/electron interaction is given by

$$O_2 + 4e^- \rightleftarrows 2O^{2-} \tag{19}$$

At the cathode, the reaction proceeds to the right. At the anode, the reverse reaction occurs.

Presumably, with sufficient oxygen available, the ceramic can continually conduct direct current by this mechanism. Experience shows that a very small amount of oxygen is sufficient. Most certainly, without oxygen molecules, direct current causes a pumping of oxygen from the ceramic compound from the region of the cathode to the anode and out into the surrounding oxygen deficient environment. In this way, the ceramic is reduced to sub-oxides and metallic constituents and reverts to an electronic conductor. Even with an oxygen environment available, operation of a zirconia conductor with DC results in a slight darkening of the ceramic adjacent to the cathode.

The reduction process is reversible, however, in that subsequent operation in an oxidation environment re-oxidizes the sub-oxides and metal molecules that may have formed in the reduction process. Because of the reversibility of the process and particularly because such compound transformations are structurally destructive (reference 50), this phenomenon is not being used for the advanced biowaste resistojet development program.

In an alternating current circuit, the oxygen ions presumably are not pumped from one electrode to another. Rather the ions oscillate within the defect structure and the reduction of the oxide is prevented. Experimental results of tests with typical biopropellants are discussed in this section and reveal no anamolies relative to compatibility of zirconia with alternating currents. While not pertinent to the biowaste resistojet operating conditions, results of a 2-hour test to expose zirconia to a severe reducing environment (H_2 at 1525°K) without electrical current flow indicates rapid reduction of the ceramic. On the other hand, a 500-hour test in a 10^{-5} Torr vacuum revealed a slight but nonharmful reduction.

Table XI lists the environmental tests conducted with ceramic heater elements. All of the elements tested were tubular heater elements with the exception of rod heaters used for tests S53-2, S53-3 and S57-1. All ceramic heaters were made by extrusion of Y_2O_3 stabilized ZrO_2 (YSZ) ceramic material except S57-1 which was an extruded ThO_2 rod doped with 15 w/o Y_2O_3. A typical chemical analysis indicated that the YSZ consisted of 12 w/o Y_2O_3, 85 w/o ZrO_2 and 3 w/o of other compounds including about 1 w/o Al_2O_3 with traces of rare earth oxides. The alumina content resulted from ball milling the YSZ in an alumina ball mill in preparing the ceramic powder mixtures for extrusion.

TABLE XI

ENVIRONMENTAL TESTS COMPLETED WITH

CONDUCTING CERAMIC HEATER ELEMENTS

Test No.	Environment	Wall Temp. ° Kelvin	Test Time, Hours	Remarks
S19-1	Air	1985	289	Cracked due to contamination.
S19-2	Air	2000	485	Electrode failure.
S19-3	Vacuum	1980	500	No problem.
S24-1	CO_2	1935	500	No problem.
S24-2	Flowing CO_2	1930	500	No problem.
S24-3	N_2	1935	500	No problem.
S24-4	Flowing N_2	1935	454	Cracked at electrode.
S24-7 *	Air	Up to 2230	111	No problem.
S24-7 *	Flowing CO_2	Up to 2125	10	No problem.
S27-2	Air	1935	280	Used for tensile test. No problem.
S27-4	Flowing H_2O	1950	500	No problem.
S27-5	Air	2350	-	Destruct Test. Electrode failure.
S53-2	Air-cyclic	2000/1570	1105	Electrode failure.
S53-3	Air-cyclic	2000/1570	856	Electrode failure.
S57-1	Air	2775	-	Destruct Test. Electrode failure.

* Insulated ceramic heater with an integrated starter heater.

All of the extruded ceramic heater elements were made by Mr. Oskar Glaser of Ceramic Conductors, Capistrano Beach, California. Typical dimensions for the tubular heater elements were 2.7 mm OD by 1.3 mm ID by 60 mm overall length. Electrode spacings which determine the heated length of the heater were typically 34 mm. The rod heaters were smaller, with OD's of 0.65 and 0.94 mm and electrode spacings of 13 and 12 mm, respectively, for the S53 and S57 parts. The S53 rod heaters were cycled once per hour to a lower power setting (1570°K) for 15 minutes. During the 45 minutes per cycle at high power, the ceramic temperature was 2000°K. These cyclic tests were conducted in a stagnant air environment.

It is questionable whether or not the small amount (about 1 w/o) of alumina in the YSZ material is desirable. The alumina is known to reduce the electrical conductivity; an undesirable event. On the other hand, the alumina appears to aid in promoting fracture strength by providing a glassy phase at high temperature. At least with the particular extruded material tested, the alumina appeared to be justified and the penalty in conductivity reduction was not large.

The vacuum environment test was conducted in a high-vacuum bell jar facility using a vapor diffusion pump backed by a mechanical pump to obtain pressures in the 10^{-5} Torr range. Tests with an air environment were conducted in partial enclosures to maintain an ambient air environment while preventing large drafts or flying insects (attracted by the glowing heaters) from interfering with the test conditions. Test S19-1, for example, was conducted without an enclosure as shown in figure 19. A premature failure occurred 289 hours into the test when the ceramic heater tube cracked. Either the tube had an impurity which showed up as a discoloration at the fracture location or a flying insect caused the contamination. Many dead insects (moths, flies, mosquitos) accumulated below the heater during the course of the test. A repeat test in air, S19-2, nearly completed the objective test time of 500 hours. At 485, the test terminated with a platinum electrode lead failure. The ceramic heater tube remained intact.

Tests with CO_2 and N_2 environments were conducted under a bell jar enclosure to maintain a one-atmosphere pressure condition. Figure 20 shows the ambient pressure facility used. Two heater tubes were evaluated simultaneously in the long-term CO_2 environment (tests S24-1 and -2). The test S24 setup is shown in figure 20 with the ceramic heaters visible side-by-side under the bell jar supported vertically by the rectangular shaped fixture. Carbon dioxide flowed through the right heater tube (S24-2) via a plastic tube attached to the bottom of the heater tube. A mass flow rate equivalent to a 10-mlb thrustor was supplied and exhausted into the bell jar from the top end of the heater tube. The bell jar environment of CO_2 was maintained at ambient pressure plus a few inches of water to exclude room air from the test environment.

A similar test was conducted with N_2 (tests S24-3 and -4). The objective of the N_2 environment test was two-fold:

1. To determine if nitrogen compounds might form which would be detrimental to the heater.

2. To evaluate the stability of the zirconium oxide in an environment lacking oxygen.

Commercial grade N_2 was used. Minute traces of O_2 were most likely present in the bell jar environment.

Figure 21 shows two of the S24 group ceramic heaters. One of them is shown wrapped with zirconia felt insulation over a length of 4.6 cm. The insulation completely covers the platinum electrodes (spaced 3.4 cm apart). The purpose of the insulation is to determine how the ceramic heater will operate when insulated, to determine if zirconia felt insulation presents a short-circuiting part to the heater tube, and to evaluate the platinum electrodes at high temperatures in an insulation enclosure. The insulated heater, part S24-7, was operated in air to temperatures of 2230°K. It was held at 2175°K for eleven (11) hours and at 2060°K (the melting point of platinum plus 10°K) for 100 hours. In addition, a 4.8 gram weight was hung from the lower end of the ceramic heater tube to hold a stress of 2.5 psi in tension in the heater tube.

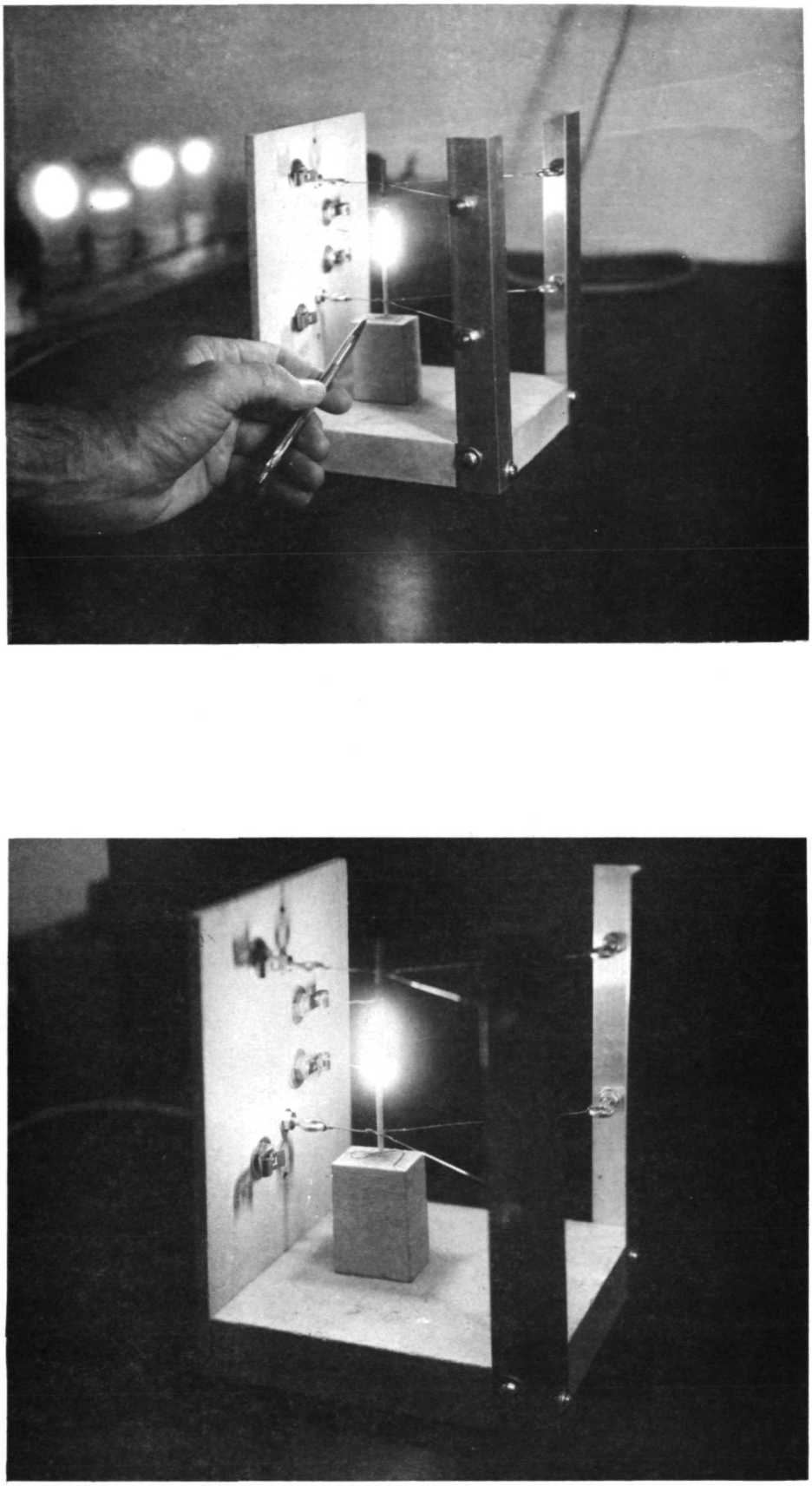

Figure 19.- Ceramic heater at 2000°K in air.

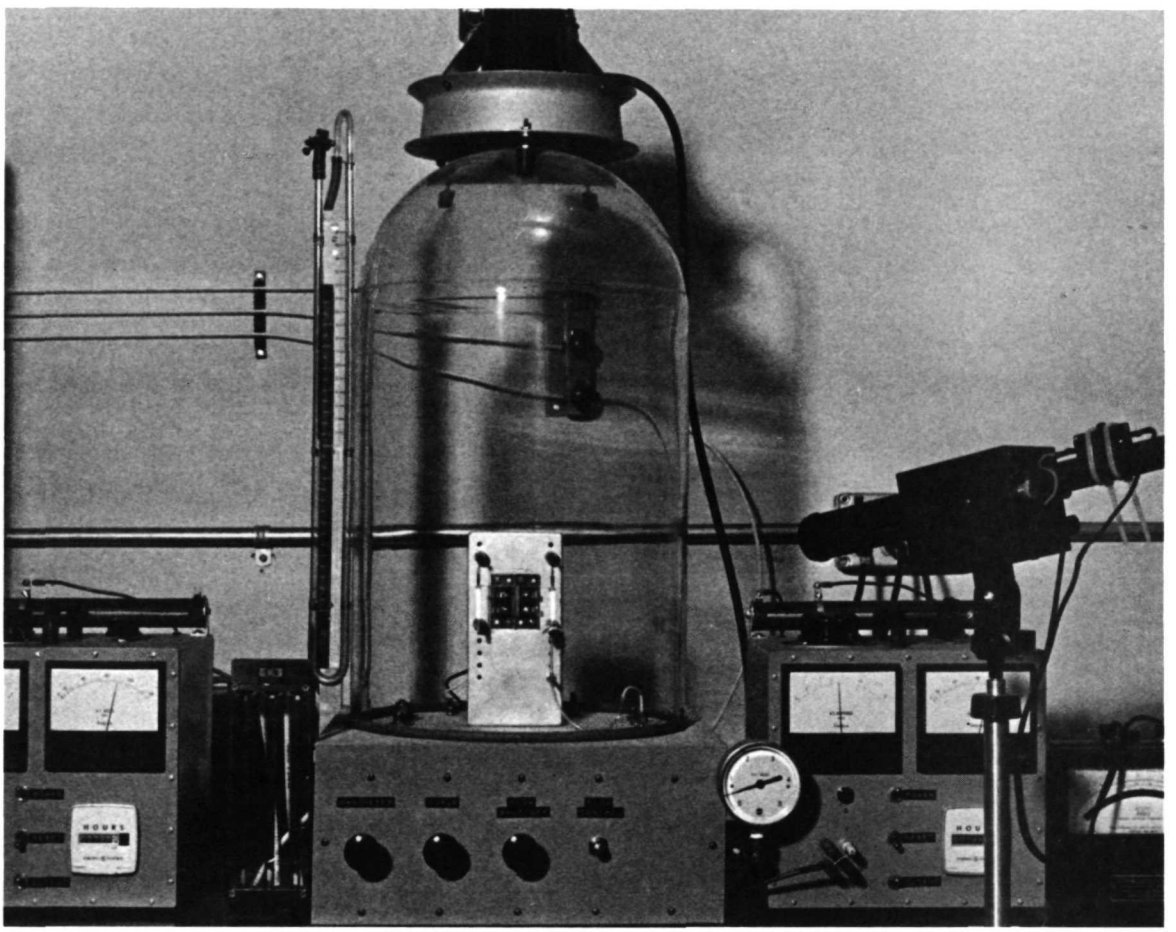

Neg. 125-4

Figure 20.- Ceramic heater environmental test facility.

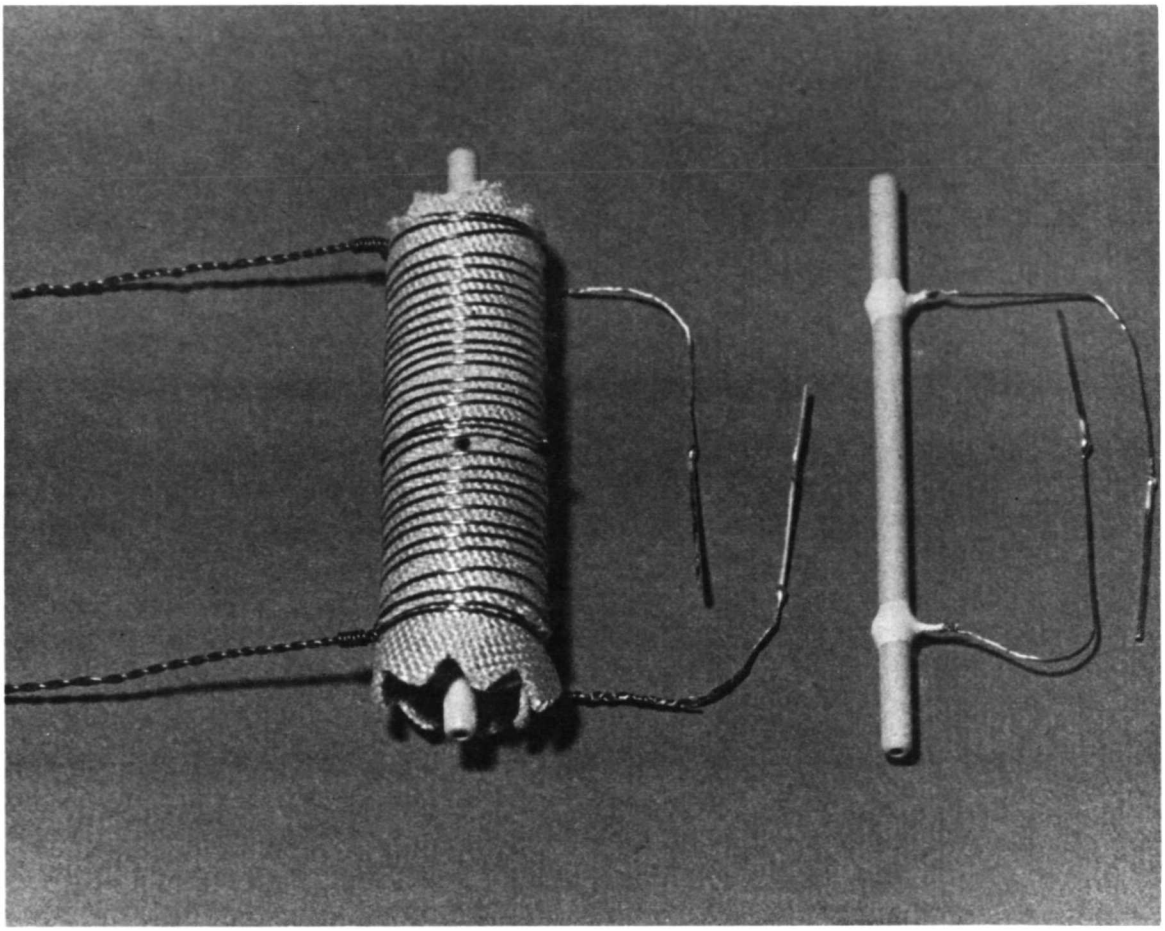

Neg. 124-1

Figure 21.- Ceramic heater with and without insulation.

Figure 21 shows a nichrome wire wound around the insulated heater to serve as a starter heater. The nichrome heater is first started. As the ceramic heater becomes conductive, it is started and the starter heater is turned off. Thus, the insulated ceramic heater represents a prototype advanced biowaste thrustor heater element.

Propellant Compatibility

Table I indicates the chemical species that would be typically present as biopropellants. These species undergo reactions in the heat exchanger of the thrustor to generate other species such as CO, O, NO, OH, H, H_2 and NH_3. Solid carbon would also be formed if heater temperatures above about 1000°K were permitted when the methane-containing propellants were used.

Five hundred (500) hour tests at typical operating temperatures of 1930 to 1950°K were conducted with the biopropellants CO_2 (tests S24-1 and -2) and H_2O (test S27-4). The objective of these tests was to verify compatibility of the YSZ against chemical corrosion with the two high temperature biopropellants. Methane propellant was not tested during this program phase. To avoid carbon deposition from the decomposition of CH_4, operating temperatures would be held below 1000°K, at which no specific problem is anticipated. The formation of free carbon at higher temperatures is viewed as a problem for all types of resistojets since it can clog any heater passage or nozzle. Table V in reference 20 indicates that carbon forms eutectics and carbides with both zirconia and thoria at high temperatures. According to Elyutin, et al., (reference 51), the reaction between carbon and ZrO_2 occurs above 2200°K, well above the intended operating condition in the advanced biowaste resistojet. ThO_2 may form ThC_2 at a temperature as low as 1375°K but only when ThO_2 and C are in intimate contact, as when mixed together as powders (reference 52).

Schroeder, et al., (reference 50) recognized that ZrO_2 could dissociate CO with the absorption of carbon into the oxide. Furthermore, a source of CO is given by the reaction equation:

$$CO_2 \rightleftarrows CO + \frac{1}{2} O_2 \qquad (20)$$

The CO, CO_2, O_2 and ZrO_2 form a complex system with several competing reactions. With the ceramic solid electrolyte material and direct current, generation of CO is promoted by the transport of O_2 from the cathode to the anode region. With alternating current, however, the degree that CO production would occur is not obvious. Y_2O_3 is known to absorb CO_2 with no apparent harmful effects.

High temperature data on compability of the ceramics with H_2O is lacking. Reference 53 suggests that the absorption of H_2O occurs with increased porosity, decreased flexure strength, and the formation of hydroxide for a CaO stabilized ZrO_2. Temperatures for the observations given in reference 53 are not known. Relating these results to a YSZ on

the basis of solubilities of the constituent compounds in cold and hot water from reference 54, Y_2O_3 is less soluble in H_2O by 3 orders of magnitude than is CaO. ZrO is completely insoluble. CaO actually decomposes in H_2O. It would appear that a YSZ would be considerably more resistant to H_2O than a CSZ (CaO stabilized ZrO).

Reference 24 indicates the insolubility of Y_2O_3 in H_2O but mentions that Y_2O_3 is highly subject to hydration. Table 8-1 of reference 55, on the other hand, indicates that hydration is a problem with CaO, not for Y_2O_3. Reference 50 conjectures that there are hydrates of ZrO_2 that are stable in the 1300 to 1500°K range and are also oxygen deficient.

Additional discussions of possible anomolies resulting from the various biopropellants and their reaction products are discussed in detail in reference 20. These anomolies and those discussed above indicate the importance of conducting propellant compatibility tests with actual heater materials at operating temperatures while passing electrical current. Tests of 500 hours duration were considered sufficiently long to verify whether or not chemical corrosion or decomposition failure modes would occur. Corrosion or decomposition problems, if they occurred, would show up as changes in electrical characteristics of the conducting ceramics and/or would be visible from a photomicrographic examination. Electrical characteristics from these tests will be compared in the next section with those for the tests in air and in a vacuum.

Photomicrographs are shown in figures 22 through 25 to indicate the general nature of the extruded YSZ conducting ceramic heater elements used and to show that no chemical reactions have occurred during tests with CO_2 and H_2O. These photomicrographs are 200X enlargements of a typical region showing a partion of the inside edge of the heater tube. Figure 22 shows unetched and etched YSZ material from heater sample S19-1 in the as received condition. Grains are not well defined in the etched view because the material is partially sintered in the as-received condition. In general, particle size is seen to be small, averaging on the order of 5 μm. Porosity is irregular, with a few large (30 to 50 μm size) voids seen in the upper left corner of the unetched figure 22 view. The S19-1 as-received photomicrographs are typical of all of the YSZ heater element samples.

Figure 23 shows the unetched (upper view) and etched condition at typical locations for the hot-tested portion of the heater after 289 hours at 1985°K in air. Air presents no problem to the ceramic heater material and this figure serves as a reference condition in assessing the CO_2 and H_2O tested heater elements shown in figures 24 and 25. The relatively ragged edge in the etched figure 23 photomicrograph is due to breakout of material as the result of polishing and etching. The figures 24 and 25 photomicrographs were prepared more carefully as reflected by the relatively smoother edge.

In the case of the test in air, the grain size in figure 23 is seen to be large (on the order of 100 μm). Small 10 μm size pores are scattered

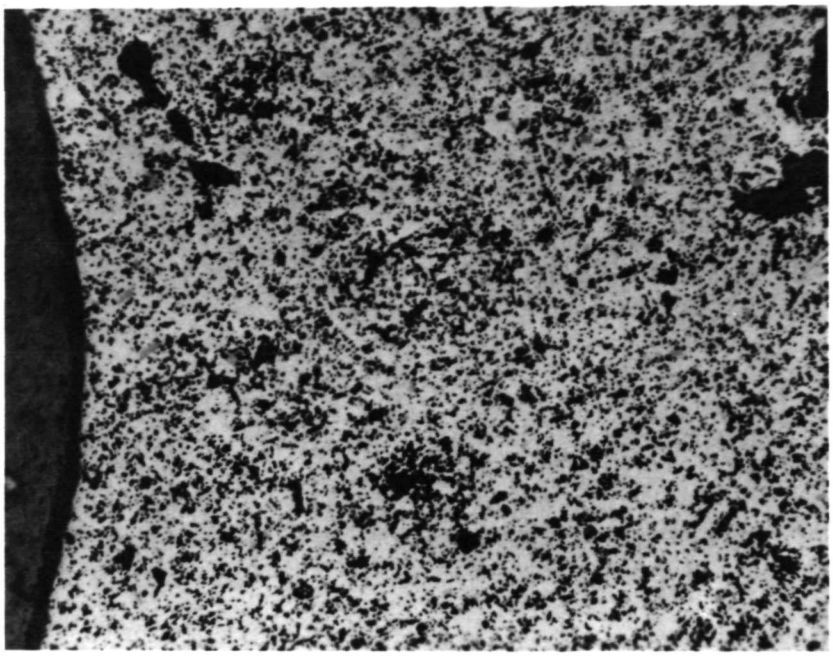

UNETCHED 200X

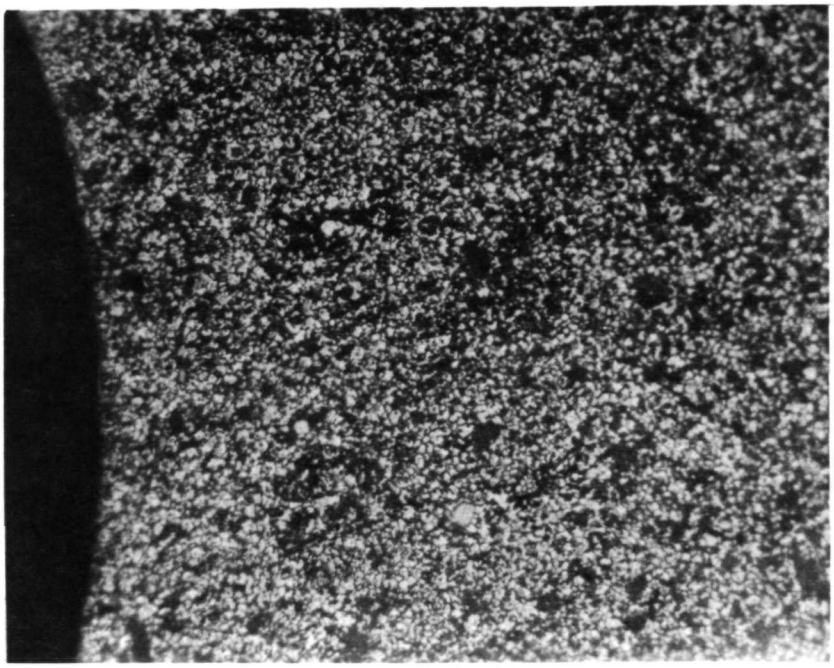

ETCHED 200X

Figure 22.- Ceramic heater tube sample S19-1 in as-received condition.

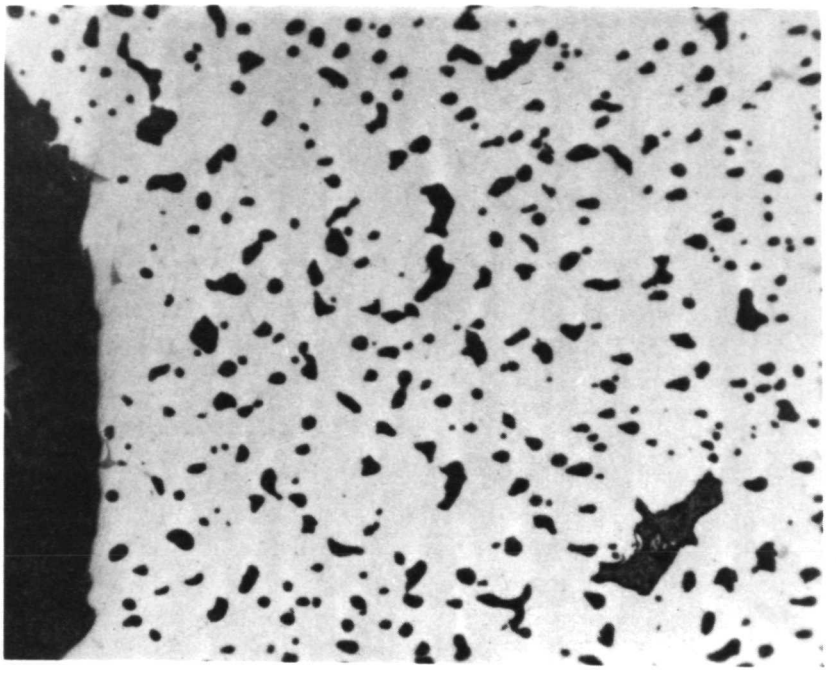

UNETCHED 200X

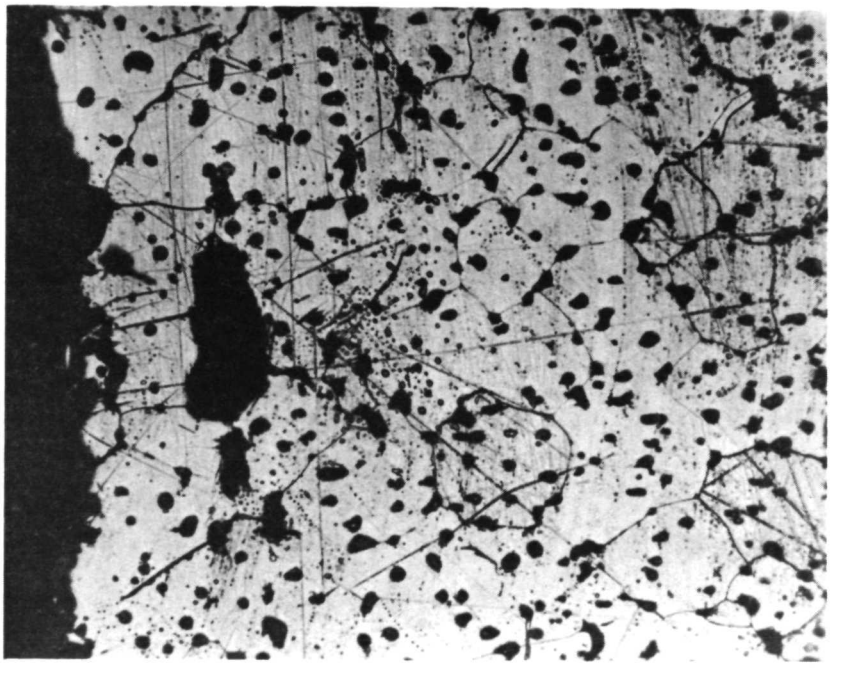

ETCHED 200X

Figure 23. - Ceramic heater tube sample S19-1 after test.

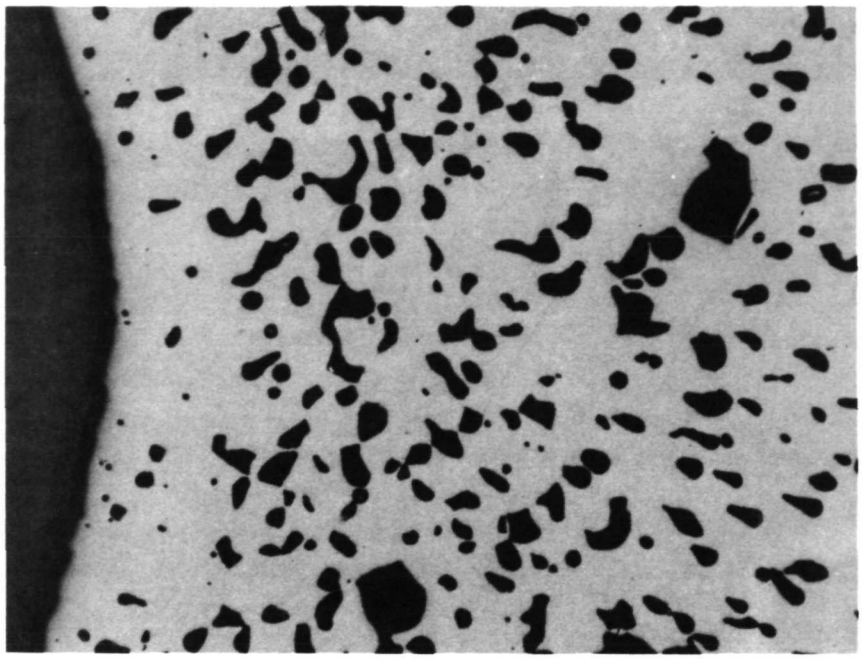

UNETCHED 200X

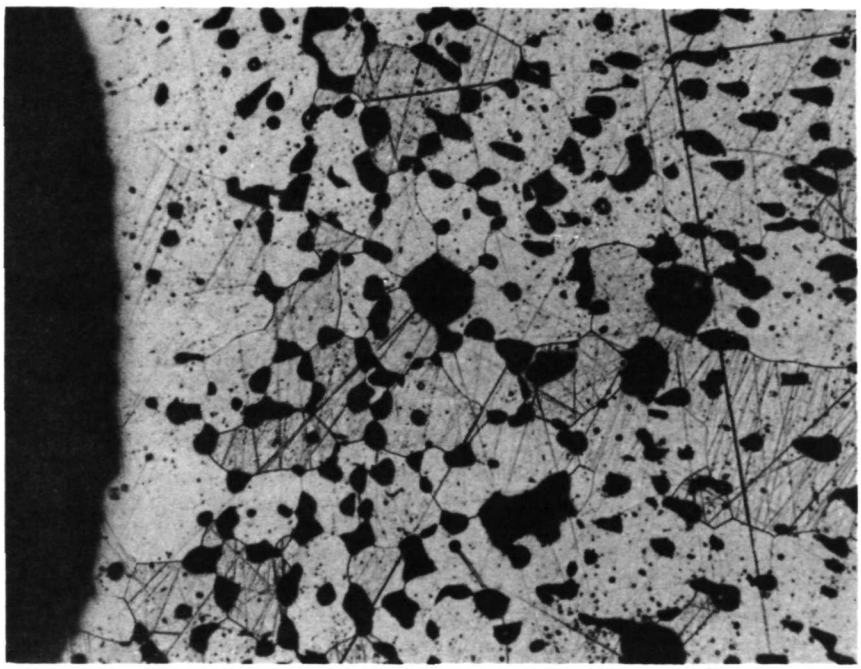

ETCHED 200X

Figure 24.- Ceramic heater tube sample S24-2 after test.

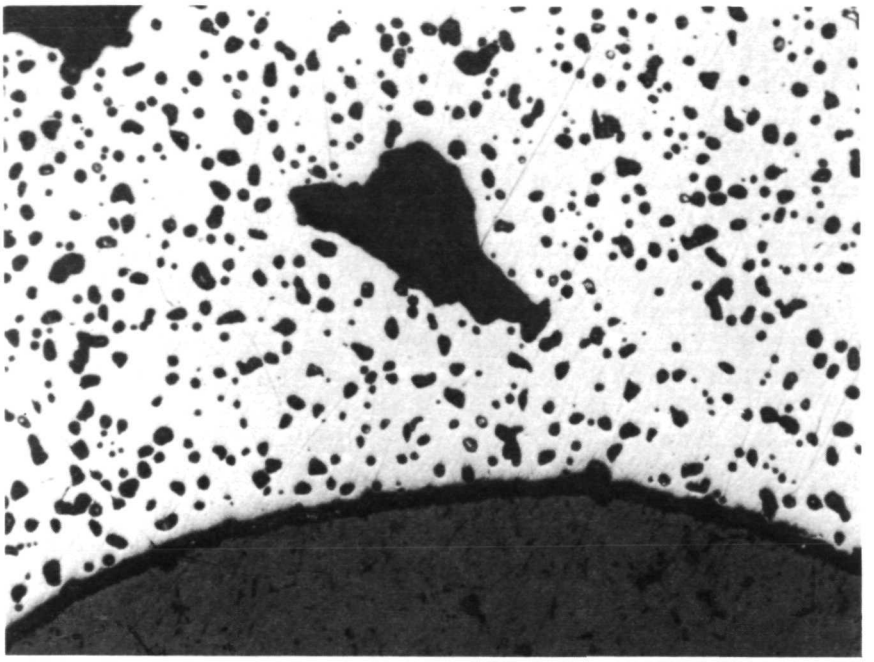

UNETCHED 200X

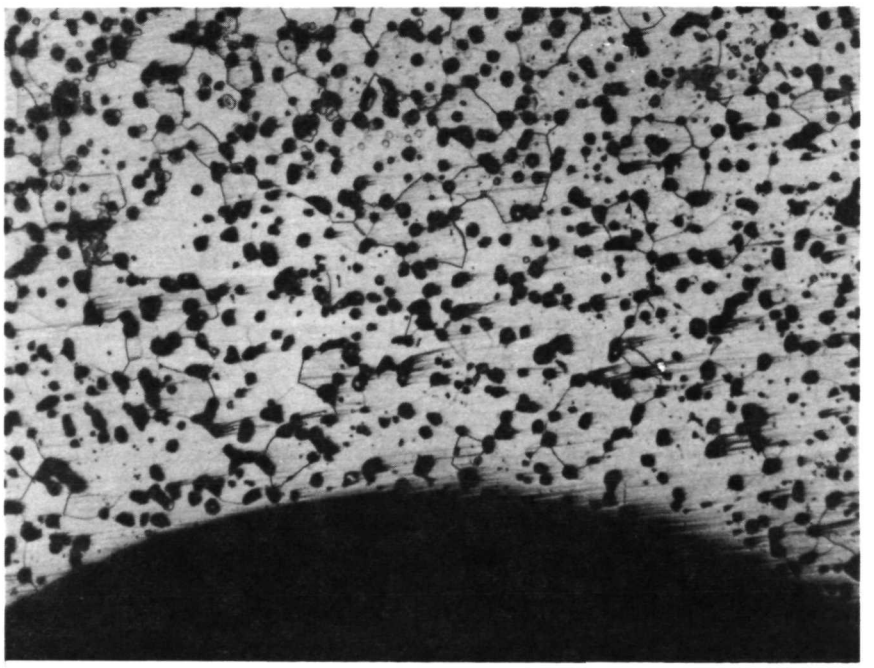

ETCHED 200X

Figure 25.- Ceramic heater tube sample S27-4 after test.

uniformly throughout the material. A very large 130 μm long void appear in the etched photomicrograph. The 100 μm long gray area in the unetched photomicrograph appears to be filled with unknown material. The smaller dark spots referred to as pores are most likely not voids at all but pockets containing, at least in part, some of the impurities and trace compounds.

Figure 24 shows the photomicrographs of a representative area from sample S24-2 operated with flowing CO_2 for 500 hours at 1930°K. In this test CO_2 flowed through the tube against the surface shown as an edge in figure 24 and exhausted into a bell jar covering the experiment. The heater tube was, therefore, exposed to a stagnant CO_2 environment on the outside. The large dark spot at the bottom of the unetched view corresponds to the identically shaped spot in about the center of the etched view in figure 24. Grain size is comparable to that for the air-tested sample, or about 100 μm on an average. The dark spots or pockets are larger in figure 24 than for figure 23 but also randomly scattered. In figure 24 near the edge, the dark spots are noticeably smaller and fewer. This is attributed to an extrusion effect rather than an effect related to the CO_2 environment. Material S24-2 for the CO_2 test was YSZ like the S19-1 material for the air test but from a different batch with ZrO_2 and Y_2O_3 taken from different batches also. A semi-quantitative spectrochemical analysis on these two materials revealed about one-half as much Al_2O_3 in the S24-2 compared to the S19-1 material. Of the order of 1/2 weight percent of ThO_2, HfO_2 and BeO, and about one weight percent of Dy_2O_3, were contained in S24-2, while none of these oxides were detected in the S19-1 sample. These oxides may explain the larger pores in the S24-2 photomicrographs. The conclusion drawn from the figure 23 versus figure 24 photomicrographs is that CO_2 is not harmful to YSZ.

Figure 25 shows photomicrographs of the as-tested S27-4 heater tube sample. In this test, steam passed through the tube against the surface shown as an edge in the figure 25 photomicrographs. The tube was exposed to air on the outside. The material in S27-4, from a batch different from S19-1 and S24-2, contained about the same amount of Al_2O_3 as in S19-1, about the same ThO_2, HfO_2 and BeO as in S24-2, and no Dy_2O_3. On the average, the grain size appears to be slightly smaller (about 70 μm) relative to the S19-1 grain size. Pores are about the same size as in S19-1 but with more of them and the S27-4 pores are seen to be more circular or elliptical as compared to those of the S19-1 material.

The large void (200 μm long) in the unetched view of figure 25 is typical of those found in the extruded parts. This particular void probably is relatively long in the longitudinal direction (into the photograph) and occurs when small air bubbles pass through the extrusion die. These voids have not presented problems during this phase of the program; however, steps will be taken to reduce their size or eliminate them in the next phase of the advanced biowaste resistojet program. Figure 26 shows a 200X and a 20X photomicrograph. The 20X figure reveals typical longitudinally stretched voids due to air bubbles in the extrusion. Comparing the smaller voids in the 200X figure 26 against the unetched figure 25, the normal sized-randomly scattered voids are seen to be generally spherical in shape.

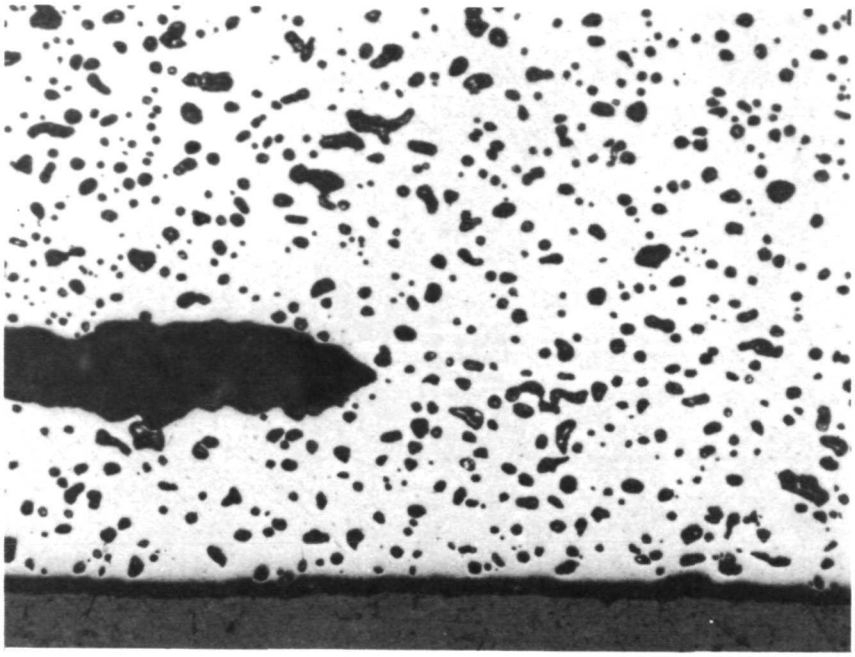

UNETCHED 200X

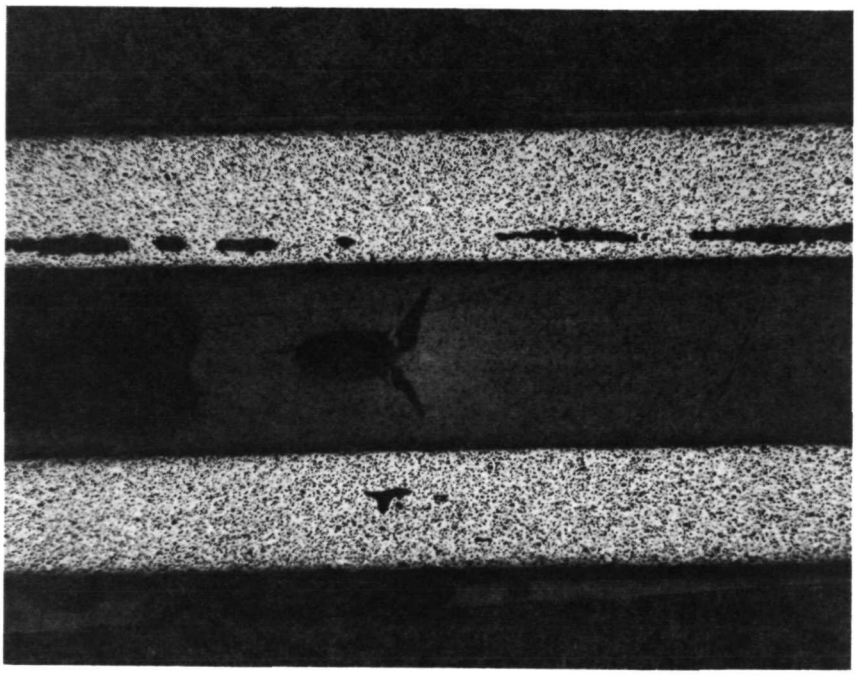

UNETCHED 20X

Figure 26.- Longitudinal section of ceramic heater tube sample S27-4 after test.

The figure 25 and 26 photomicrographs indicate that there is no apparent chemical reaction problem in heating steam with YSZ ceramic heaters. The S27-4 test condition was 1950°K for 500 hours. Based on the CO_2 and H_2O test results after 500 hours exposure, it appears that the YSZ material will be suitable for thousands of hours of hot-time exposure with these biopropellants.

A 500-hour test at 1980°K was conducted on heater S19-3 in a vacuum. This material was identical to the S19-1 shown in figures 22 and 23. The test S19-3 ceramic heater was started in air using a nichrome wire-wound preheater and was then covered with a bell jar and pumped down to vacuum donditions. For the first 90 hours, bell jar pressure ranged from 0.5 to 1×10^{-4} Torr. For the final 410 hours, pressure was in the 10^{-5} Torr range. The objective of this test was to determine if a relatively hard vacuum would cause a problem (such as reduction) with the YSZ material. In the present thrustor design (figure 17), the ceramic heater is completely surrounded by the propellant at chamber pressure. However, it may be desireable in final thrustor designs to expose one side of the heater to a vacuum environment. The S19-3 test serves to verify that this environmental arrangement is practical. The complete vacuum environment is considered more severe than vacuum on one side. In the later case, any reduction tendency would be compensated for by the tendency of oxygen ions to diffuse to the region of the vacuum.

Figure 27 presents photomicrographs, unetched and etched, for the S19-3 heater element. The two photomicrographs are of the same region and can be correlated by the prominent dark spots near the bottom of the etched view which corresponds to almost mid-way up in the unetched view. Comparing figure 23 for air at 289 hours against 27 for vacuum at 500 hours, the grain size is considerably smaller for the vacuum-tested sample S19-3. Average grain size in the S19-3 photomicrograph is about 20 μm versus about 100 μm for the in-air S19-1 sample. Pore sizes are also smaller in the S19-3 sample and of greater number density.

These results, figures 23 versus 27, are especially interesting and significant. Grain growth is believed to proceed rapidly during the first hours of testing, particularly while final sintering is occurring. The smaller grained structure is considered to have the best thermal-mechanical strength. If a vacuum curing could be used to develop the small grain size as indicated by the test S19-3 results and if subsequent exposure to the biopropellants resulted in relatively slow continued grain growth, the vacuum curing might be used to develop better thermal-mechanical strength characteristics. This approach will be investigated further during the next program phase and would be of value for solid electrolyte applications of YSZ as well as for the advanced resistojet application.

A conclusive explanation for the smaller grain size in the S19-3 vacuum test cannot be made at this time. Two possible effects can be considered based on the fact that minute impurities or voids within the material tend to suppress grain growth. The vacuum condition would tend to increase the evaporation rate of certain lower vapor pressure trace impurities causing

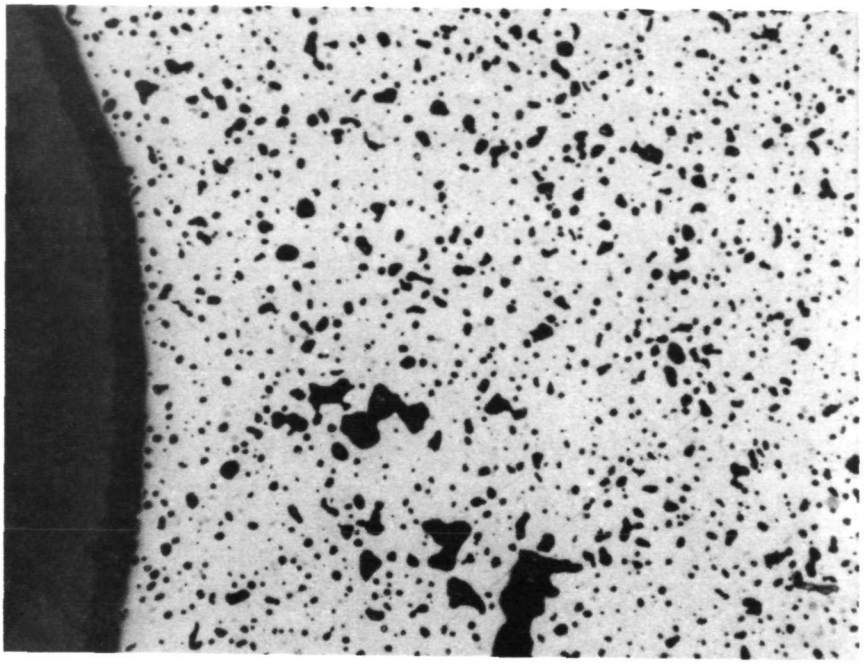

UNETCHED 200X

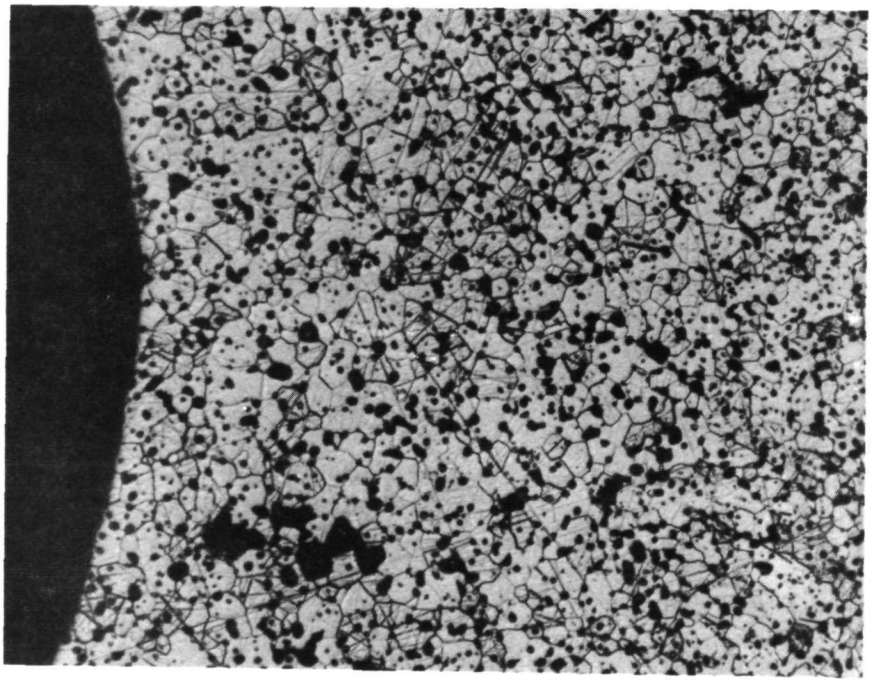

ETCHED 200X

Figure 27.- Ceramic heater tube sample S19-3 after test.

these to be dispersed or to form small voids. On the other hand, a partial reduction of the oxides to suboxides and metallic elemental particles could have the effect of a dispersion of particles and suppression of grain growth.

The post-test appearance of the S19-3 (vacuum) heater was similar to that of the S19-1 (air) heater in that both parts had a satin-like lustre. The S19-3 part was a light yellow-orange color while the S19-1 part was pure white. The color of the S19-3 part indicates that some suboxides did form. The degree of color change was slight and suggests that the degree of suboxide formation is not significant nor harmful. The formation of some suboxides or metallic elemental particles is further substantiated by a small 15% decrease in resistance for the S19-3 test relative to 4% decrease for the S19-2 test in air (see table XI). These changes in electrical characteristics are discussed in detail in the next section.

The test in nitrogen serves as a further evaluation of the ceramic heater's stability in a depleted oxygen environment. In the nitrogen tests (S24-3 and -4), the post-test examination revealed a porcelain white color to the ceramic indicating that suboxides did not form. Ceramic heater S24-4 was operated with nitrogen gas flowing through the tube. The outside of the tube was in a relatively stagnant N_2 environment as was the S24-3 ceramic heater.

The non-flowing ceramic heater S24-3 operated 500 hours at which time the test was terminated. The flowing heater S24-4, however, suffered a failure due to fracturing at one of the electrodes at 454 hours into the test. Both heaters were operated at constant wall temperatures midway along the heated length of 1935°K. An examination of the break in S24-4 revealed a gray color in the immediate vicinity of the break. This was apparently due to diffusion of electrode metal into the ceramic. In previous tests in air, CO_2 and vacuum, relatively slight coloration of the ceramic was noted at the electrodes where the electrode metal touches the ceramic heater. From the increased extent of the coloration in the S24-4 broken section, it appears that electrode metal diffusion into, or reaction with, the zirconia heater is accelerated in the nitrogen environment, It is also suspected that the electrode cement used was contaminated with chlorine, known to be harmful to zirconia.

Two Pt-20 Rh alloy tube samples were cut from a common tube 0.016 cm (.040 inches) I.D. and 0.021 cm (.054 inches) O.D. These tubes were heated by electric resistance heating in a bell jar to hold a vacuum environment on the outside of the tubes. The tubes were brazed to stainless steel supply and exhaust tubes to provide for the passage of a biopropellant gas on the inside of the tube. Test item S41-1 was supplied with 1.1 weight percent O_2 and the balance commercial grade CO_2 while test item S41-2 was supplied with commercial grade CO_2. The mixture was premixed by Air Products Co. A maximum tube wall temperature was set for both tube samples at 1500°K. The test was continued for 215 hours at which time tube sample S41-1 developed severe leakage. Cracks were visible near the inlet end at a station corresponding to 1360°K in the S41-1 sample.

Table XII identifies the stations along each tube examined micrographically. The stations were chosen to correspond to the same tube wall temperature in both samples. The tube samples had overall lengths of 65 mm between their braze joints where they were joined to the stainless steel tubes. The mass flow rate of gases used for this test was about 4×10^{-4} grams per second.

TABLE XII

PLATINUM - 20% RHODIUM TUBE SAMPLE TEST CONDITIONS

Station	Tube Wall Temp. °K	Distance from Upstream braze joint, mm	
		S41-1	S41-2
1	1360	17	17
2	1500	35	35
3	1350	54.5	52
4	1220	60	58

Unetched photomicrographs at 200X magnification of the two upstream stations 1 and 2 are presented in figures 28 and 29 comparing typical wall sections for the S41-1 and -2 samples. The station 1 location for S41-1 shown in the upper photomicrograph of figure 28 reveals grain boundary corrosion in the form of connected voids. A typical zig-zag path is seen slightly to the right of center in the upper figure 28. Relatively little corrosion is apparent in the S41-2 sample at station 1. Moving downstream to the maximum temperature station 2, more severe material depletion is seen for the upper case (S41-2) in figure 29. Here the voids do not connect with the O.D. of the tube and no leakage was apparent. The material depletion near the I.D. indicates a carbonyl type corrosion is occurring at station 2 for the $CO_2 + O_2$ mixture with little or no corrosion for the S41-1 case (CO_2 alone).

Figure 30 indicates the condition of tube S41-1 at the downstream stations 3 and 4. No corrosion was apparent at these stations for the S41-2 tube. Comparing station 3 in figure 30 against station 1 (upper figure 28), for the S41-1 sample at about the same wall temperature, grain boundary corrosion appears to be at least as severe at the downstream station 3 or possibly more so. The S41-1 sample at station 1 did leak as was evidenced by surface eruptions visible in the macrophotos. Smaller but similar eruptions were visible at the station 3 location indicating that that station would have soon developed leakage paths also.

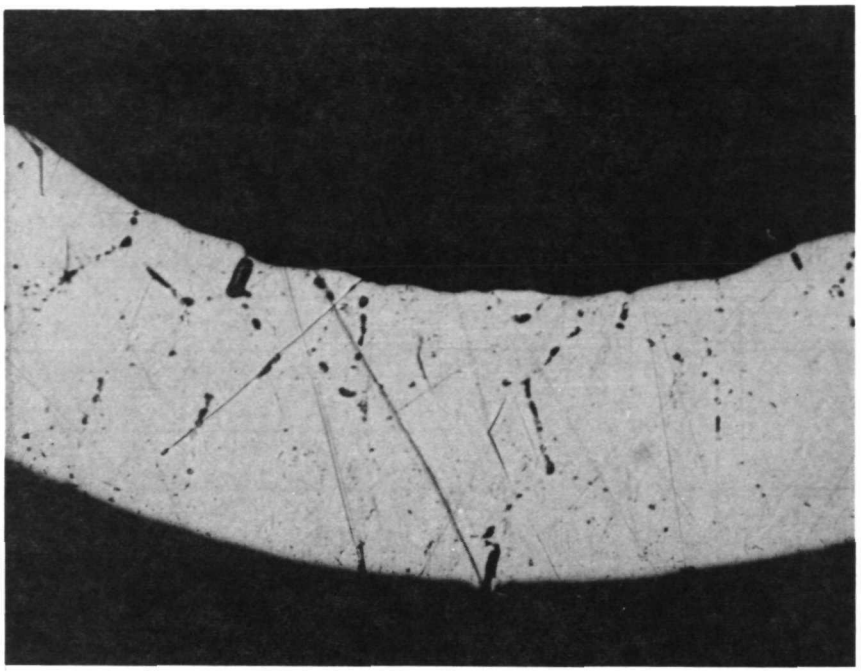

SAMPLE S41-1, CO_2 + 1.1% O_2 200X

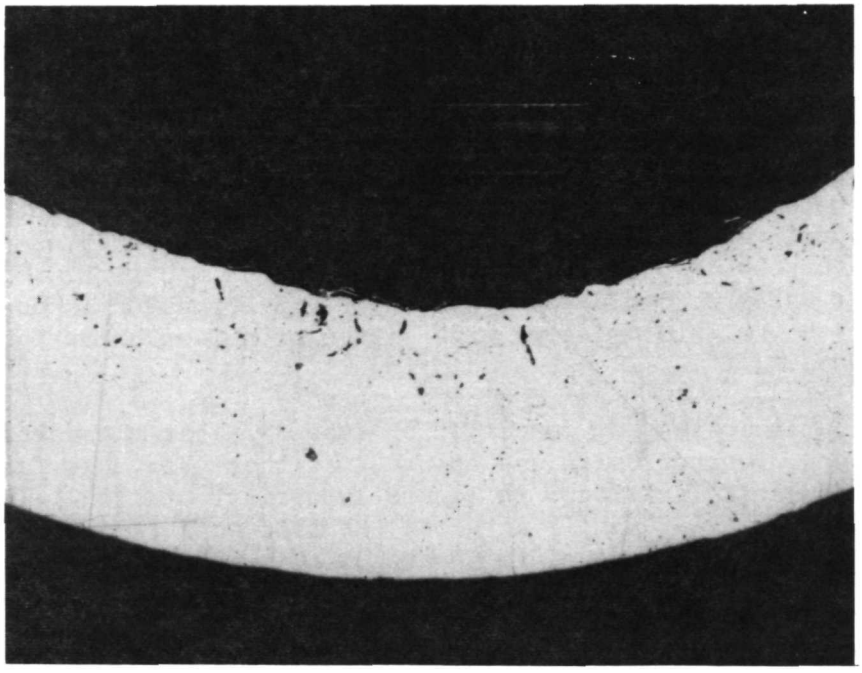

SAMPLE S41-2, CO_2 200X

Figure 28.- Pt-20 Rh tube sample at station 1 (1360^{o}K)

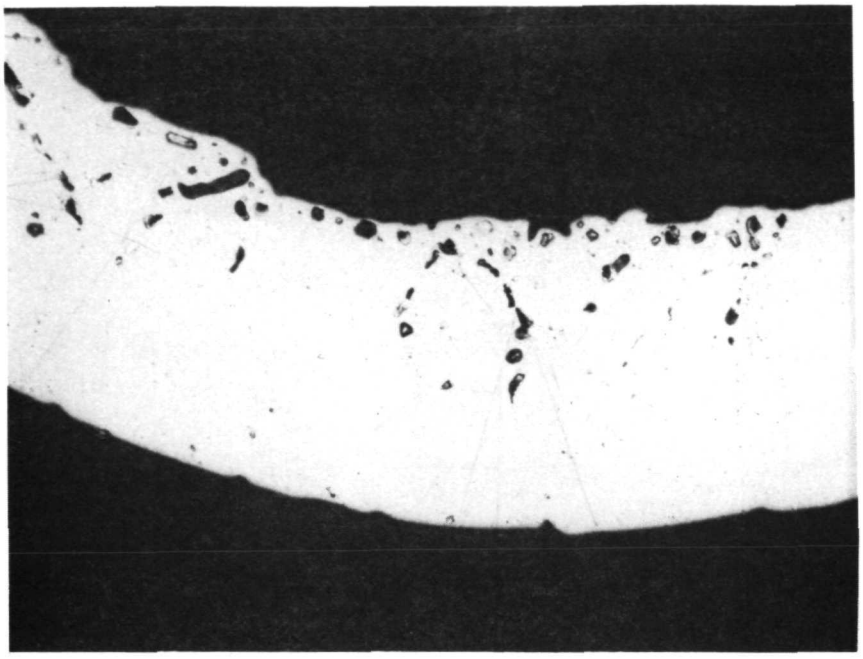

SAMPLE S41-1, CO_2 + 1.1% O_2 200X

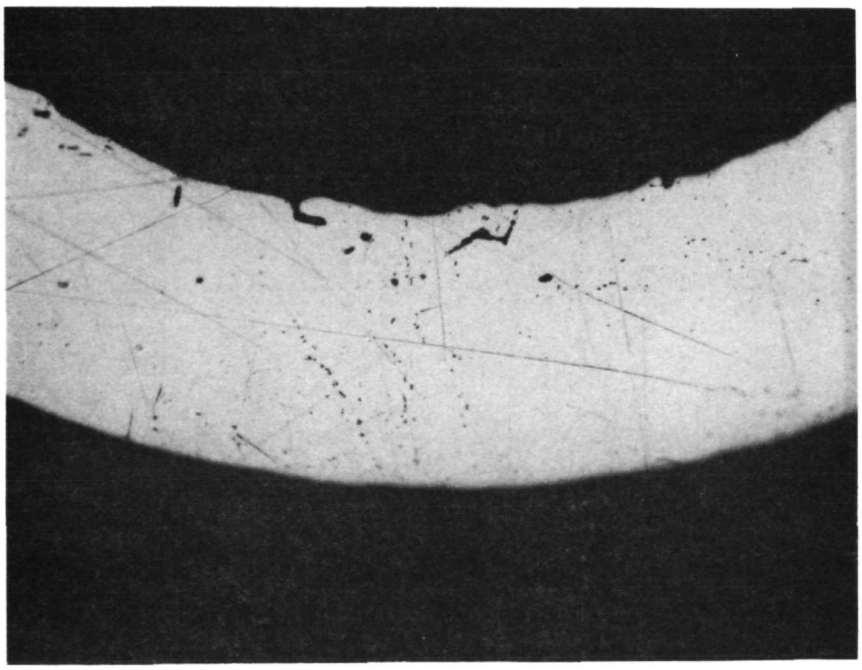

SAMPLE S41-2, CO_2 200X

Figure 29.- Pt-20 Rh tube sample at station 2 ($1500^{o}K$)

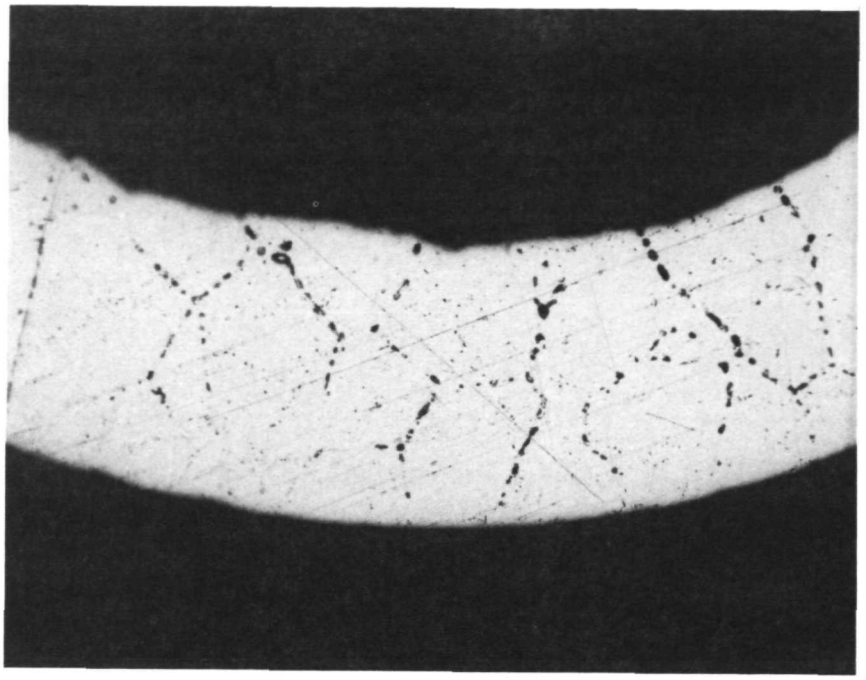

STATION 3 , 1350°K 200X

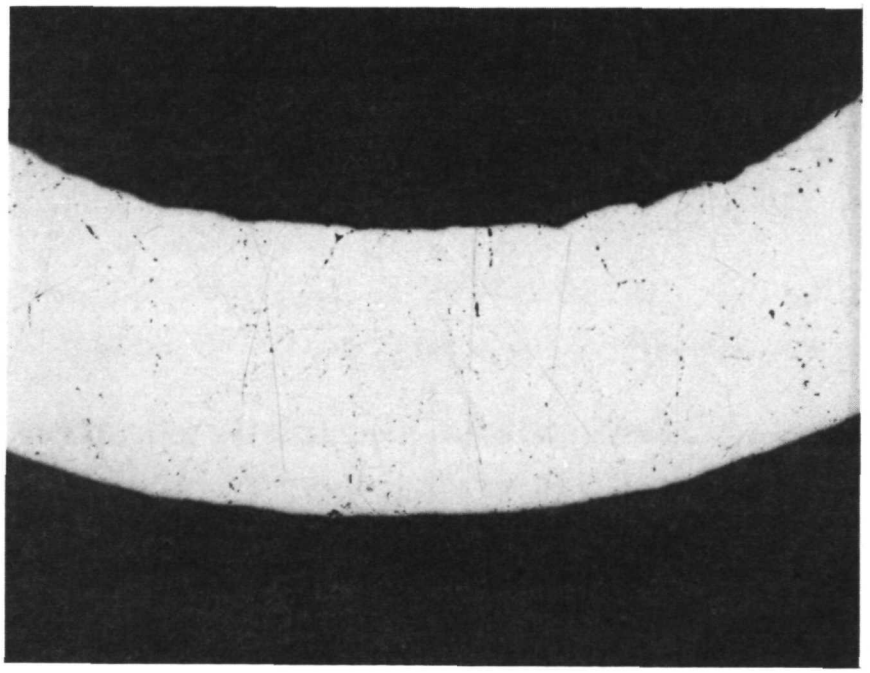

STATION 4, 1220°K 200X

Figure 30.- Pt-20 Rh tube sample S41-1, CO_2 + 1.1% O_2.

The conclusion reached from these observations is that if the corrosion was due to oxidation alone, oxygen would be consumed in passing through the tube and a lesser reaction would be apparent downstream at station 3. Another corrosion mechanism believed to be a carbonyl reaction seems to be evident. While one would expect the addition of a trace of oxygen to CO_2 to suppress the formation of CO by shifting the equilibrium equation

$$2CO_2 \rightleftarrows 2CO + O_2 \tag{21}$$

to the left, it appears that intermediate reaction kinetics are involved and that the trace addition of O_2 is increasing the mass fraction of CO.

It was also considered possible that the Pt-20 Rh alloy was contaminated and that oxidation corrosion was occurring at the grain boundaries where the impurities concentrated during grain growth. A spectrochemical analysis was conducted on the as received Pt-20 Rh tube material and revealed minor amounts of impurities as shown in table XIII.

The furthest downstream station examined, station 4, revealed minor corrosion (see lower figure 30) and indicates that Pt-20 Rh can be used at temperatures to about 1200°K without severe problems with CO_2, with or without a trace amount of oxygen. Pt-20 Rh will be used for the regeneration coil with temperatures not expected to exceed 1000°K. TD platinum will be used for the nozzle to avoid carbonyl corrosion in this region.

TABLE XIII

RESULTS OF SEMIQUANTITATIVE SPECTROCHEMICAL ANALYSIS

OF PT-20 RH TUBE SAMPLE

Element	Amount, w/o
Pt	Remainder
Rh	20.
Au	0.041
Fe	0.053
Cu	0.0003
Pd	0.0083
Ti	0.020
Ca	0.0011
Other	Nil

Electrothermal Characteristics

A simple electrical circuit indicated in the figure 31 schematic was used to determine electrothermal characteristics of the various conducting ceramic configurations tested. These included rods, single hole tubes and multiple hole tubes of stabilized zirconia and rods of thoria. In each test, a ballast resistance R_B was used for stability with the negative resistance characteristic ceramic heaters. In the section THRUSTOR DESIGN: Ceramic Heater Concept, the ballast resistor is discussed and it is pointed out that about 20% of the total power P_T is dissipated in the ballast resistor. For the test results which follow, the ballast resistor values used were arbitrary values generally ranging from about 10% power dissipation in the ballast resistor at low total power to 30% at high total power. The 20% value being considered in the thrustor design at full power is realistic and offers adequate electrothermal stability.

For some of the data presented (figures 32 through 35), the power distribution for the particular test is presented as a ratio of the ceramic heater power P_C to the total power P_T. The power ratio can be shown to be equivalent to the voltage ratio E_C/E_T and also the resistance ratio R_C/R_T for the figure 31 series circuit.

Since

$$P_C = E_C I = I^2 R_C \tag{22}$$

and

$$P_T = E_T I = I^2 R_T \tag{23}$$

then

$$P_C/P_T = E_C/E_T = R_C/R_T = \frac{R_C}{R_C+R_B} \tag{24}$$

The ballast resistance and voltage follow from

$$R_B = R_T - R_C = R_C \left(\frac{1}{P_C/P_T} - 1\right) \tag{25}$$

and

$$E_B = E_T - E_C = E_C \left(\frac{1}{P_C/P_T} - 1\right) \tag{26}$$

Figures 32 and 33 present typical data for a single stablized zirconia heater. This tube was operated at an average temperature of 2000°K in air for 485 hours. The test was terminated by a power lead failure that was a function of the test geometry. The leads supplying power to the conducting ceramic are made of fine stranded platinum wire to prevent excessive conductive

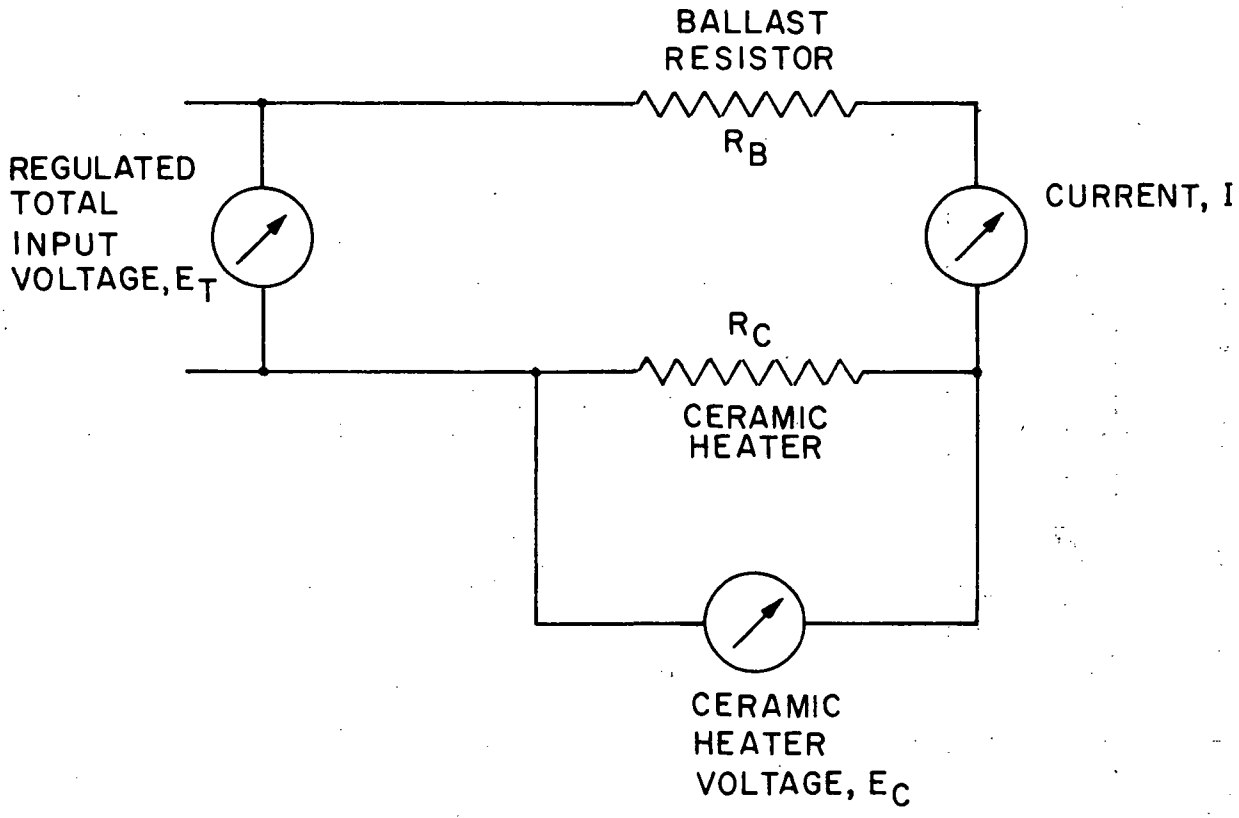

Figure 31. - Ceramic heater electrical circuit.

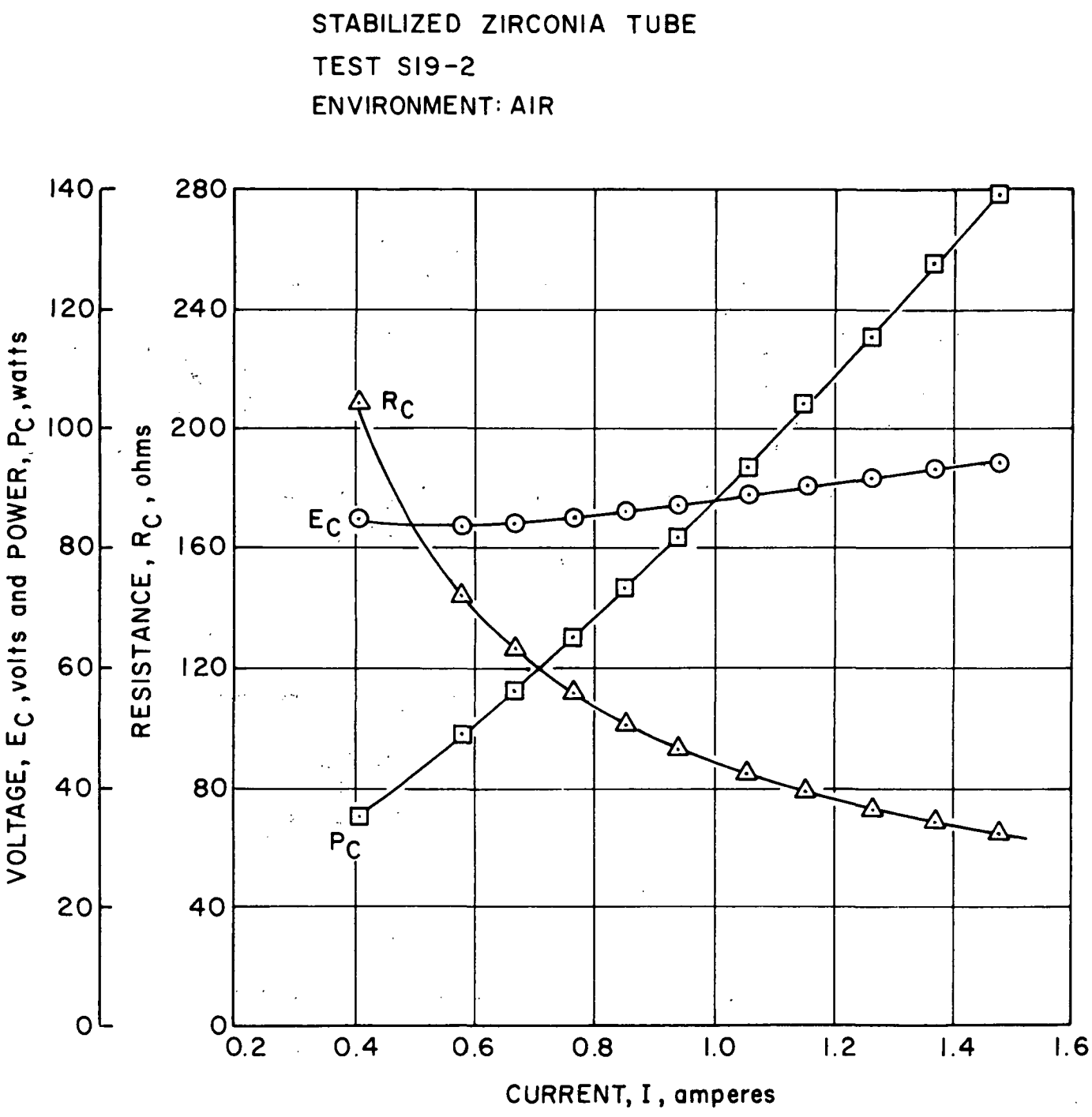

Figure 32. - Ceramic Heater Electrical Characteristics in Air.

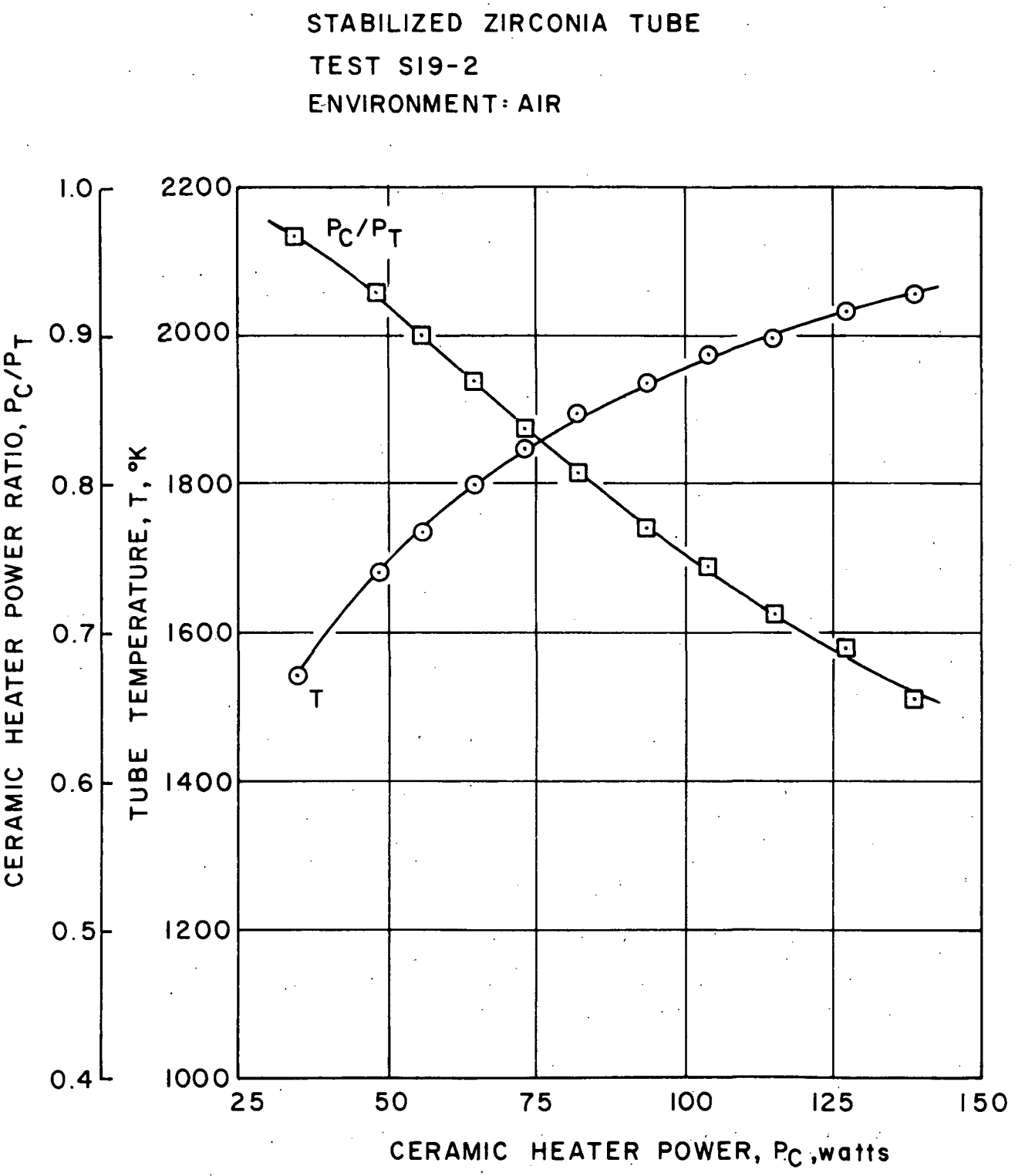

Figure 33. - Ceramic Heater Performance in Air.

heat losses from the wire-ceramic junction. This design forces the wire near the junction to run at a high temperature that is not greatly lower than its melting point. Redesign of the lead and junction to provide a larger wire lead in the critical area and a more favorable temperature gradient should prevent further problems of this sort. No degradation of the ceramic tube itself was noted at the conclusion of the test.

Prior to setting the 2000°K condition in test S19-2, the ceramic heater was operated with typical values of ballast resistance to determine its control characteristics. With a ballast resistance consuming approximately 25% of the total power input to the ceramic heater circuit, it was possible to operate the heater stably to a temperature of less than 1400°K. At lower temperatures, control became difficult when small changes in the thermal environment occurred. With an extreme 2% - 98% power distribution (ballast-to-heater), control down to 1550°K was possible. Thus, there should be no difficulty in obtaining favorable power distributions, where most of the power is dissipated in the ceramic heater. The conducting ceramic heater concept is, therefore, very attractive for biowaste resistojets.

Figure 32 shows ceramic heater voltage varying slightly from 85 to 94 volts for current changing from 0.41 to 1.48 amperes. The corresponding temperature of the ceramic heater tube is shown in figure 33 to increase from 1450 to 2060°K. Temperatures are determined by correcting a narrow band (0.65 micron) pyrometer reading for the emissivity of the ceramic corresponding to wave length and temperature.

In the S19-2 test, a bank of incandescent lamps was used as a ballast resistor. These can be seen in the top view of figure 19. Consequently, the ballast resistance varied from about 6.4 ohms at the lower power condition (0.41 amperes) to about 32 ohms at the high power condition (1.48 amperes). Total voltage required for this test ranged from 88 to 143.5 volts and was controlled by an autotransformer (Variac) operating from a 120VAC service. Had a constant resistance ballast been used, a nichrome resistor for example, ballast voltage drop would have ranged from 6.5 to 23.5 volts for a total applied voltage E_T of 91.5 to 117.5 volts. The corresponding ballast resistance would be 15.9 ohms. These examples are given merely to indicate how the ballast resistor - ceramic heater circuit characteristics are affected by the kind of ballast resistor used.

In a thrustor, the situation is again different. Nominally the thrustor would operate at about constant ceramic heater temperature with the power level varying to suit the enthalpy rise requirements and mass flow rates of the biopropellants (CO_2 and H_2O). In the case of CH_4, the thrustor would operate using power to the ballast resistor and starter resistor without power to the ceramic heater. Using a noble metal coil for the ballast resistor, R_B would be dependent on operating temperature.

Consider the case of CO_2 and H_2O propellant with typical respective total power levels of 160 and 192 watts per table XV of the PERFORMANCE PREDICTIONS section. R_B would be nearly the same for both of these cases since the ballast resistor temperature would be nearly the same for both propellants. R_C would be the same in both cases with the ceramic

heater temperature being controlled to the same set point value. Since $R_T = R_C + R_B$ = constant,

then from equation (23)

$$I = \sqrt{P_T/R_T} = P_T/E_T \tag{27}$$

therefore

$$E_T = \sqrt{P_T R_T} \tag{28}$$

and the ratio of the total applied voltage E_T for the H_2O relative to the CO_2 case is $(192/160)^{1/2}$ or 1.1. Therefore, if the ballast resistor - ceramic heater were sized to operate at 100 volts with CO_2, a voltage of about 110 volts would be used for H_2O. Power control/adaptation requirements are seen to be minimal in this situation.

Electrothermal data similar to that for test S19-2 in air (figures 32 and 33) were obtained in a vacuum environment of 10^{-5} Torr. These data from test S19-3 are presented in figure 34 and 35.

In comparing figures 32 and 33 for the in-air test with figures 34 and 35 for in-vacuum, some differences in electrical performance are obvious. Some difference can be attributed to having taken the characterization for the air test at the beginning of the test versus waiting for some 200 hours into the vacuum test for the S19-3 data. The effect of test time on the various parameters is discussed below. Comparing the power consumption as a function of temperature from figures 33 and 35:

Temperature, °K	Power Consumption, watts S19-2 (air)	S19-3 (vacuum)
1600	40	31
1800	66	67
2000	114	137.5

a crossover occurs. At 1600°K more power is required in air as one would expect to supply both convective as well as radiation heat transfer losses. In the vacuum, convective losses are negligible small. A crossing over occurs at about 1800°K with both cases consuming about 66 watts. At 2000°K, more power is required for the in-vacuum case. This clearly demonstrates that emissivity of the ceramic surface is higher in the in-vacuum case relative to the in-air case. Post test examinations of the ceramic heater surfaces revealed a semi-glossly crystalline-like pure white surface for S19-2 (air) versus a similar surface but yellow-orange in color for S19-3 (vacuum). Visually, but not conclusively relative to total emission, the S19-3 ceramic heater would appear to have a higher emissivity.

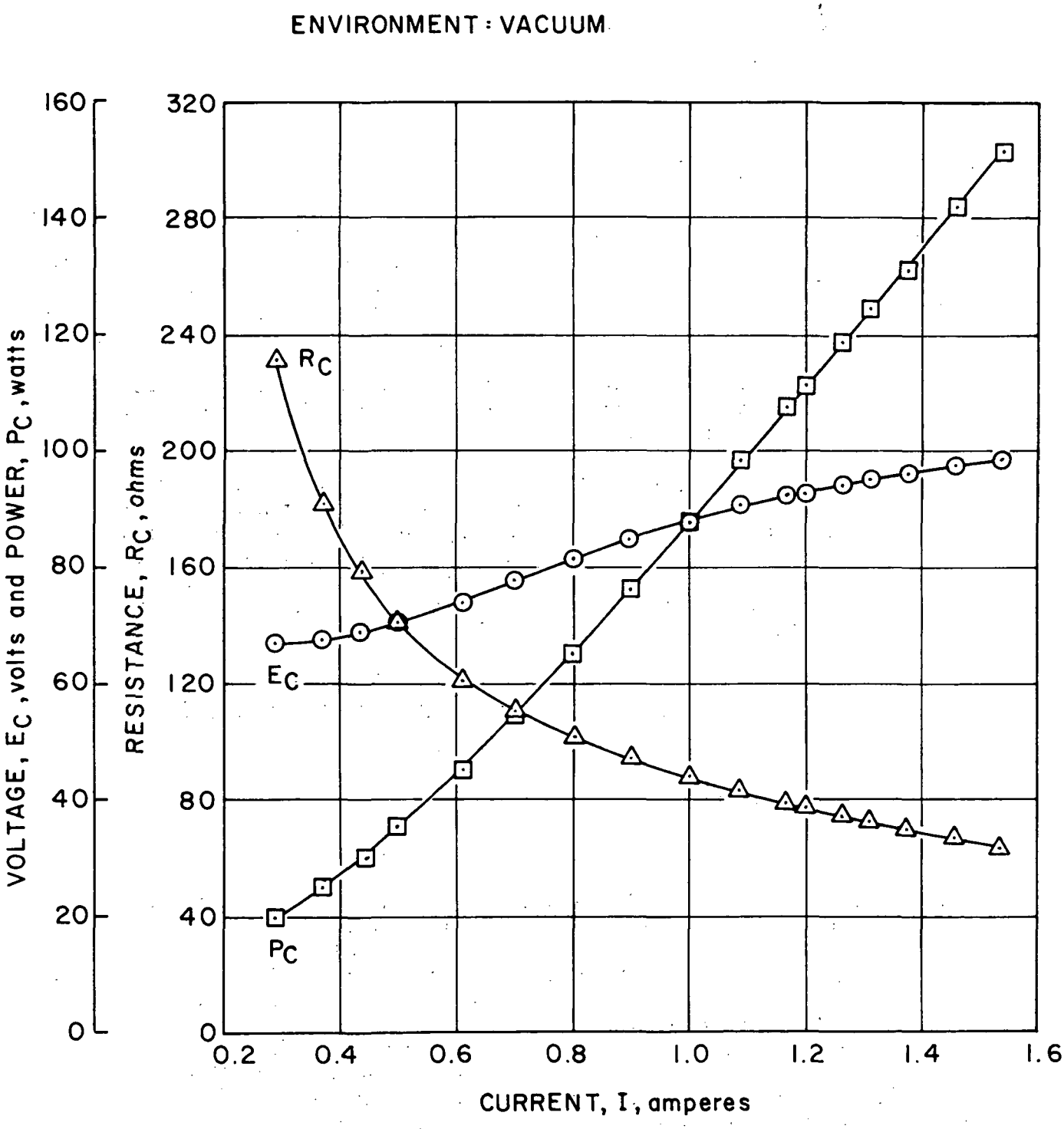

Figure 34. - Ceramic Heater Electrical Characteristics in Vacuum.

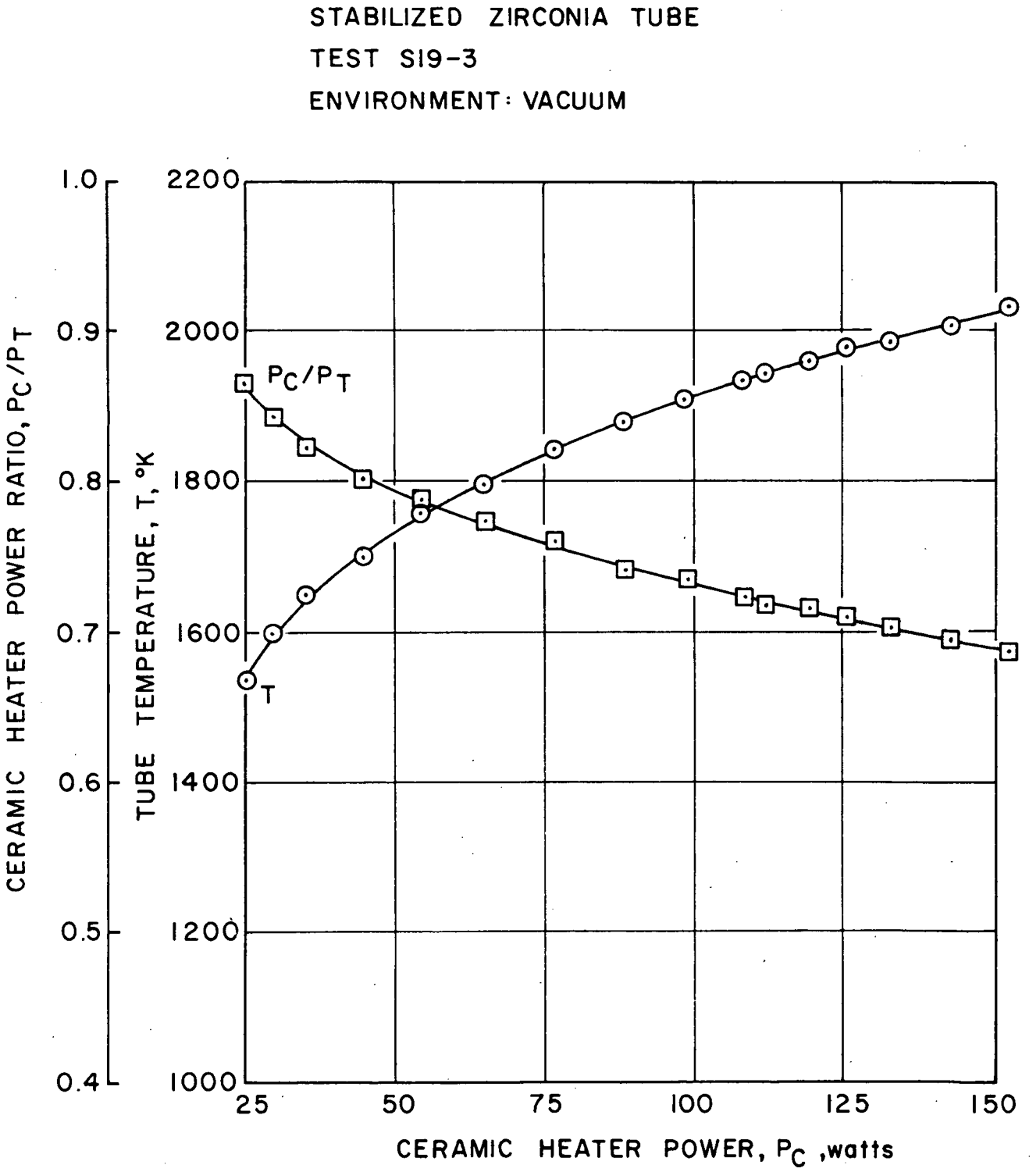

Figure 35. - Ceramic Heater Performance in Vacuum.

The flatter P_C/P_T curve for S19-3 (figure 35) relative to the in-air case (figure 33) is the result of having used a constant ballast resistance of 30 ohms for the S19-3 test. For S19-2, a light bulb bank was used for ballast and resulted in a ballast resistance varying with power from 6 ohms to 32 ohms, low to high power.

Over the time span of 500 hours for tests S19-2 and -3 at constant observed temperature, power increased about 14% for both cases. The measured resistance increased about 6% for S19-2 (air) and decreased about 2% for the S19-3 (vacuum). The ceramic heater outer wall temperature is measured by a precision optical pyrometer and observed temperature is calculated using an emissivity correction. The increase in power can be attributed to two factors:

1. An increase in the emissivity of the ceramic heater surface.

2. A roughening of the surface, which can increase the effective radiating area.

The emissivity effect is considered to be the major cause of the observed power increase. Barely visible to the naked eye is a slight roughening due to minute crystal growth which would contribute some small effect through an effective area change.

Interpreting the power increase as an increase in emissivity, the measured temperature corrects to a lower (by about 50°K) temperature. This follows from the heat transfer equation and the dependence of radiated power on emissivity and on the fourth power of temperature. For example, for the S19-2 test in air:

$$Q_{loss} = 0.018\ (T_S - T_A) + 0.154 \times 10^{-10}\ \varepsilon\ T_S^{\,4} \qquad (29)$$

where T_S is the ceramic heater surface temperature in °K, T_A is the ambient air temperature in °K, ε is the emissivity and the heat loss rate is in watts. The first term in equation (29) is the convective heat transfer term. The estimated 50°K lower temperature interprets into a 10% and 13% increase in resistance from the figure 32 and 34 resistance curves, respectively. The actual net change in resistance over the 500 hours of testing is found to be about 4% decreasing for test S19-2 and 15% decreasing for test S19-3. While true temperature decreased about 50°K over the 500-hour test time (observed temperature being held constant), the average true temperatures for the S19-2 and -3 tests are estemated to be 2015°K and 1980°K, respectively.

Based on the yellow-orange color taken on by the S19-3 ceramic heater in vacuum relative to the pure white color in test S19-2 and on the apparent 15% decrease in resistance (relative to 4% for S19-2), the following is concluded:

1. The vacuum environment resulted in a minor reduction of some oxides constituents in the ceramic heater to probably sub-oxide compounds.

2. Sub-oxide formation would account for the yellow-orange color change.

3. Sub-oxide formation would account for the larger decrease in resistance of the S19-3 than the S19-2 ceramic heater. That is, conductivity is increased with a conversion of normal oxide forms to sub-oxide forms.

It is important to note that 500 hours exposure to the bell jar vacuum did not result in any significant problem. The ceramic heater appeared normal (other than for color) and indicated suitability for vacuum service for lifetimes of the order of 1000 hours.

Normally in a thrustor application, a biowaste propellant will be flowing through the thrustor. However, it may be desirable to expose some ceramic heater surfaces to vacuum on one side. The purpose of test S19-3 was to verify that the vacuum environment would not present an obvious problem area.

Figure 36 presents performance data for the left-hand ceramic heater tube (S24-1) shown in figure 20 taken after 500 hours exposure to CO_2 at a wall temperature of 1935°K. Power consumption for this condition was 122 watts. Performance characteristics for the S24-2 heater tube (see table XI) were similar with a mean wall temperature of 1930°K being held for the 500-hour test.

While both the S19 (figures 32 through 35) and S24 heater tubes are of stabilized zirconia, they were made from different sources of the stabilizer (yttria) and slight differences in electrical characteristics are to be expected. This is mentioned so that minor differences between figure 36 data with previous data are not compared and related to environmental differences alone. Data taken on S24-1 in air and CO_2 revealed essentially no differences in the electrical characteristics. Thermal convection effects with these two different heat transfer fluids were not obvious because of the large radiant heat transfer associated with the bare heater tube at the high test temperatures.

Variable flow data were taken on the S24-2 heater tube without insulation from no flow to a typical 10 mlb thrustor flow of 0.023 grams per second. Wall temperatures measured along the tube with CO_2 flowing from bottom to top in the figure 20 setup were as follows at the extreme flow conditions:

Flow Rate, g/sec	Wall Temperature, °K		
	Bottom	Middle	Top
0	1920	1930	1930
0.023	1830	1930	1940

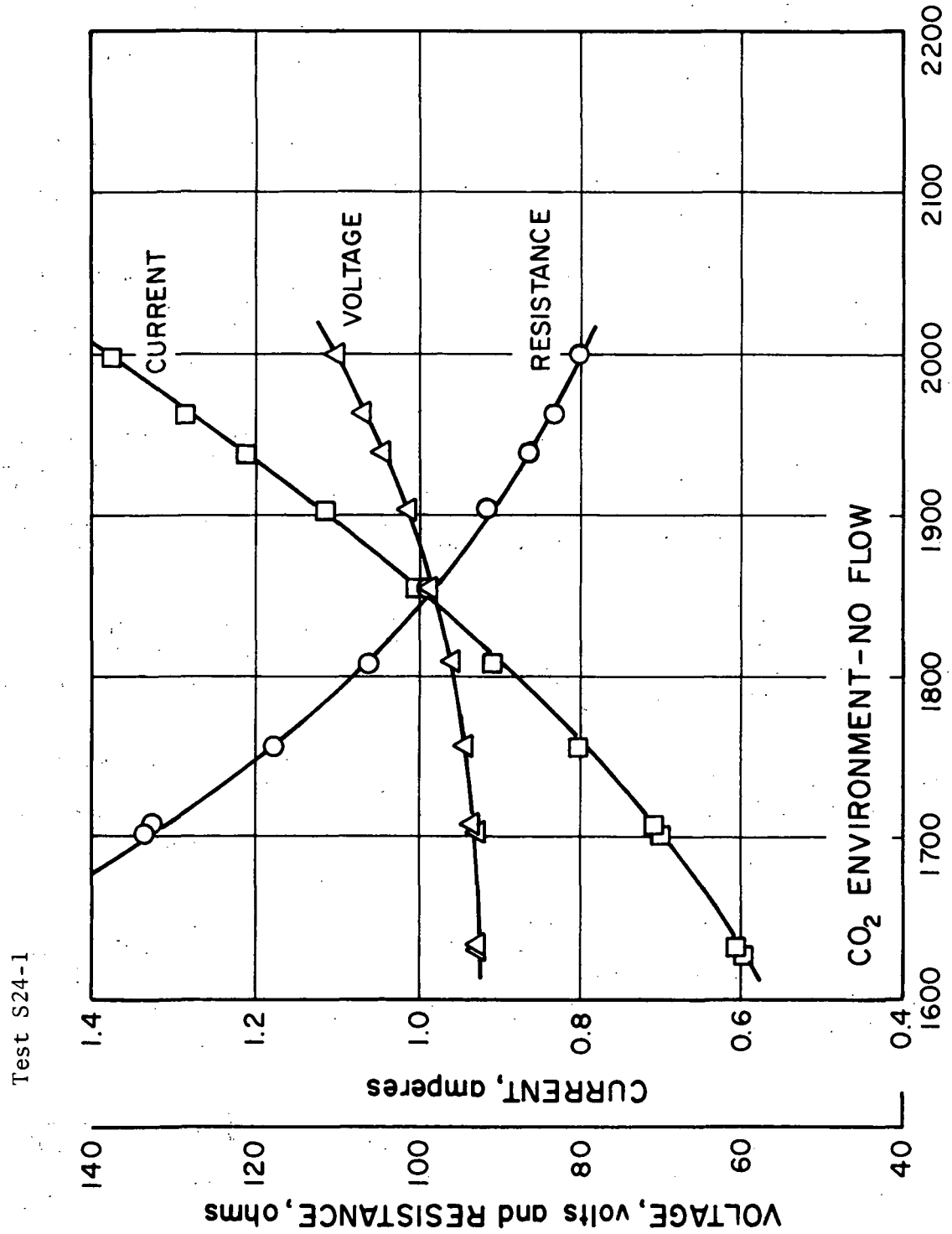

Figure 36.- Electrical characteristics of uninsulated ceramic heater.

Power consumption varied from 118 watts at no flow to 143 watts at the 0.023 grams per second condition. An energy balance calculation indicates that the leaving gas temperature was 1600°K with cold 300°K CO_2 entering the ceramic heater tube.

The ceramic heater tube is a very favorable heater configuration. With flow into a metal tube a large temperature drop would occur as the result of cooling at the inlet end of the heated section. The ceramic tube has compensating electrical characteristics which adjust to the large inlet cooling load. With a decrease in tube wall temperature, there is a large relative increase in local electrical resistivity. The ohmic heating shifts favorable and considerably toward the cooler region helping to maintain a more uniform temperature gradient than would occur in a metal tube. Thus, for a given tube length, considerably more energy can be transferred to a gas with a ceramic heater as compared to a metal heater tube.

The mean convective heat transfer coefficient for the 0.023 grams per second flow condition is about 0.027 watts/cm^2-°K based on the experimental data. This agrees with a theoretical value based on a Nusselt number of 3.65 corresponding to a constant wall temperature and laminar flow. That is

$$Nu_D = \frac{hD}{k} = 3.65 \qquad (30)$$

where D is the ceramic heater tube inside diameter and k the thermal conductivity of the gas.

Figure 37 presents electrothermal data obtained with a thoria rod heater element in air. This heater was powered up to failure which occurred at a rod temperature of 2775°K. The failure occurred in the platinum wire electrode which actually melted under the electrode cement. The electrode had not been thermally sized for this high temperature condition. Thoria has a significantly higher resistivity as compared to zirconia and requires a greater preheater temperature for ignition. For comparison purposes, the zirconia rod heaters tested could be stably operated to as low as 1400°K while the particular thoria rod heater tested (S57-1) would not operate below about 1900°K. For the figure 37 data, voltage is seen to be relatively constant, dropping from 90.7 volts to 85.8 and then increasing to 88.7 volts as temperature increases.

Figure 38 presents electrical characteristic data for the insulated demonstration heater with a CO_2 mass flow rate of 0.022 grams per second. This mass flow rate is typical of a 10 mlb thrustor (at a specific impulse of 200 seconds). The simple tubular ceramic heaters being used for preliminary tests happen to have a size more closely associated with a 10 mlb thrustor. Comparing figure 38 to figure 36 for a no-flow situation, the voltage trend is seen changed to a downward one. This is the result of the flowing propellant and in part the result of flowing cold (298°K) CO_2 into the heater. This presents no problem. In a realistic regenerative heater, the propellant to the ceramic heater would be about 900°K and the

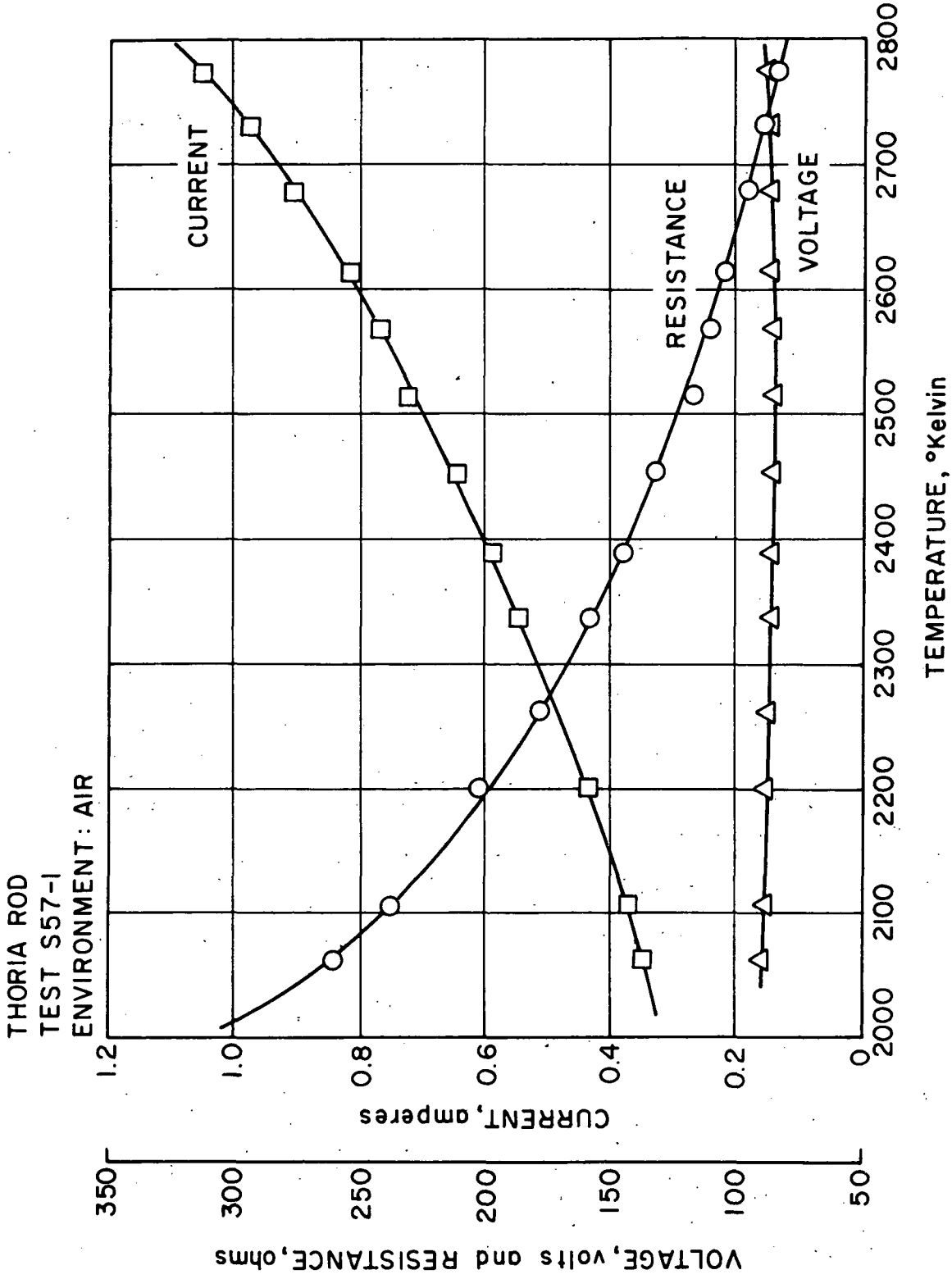

Figure 37. - Electrical characteristics of a thoria rod ceramic heater.

Chamber Pressure = 1.0 atmospheres
Inlet Temperature = 298°K
Test S24-7

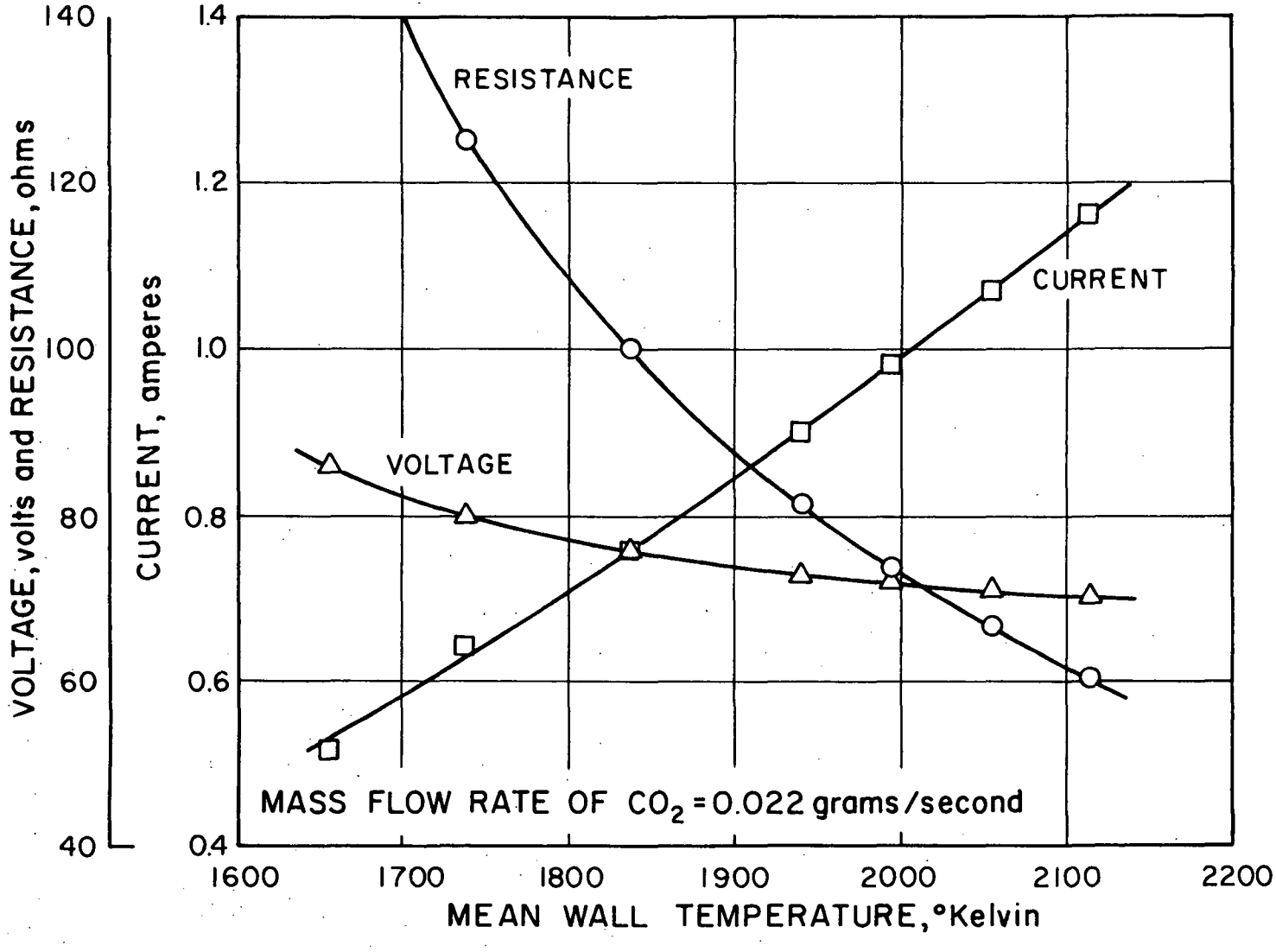

Figure 38. - Electrical characteristics of insulated ceramic heaters.

voltage would be relatively constant. Correspondingly less power (lower voltage-lower current) would be used in this situation for two reasons:

(1) The required propellant temperature rise in the ceramic heater would be reduced to about one-half.

(2) The regenerative section of the thrustor would present an increased temperature surface (relative to the figure 38 case) and reduce heat losses from the ceramic heater.

In all of the data presented here, the ceramic heaters were operated in a stagnant ambient temperature environment resulting in greater heat losses than would be experienced in a thrustor assembly.

Power consumption of the insulated heater is greatly reduced compared to a bare heater tube as shown in figure 39. For example, at 2000°K electrical power is reduced from 141 watts to 38 watts with the 0.5 cm thick zirconia felt insulation shown in figure 21. The data of figure 39 are for two different heaters from the same group, the bare S24-1 and the insulated S24-7. Ceramic heater tubes from each group tested have had essentially the same performance characteristics, therefore, the figure 39 data are a valid evaluation of the insulation performance.

Corresponding to the figure 38 data, final gas temperature and power distribution curves are shown in figure 40. The mean wall temperature given by the abcissa corresponds to the measured electrical resistance for a uniform (no-flow) wall temperature case. The mean wall temperature physically occurs about 60 percent of the way along the heated portion of the tube from the inlet end electrode. The negative resistance characteristic of the ceramic heater is a fortunate property from a gas heating device point of view. In a metal tube used to resistively heat a gas, an extreme temperature gradient occurs along the tube as the result of a flowing in a cold gas and the particular electrical characteristics of the metal. In the ceramic heater, a compensating power distribution effect results from the ceramic's negative resistance characteristic. As the inlet end of the tube is cooled by propellant, its local resistance increases considerably for the local I^2R (ohmic) heating also increases considerably. For the flow conditions indicated in figures 38 and 40, a metal tube would suffer a temperature gradient along the heated length in excess of 1000°K. For the ceramic tube, the temperature gradient along the tube is about 200°K. Thus, for a given length, size, and maximum temperature, the conducting ceramic heater tube becomes a much more efficient heating device than a resistively heated metal tube.

Figure 40 indicates the amount of total electric power used and how much actually goes into the propellant. The difference, the power loss, is comparatively large as the demonstration heater data are for a cold ambient environment. The final gas temperature is, therefore, seen to be relatively low compared to the mean wall temperature. Figure 41 indicates how the final gas temperature changes with mass flow rate, again CO_2, for a cold inlet condition of 298°K and constant mean wall temperature of 1940°K. Also shown are pressure drop for the power condition and for a cold flow

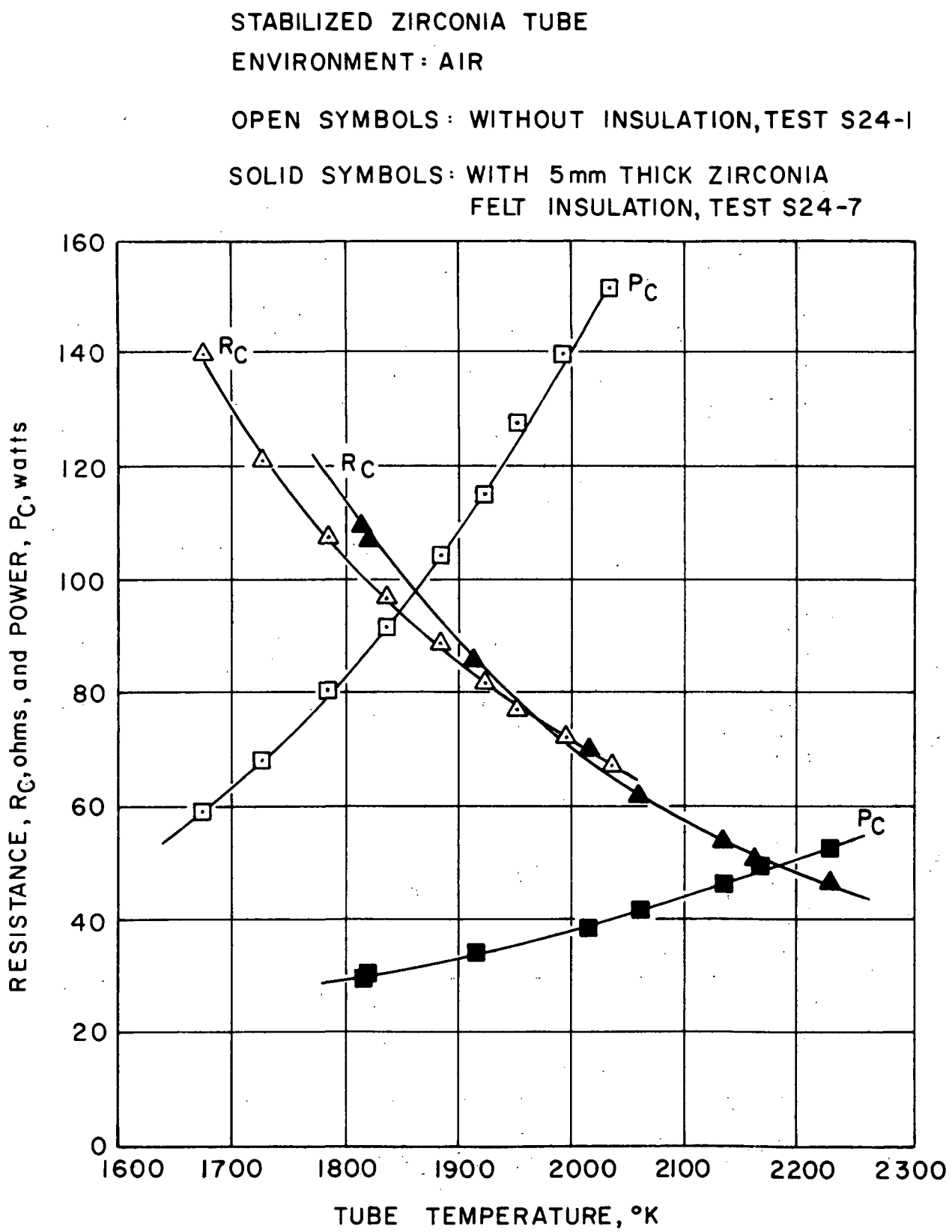

Figure 39. - Ceramic heater performance.

Chamber Pressure = 1.0 atmospheres
Inlet Temperature = 298°K
Test S24-7

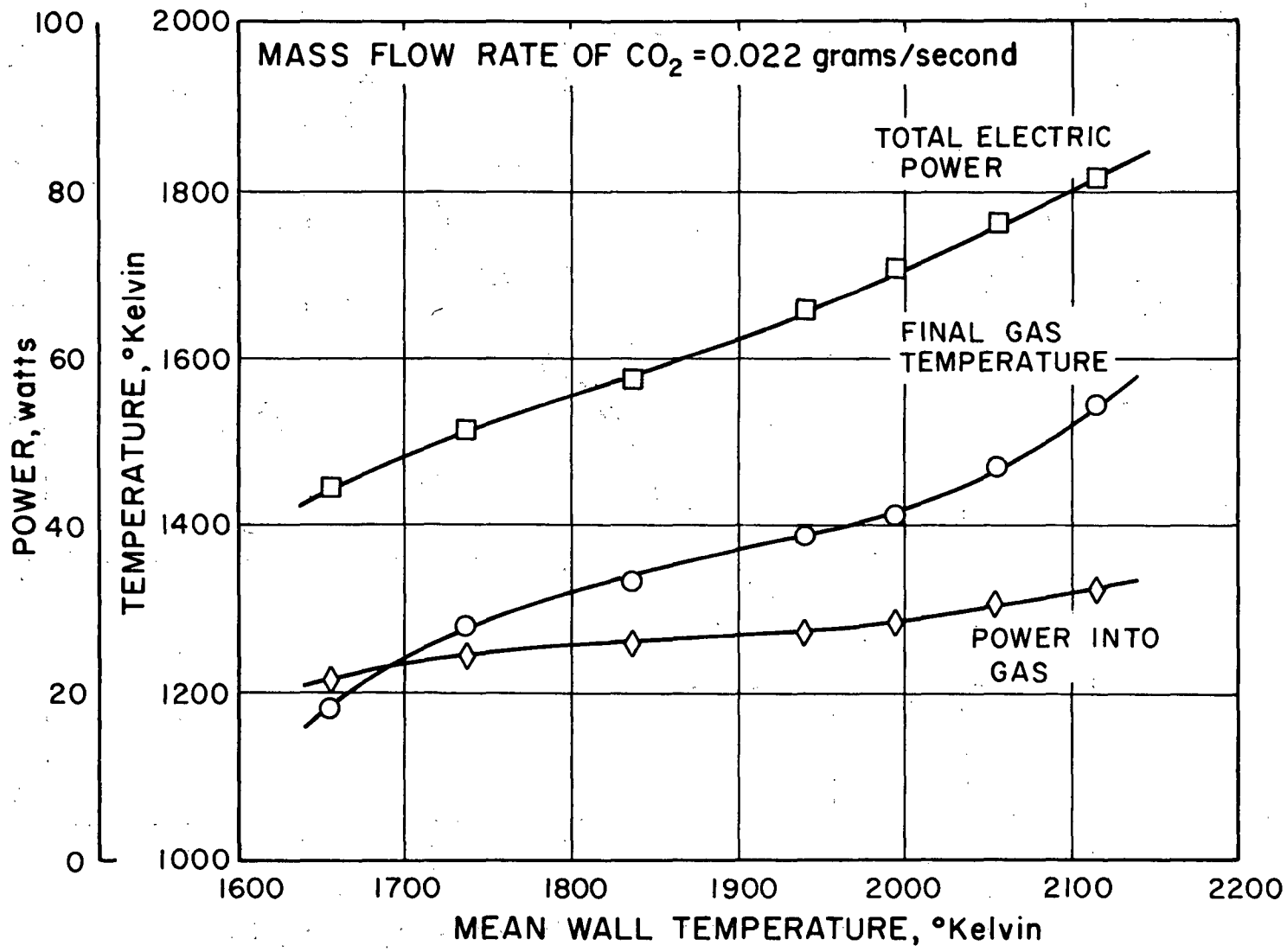

Figure 40. - Thermal performance of a single passage ceramic heater.

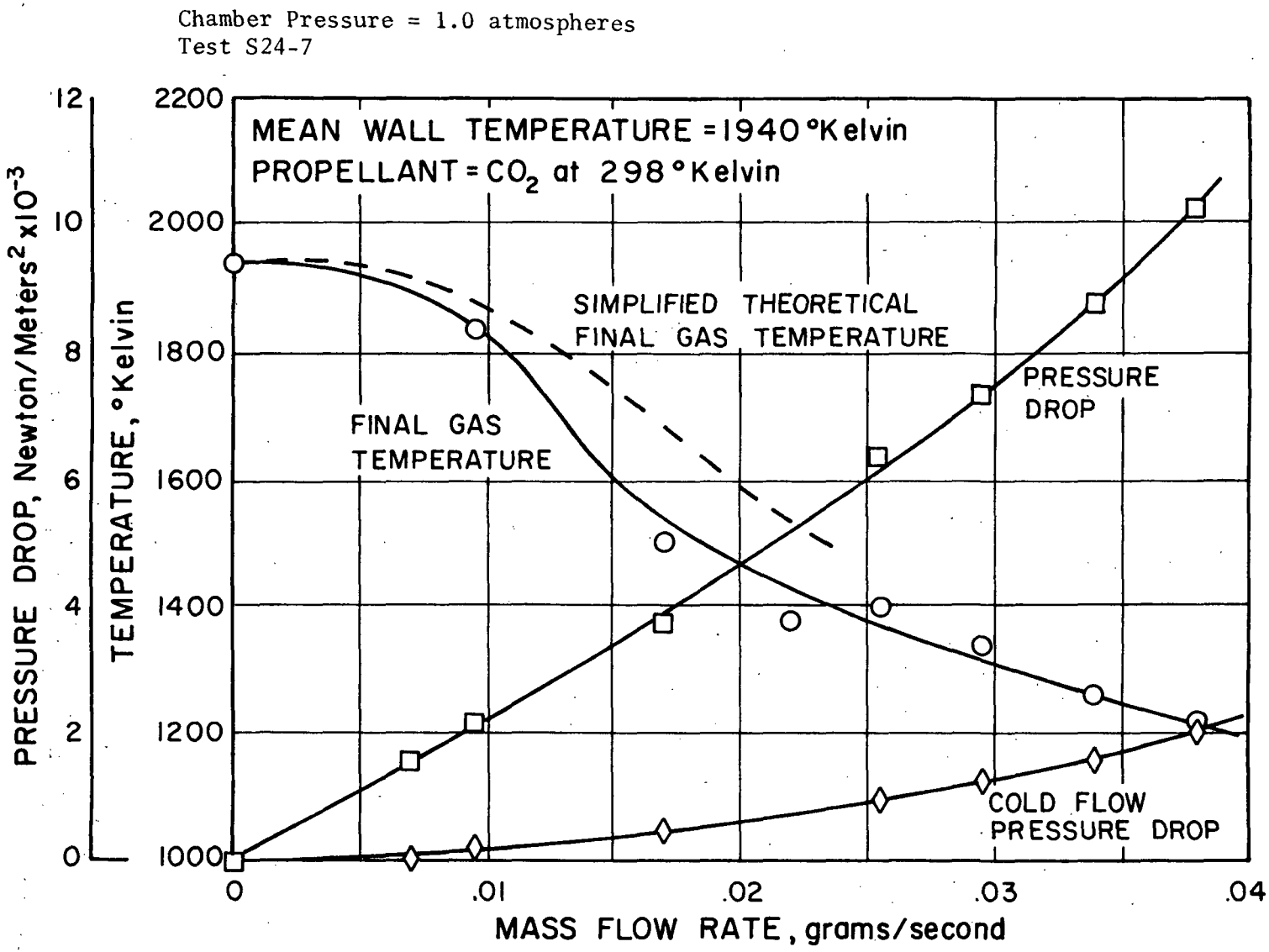

Figure 41. - Effect of mass flow rate on single passage ceramic heater.

condition. The pressure drop occurs over a total ceramic tube length of 60 mm, of which 34 mm are heated. Reynolds numbers are low for the figure 41 data, 450 based on diameter, for example, at 0.025 grams per second. Therefore, the flow in the ceramic heater tube is quite laminar. At flow rates up to about .015 grams per second, the Nusselt number closely follows the theoretical 3.65 value corresponding to a constant wall temperature situation and then increases rapidly to 6.0 at 0.04 grams per second as entrance effects become significant.

From structural and thermal efficiency points of view, it is desirable to have a relatively short ceramic heater. Consider a hypothetical thrustor requirement calling for 10 mlb of thrust at a specific impulse of 180 seconds with CO_2. The corresponding mass flow rate would be 0.025 grams per second. Consider for the moment, that the ceramic heater is used without regenerative cooling and has a cold (298°K) inlet condition. Then from figure 41, it is seen that a final gas temperature of about 1400°K would result with a mean wall temperature of 1940°K. Incidentally, the maximum wall temperature occurring at the downstream end of the heated portion of the ceramic tube is 1960°K at this flow condition.

A higher final gas temperature can be achieved by using a multiple channel ceramic heater tube. This is shown in the THRUSTOR DESIGN: Thermal Analysis section by equations (1) through (3). Equation (2) has been used to indicate the gas temperature curve shape for variable flow as shown dashed in figure 41. The hypothetical case of 0.025 grams per second was used as a reference point with the following values of the variables:

$T_{wall} = 1940°K$

$T_{gas\ initial} = 298°K$

$L = 34$ mm

$\dot{m} = .025$ g/sec

$k = 0.10$ watt/(m - °K)

$C_p = 1.34$ (watt-sec)/(g - °K)

$Nu = 4.0$

Taking n at unity for .025 g/sec, then other flow rates represent multiple channel cases corresponding to integer values of n. For example, for n equal to 5, the mass flow is divided into five (5) passages of 0.005 g/sec each. The simplified (dashed) curve in figure 41 is presented to justify the S-shaped curve fit to the final gas temperature data. The use of more accurate values of the independent variables and accounting for the change in the variables with the changing flow conditions would result in close agreement with the experimental results. It is entended here to indicate how rapidly the final gas temperature closes on wall temperature as multiple passages are used to divide the propellant flow.

Using a 5-hole heater, again for the hypothetical case above, the mass flow rate per passage is 0.005 grams per second and a final gas temperature of 1910°K is indicated by the experimental data of figure 41. With the incorporation of regenerative heat recovery and an entrance temperature of 850°K into the ceramic heater, the final gas temperature would be even closer to the wall temperature.

Test S24-7 demonstrated feasibility of insulating a zirconia heater tube with zirconia fiber insulation to effect an improvement in the thermal characteristics of the ceramic heater. While non-optimum electrodes were used, this test also demonstrated that temperatures far in excess (2230°K) of the electrode material melting point (2050°K) could be attained with a relatively well insulated ceramic heater. Finally, the S24-7 test demonstrated an integrated starter heater with a ceramic heater tube. No problems were encountered in the 111 hours of testing of the insulated heater assembly.

Thermomechanical Considerations

Thermomechanical considerations applicable to the specific mechanical design presented in the THRUSTOR DESIGN section were discussed in that section. Other related considerations are presented in this section, including a tensile creep test conducted on a stabilized zirconia heater element and a discussion of ceramic-to-metal seals and joints.

The permanent or plastic deformation of a material with time under conditions of constant load and constant temperature is an important engineering property commonly known as creep. Creep may be due to compressive, tensile or shear loads, or combinations of these. Tensile-creep properties of the ceramic heater material is lacking in the literature and is important to the design of a biowaste resistojet ceramic heater. Test S27-2 (table XI) served as a preliminary evaluation to determine the order of magnitude creep rates to be expected at a typical operating temperature. The heater tube was operated at 1935°K wall temperature for three periods of time as shown in table XIV for a total of 280 hours. Before and after each run period, the overall length of the heater tube was measured to determine the total elongation for each period. Wall temperature was relatively constant (within 20°K) over the entire heated length of 35 mm. A tensile load of 87.0 grams (0.192 pounds) was applied to the heater tube corresponding to a stress of 157 kN/m^2 (22.6 psi). This stress is typical of the hoop stress in a ceramic heater tube flowing propellant and surrounded by vacuum.

TABLE XIV

PRELIMINARY TENSILE CREEP DATA FOR

AN YTTRIA-STABILIZED ZIRCONIA TUBE

Test Period	Time, Hours	Elongation, mm	Rate of Elongation, (mm/mm) /hour
1st	64.4	.356	15.8×10^{-5}
2nd	71.9	.102	4.05×10^{-5}
3rd	143.5	.140	2.8×10^{-5}

The initially high rate of elongation observed during the first test period is attributed to final curing and sintering of the ceramic during the first few hours of testing. Had the tube been operated for several hours without a tensile load before the test, it is believed the measured elongation rate for the first period would have been lower. On an average, it appears that the tensile elongation rate (allowing for an adequate presintering period) is about 3 to 4 $\times 10^{-5}$ per hour for the zirconia tube at 1935°K and a 157 kN/m^2 load.

A detailed discussion of creep deformation and endurance stress is presented in reference 20. Compressive creep data are presented for thoria and zirconia at high stress levels (above 2 x 10^4 kN/m^2). These are extrapolated using an Arrhenius equation to relate steady-state creep rate to stress and temperature. Grain size and impurities affect the creep rate significantly. Large grain material has the lowest creep rate. The endurance limit is noted to occur at about 5% total elongation for zirconia and about 10% total elongation for thoria. Relative to tensile creep, it is suggested in reference 20 that endurance stress be guesstimated in the ratio of the ultimate stresses related to compressive creep data.

Using the 3 to 4 x 10^{-5} per hour creep rate for the preliminary tensile creep data of table XIV the time to 5% creep (assumed endurance limit) would be about 1430 hours. To extend this to about one year, the applied tensile stress would have to be limited to about 25 kN/m^2 (4 psi). Compressive stress would have to be limited to about 250 kN/m^2. The thrustor design presented in figure 17 is predicated on minimizing ceramic heater stress levels to even lower values to insure long lifetime.

The biowaste resistojet configuration presented as figure 17 in the THRUSTOR DESIGN section utilizes ceramic-to-metal seals between the alumina heater support and several metal parts (nozzle flange, regenerator coil and electrode tube). In addition, the electrode wires must form a psuedo bond to the ceramic heater tube. The electrode wire bond is not necessarily continuous or classified as a hermetic seal type bond, but it must provide a sufficient electrical conduction path between the wire and the ceramic to avoid local hot spots or arcing. A variation to the figure 17 design is the one discussed in the THRUSTOR DESIGN section in which a metal nozzle serves as the downstream electrode. In this case, a ceramic-to-metal joint is, in effect, required. Other variations which may prove to be attractive may require ceramic-to-metal seals or joints and may require service temperatures to as high as 1400°K.

A literature search (reference 56) was conducted to determine which techniques were available to effectively metallize ceramic parts to make seals and joints which are applicable to the zirconia and thoria ceramics. In addition, preliminary experimentation was conducted to evaluate a few attractive techniques. Included were test samples of zirconia to which platinum was applied by diffusion bonding and by brazing with an intermediate alloy, and samples of zirconia tubes of different diameters which were joined by sintering.

As a result of the literature search three techniques for metallizing the ceramic heater at joint/seal and electrode locations which appear promising were found as follows:

1. Hydride brazing process

2. Active metal brazing process

3. Deposition by sputtering followed by brazing.

Both the hydride and active metal processes utilize metals which have an affinity for the ceramics. Typical metals are Ti and Zr. In the case of the hydride process, the metal is deposited on the ceramic indirectly through hydride compounds, typically TiH_2 and ZrH_2, which are reduced in the firing process. The active metals themselves can be applied as a constituent of a braze alloy being used or as a separate braze material in the form of wire or powder. Both the hydride and active metal processes are one-shot processes in that the wetting of the ceramic by the active metal and joining of the ceramic to a metal part are accomplished in one furnace firing. In the case of deposition by sputtering, a mechanism for chemical bonding of the applied metal and the ceramic is necessary. This can be accomplished by sputtering a thin film of an active metal followed by the desired base metal to be used in the joint.

Zirconium appears to be the preferred active metal used and is found not to react with zirconia at temperatures below 1800°K. To achieve a bond using zirconium it is not necessary for a reaction to take place, however, as a strong bond due to chemical forces at the interface of the metal and the oxide can occur. In an oxidizing atmosphere such as exists with the biopropellants CO_2 and H_2O, the Zr would tend to oxidize.

Battelle's Columbus Laboratories (reference 57) have reviewed ceramic-to-metal seal requirements for the ceramic heater assemblies being studied for biowaste resistojets. Battelle has suggested that vapor-deposition cladding of the ceramic tube followed by brazing or diffusion bonding can be used to join noble metal tubes to ceramic heaters, for example. Achieving a strong adhesion to the ceramic tube may, however, require an intermediate material. Metallic zirconium deposited by vacuum evaporation and chromium carbide deposited by thermal decomposition of an organometallic compound are being considered as candidate intermediates. These materials would be applied as very thin micron-thick coatings to interface the platinum coating to the zirconium.

Another possible joining mechanism for zirconia heater tubes may be possible from the fact that zirconium is unstable toward platinum in a reducing atmosphere. A highly stable compound, $PtZr_3$ is formed as follows:

$$\frac{1}{3}Pt + ZrO_2 + 2H2 \xrightarrow[1500°K]{} \frac{1}{3}PtZr_3 + 2H_2O \qquad (31)$$

This reaction may provide a mechanism for the joining of zirconia to platinum without an intermediate material. Platinum can be physically deposited onto zirconia but, unless such an interaction occurs, a bond capable of thermal cycling is not assured. Relative to the mechanical bonding of platinum directly to zirconia, a rough or porous ceramic surface is desirable to promote interlocking of the constituents.

Sample ceramic heater tubes made of zirconia have been successfully metallized with platinum. A platinum powder based slurry was prepared which can be applied to the ceramic tubes by brushing, dipping or spraying. The

slurry was applied to green (uncured) ceramic tubes. These tubes were then cured at about 2000°K in an oxidizing atmosphere at which time the platinum adhered to the tubes while organic materials in the slurry were burned off. Bands of platinum metal applied by this technique are shown in figure 42 on sample zirconia heater tubes. The lower photo is a micrograph of one of the metallized sections. The platinum metal is seen as the discontinuous particles on the ceramic substrate. The platinum is believed to have become discontinuous during polishing of the sample, the platinum being soft relative to the hard ceramic substrate. Macro photos reveal an apparent continuous coating.

The photomicrograph interface is sharp and clean, revealing no apparent chemical interaction in the figure 42 case. Grain structure is seen to be larger for the S39-1 sample photomicrograph in figure 42 as compared to the S19-1 case shown in figure 22. This is apparently the result of a higher sintering temperature used to prepare the S39-1 sample.

Preliminary tests were conducted with zirconium hydride to effect a metallizing of zirconia heater samples with platinum-gold alloy having a melting temperature of about 1880°K. Indications were that this process will yield suitable joints having adequate strength and sealing properties. Achieveing a high quality joint, however, requires specially controlled conditions for the hydride process; the pure zirconium hydride is pyrophoric.

Preliminary tests were conducted using palladium foil to interface platinum foil with zirconia heater samples. The Pd has good wetting properties and this approach appears attractive. The samples made by this technique were not examined metallographically; however, they indicated that a structurally good bond could be obtained with the Pd interfacing.

Ceramic-to-ceramic joint samples were prepared by sintering together matched ceramic tubes. The O.D. of a smaller tube was matched to the I.D. of a larger tube. These parts were sintered together. Short sintering times (or the order of 10 minutes) were used and revealed positive results. Care must be taken on the fit and concentricity between the parts to be joined. Longer sintering times (of the order of one hour) should yield excellent joints by this techniques. This technique would be applicable to joining a ceramic nozzle to a ceramic heater tube.

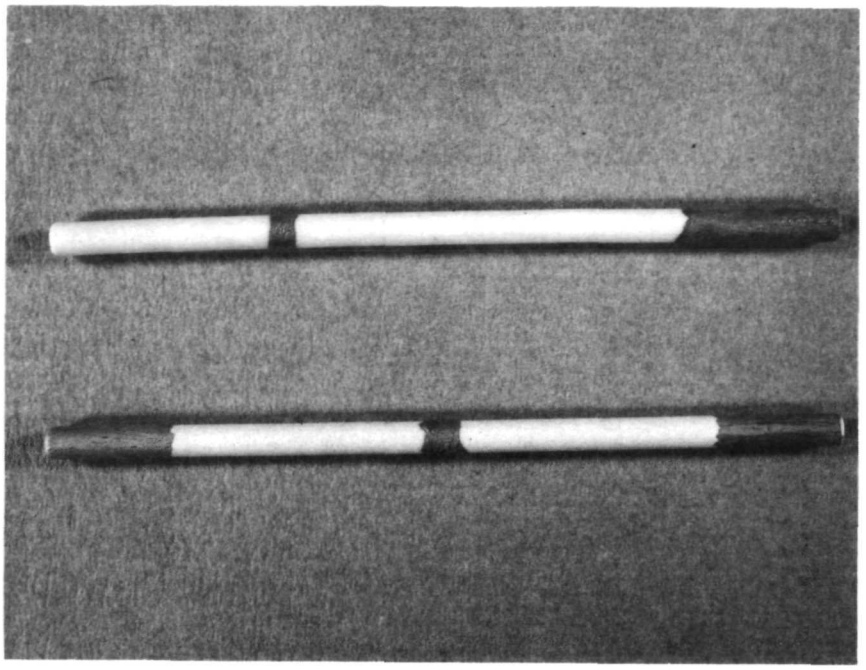

SAMPLES S39 and S47 1.7X

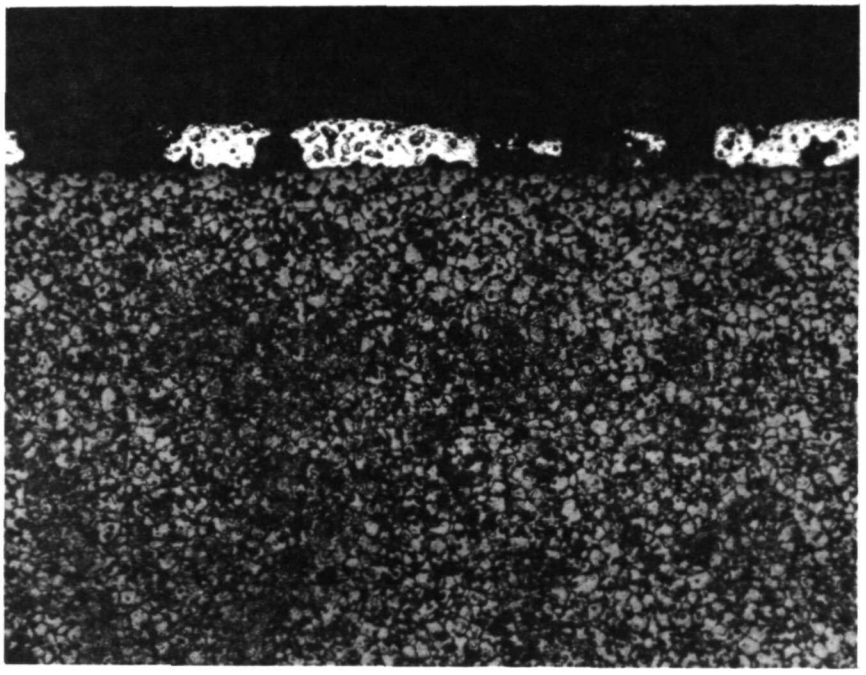

SAMPLE S39-1 ETCHED 200X

Figure 42.- Zirconia heater tubes metallized with platinum.

PROOF OF CONCEPT

A proof of concept test was conducted on a multiple-passage conducting ceramic heater tube. A complete heater assembly was used including a platinum wire starter-ballast coil, an alumina starter-ballast support, zirconia felt insulation and Pt-Rh alloy radiation shields. Figure 43 shows the assembly at the top. In the middle is an alumina support tube. Twenty four longitudinal holes in the wall of the support tube carry the starter-ballast coil. In the foreground is the multiple-hole ceramic heater tube with its electrode wires. The electrode wires can be seen in the upper assembly view as well as two twisted wires on the right hand end which connect to the starter-ballast coil.

A regenerator coil (see THRUSTOR DESIGN section) was not used in the proof of concept test. Ambient temperature (298°K) carbon dioxide propellant (the poorest propellant for heat transfer) was used. With the 298°K inlet condition, a severe temperature ratio situation existed. For example with an exit gas temperature at 1900°K, an exit to inlet temperature ratio of 6.3 occurs which could present a thermal instability condition in the parallel flow channels (see Thermal Analysis section). In addition, an extreme axial temperature gradient occurs, with a more severe condition at the inlet end electrode than would normally occur in the complete thrustor assembly. Typically, the regenerator would provide 850°K at the ceramic heater inlet for a temperature ratio of 2.2, well below the flow instability limit. Thus, the proof of concept test was a severe thermal test of the ceramic heater.

In one of the first tests of the figure 43 assembly, the space between the ceramic heater tube and the alumina support tube was filled with yttria stabilized zirconia felt insulation (Zircar made by Union Carbide). An interesting anomaly was noted in this test. At an abnormal flow condition, an instability could be induced where electrical current began conducting through the zirconia felt insulation. In subsequent tests, the felt insulation was kept from touching the conducting portion of the ceramic heater tube. This prevented any short circuiting by the zirconia felt insulation.

The use of zirconia felt in the inner cavity between the alumina support and ceramic heater tube is advantageous and reduces thermal losses considerably. For instance, the no-flow thermal losses for three different cavity situations compare as follows for a ceramic heater wall temperature of 1930°K.

Test No.	Cavity Situation	Power Loss, watts
S51-5	No insulation	98
S51-6	One layer of Pt-Rh foil inside alumina support	86
S51-2	Zirconia felt insulation	48

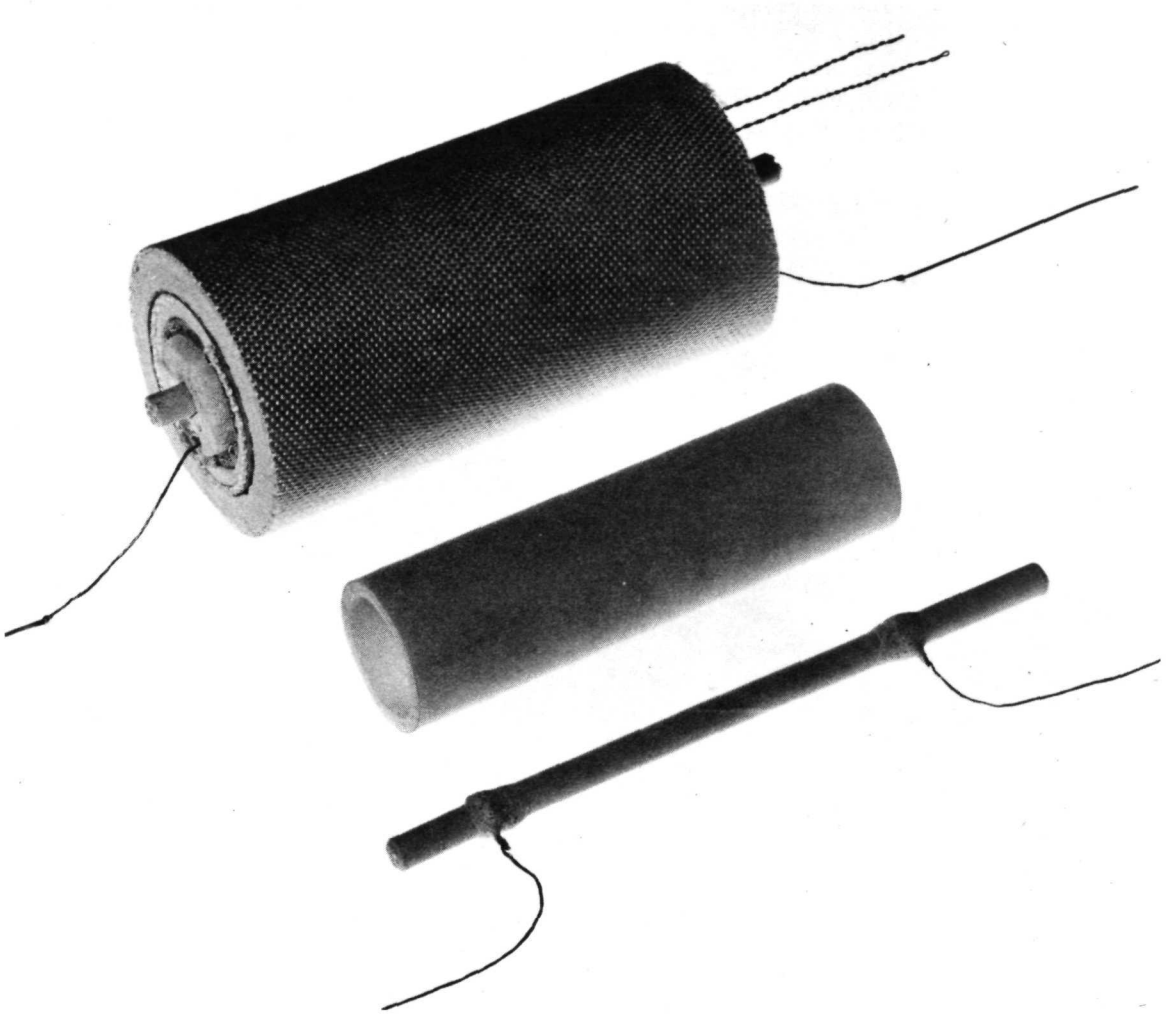

Figure 43.- Proof of concept multiple-hole conducting ceramic heater assembly.

Compared to the case of no insulation, the single radiation shield (test S51-6) reduced the no flow power loss by 12 watts. With zirconia felt, however, the power loss was reduced to one-half the case of no insulation. Zirconia felt is seen to provide effective insulation for the ceramic heater tube.

The alumina support tube used in the proof of concept test was different than the one proposed for the biowaste resistojet assembly (see THRUSTOR DESIGN section). The support tube used and shown in the center of figure 43 had an inside diameter of 1.3 cm whereas the proposed thrustor design will have a cavity diameter of about 1.6 cm. Therefore, a greater thickness of zirconia felt insulation can be accommodated resulting in lower losses than those experienced in the proof of concept test.

Figure 44 presents the electrical characteristics of the multiple-passage ceramic heater without insulation and tested in a stagnant air environment. These data can be compared with those for a single passage heater tube presented in the COMPONENT TESTS section. The trends are very similiar. Compare figure 44 with figure 36, for instance. The differences due to an air environment for the figure 44 case versus CO_2 for the figure 36 case are negligible. The multiple passage heater has been sized to have a slightly higher voltage and current to satisfy the power requirements of the larger multiple passage heater. At 1900°K, for example, the figure 44 data shows a voltage of 125 volts at a current of 1.72 amperes. This same heater in the figure 43 assembly with out flow operates at about 58 volts and 0.79 amperes with a 1900°K ceramic heater temperature.

Performance of the proof of concept heater assembly flowing CO_2 propellant is presented in figures 45 and 46. A heater temperature of 2000°K (maximum toward the downstream electrode) was maintained for this test. These data are for test S51-6 without zirconia felt insulation in the alumina support cavity. Power consumption would be reduced about 40 watts from the figure 45 power curve with the felt insulation. For a 25 mlb thrust and a specific impulse of about 192 seconds, design mass flow rate of CO_2 would be 0.059 grams per second. The voltage for the figure 45 case is seen to be about 122 volts. With felt insulation the voltage would drop to about 108 volts. In a thrustor assembly, thermal losses would be reduced further with a final ceramic heater voltage of about 100 volts and a total voltage across the ballast and ceramic heater of about 120 volts.

Figure 46 presents the pressure drop occuring in the multiple passage heater tube as a function of flow rate. Both cold flow and 2000°K heater temperature data are shown. Comparing these data to those of figure 41 for a single passage heater tube, the pressure drop is seen to be greatest for the multiple passage tube for the same flow rate. Excessive shrinkage occurred in the fabrication process for the S51 series of multiple passage heaters. Passage diameters of 0.635 mm resulted compared to design diameters of 0.71 mm (per figure 5). Pressure drop with the design passage size will be reduced to less than one-half of the figure 46 values. Assuming a cavity pressure surrounding the heater tube equal to the heater tube inlet pressure (regenerator outlet pressure), the compression loading at the heater exit end will

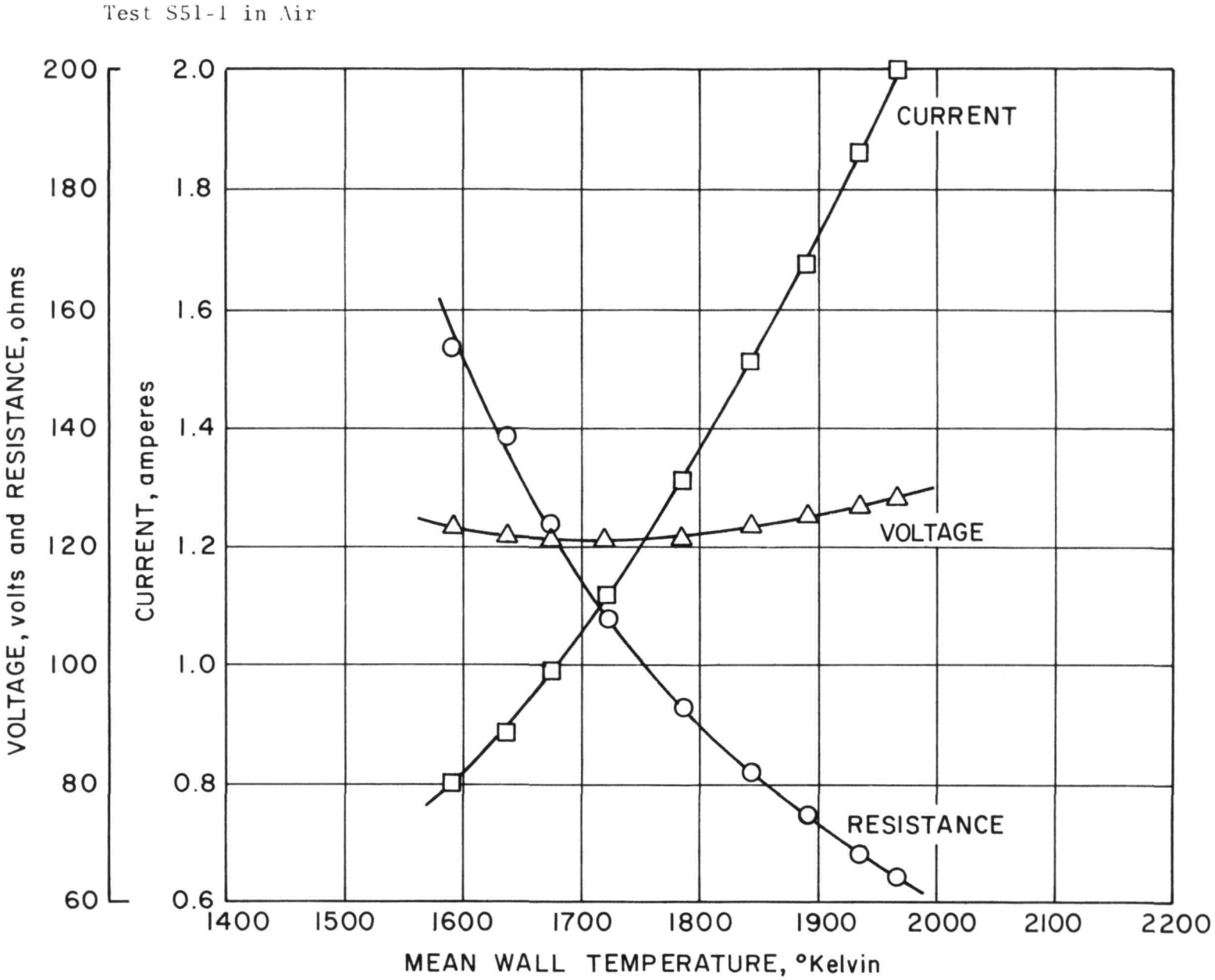

Figure 44. - Electrical characteristics of uninsulated - multiple hole ceramic heater.

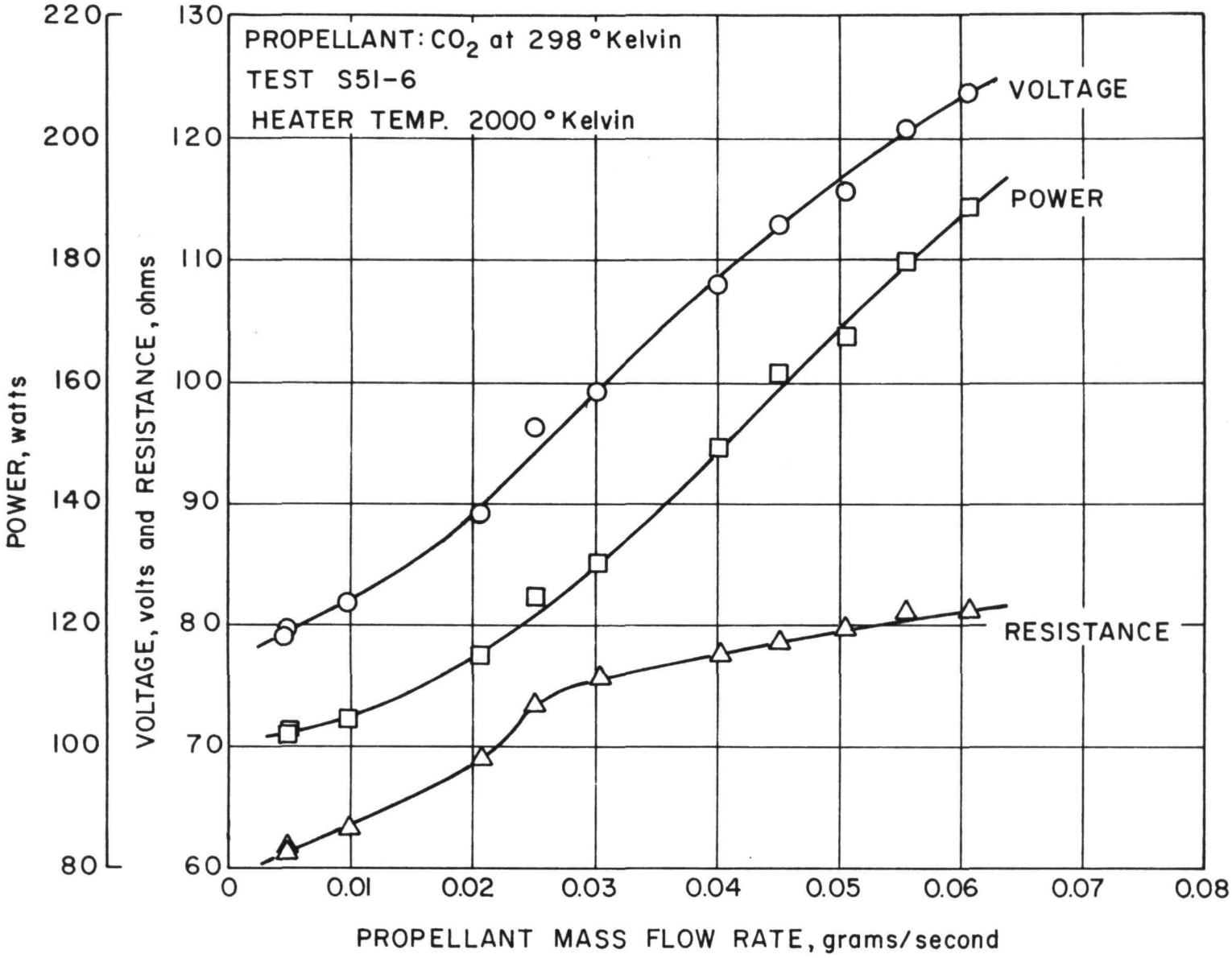

Figure 45. - Proof-of-Concept heater electrical characteristics.

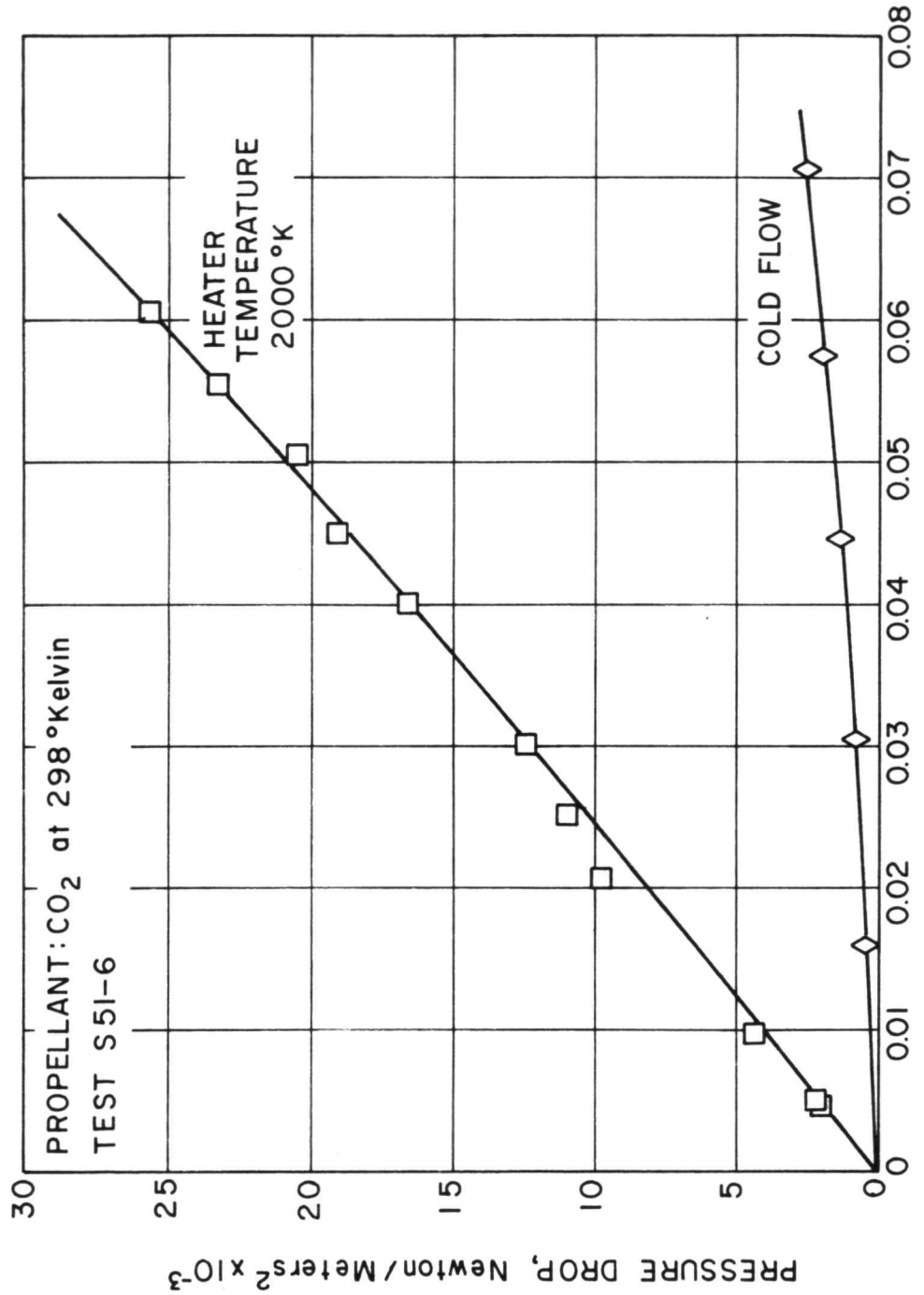

Figure 46. - Proof-of-Concept heater pressure drop.

correspond to about 10 kN/m^2. This will result in a negligible creep stress relative to the allowable creep limited compressive stress of 250 kN/m^2 (see Thermomechanical Considerations in the COMPONENT TESTS section).

Final gas temperatures in the proof of concept heater test were not measured because of the difficulty in instrumenting the small flow rates (less than 0.1 grams per second) and high temperatures (up to 2000°K). Energy balance calculations were made, however, and related to gas temperature through gas enthalpy rise and Mollier data. These calculations indicated that with a maximum heater wall temperature of 2000°K and design mass flow of CO_2 (0.059 grams per second), a final gas temperature of over 1900°K was reached. A precise determination of the final gas temperature was not possible because of uncertainties (about 3% of total power) in the end losses in the proof of concept heater. More precise temperature data can be obtained by incorporating a precision calorimeter into the heater exhaust flow. This was not done during this phase of the program.

Figure 47, a photomacrograph of an S51 series multiple heater tube is presented to indicate the 6 hole pattern used. This photo shows the S51 sample as cut on a diamond saw which caused some chipping of the outer edge of the tube. Figure 48 shows photomicrographs of typical regions of the as-received and as-tested sample S51-1 after 38 hours of operation. The as-received photomicrograph indicates that the ceramic material (YSZ) was well sintered. The post-test photomicrograph reveals porosity similiar to that observed in the single passage tubes (see figures 23 through 27). The material visible in the passage of the post-test photomicrograph of figure 48 is epoxy material used to pot the sample.

PERFORMANCE PREDICTIONS

The performance characteristics of biowaste resistojets utilizing the propellant candidates CO_2, H_2O, and CH_4, the biowaste fluids expected from typical space station sources, have been defined. Earlier performance estimates were based on long residence times in the thrustor and were expected to result in chemical equilibrium in the heat exchanger with the chemistry frozen through the nozzle (reference 58). In the study of reference 59, finite chemical kinetic solutions were used to assess the flow processes through the thrustor. From this, it was concluded that the chemical processes, for all practical purposes, were frozen at the thrustor inlet. In the case of methane, however, this is only true below about 1000°K, above which temperature the formation of solid carbon occurs (References 3 and 4).

The chemical kinetic solutions were obtained using a computer program for several propellants including those of table I. A simple tubular heat exchange model was employed. A long heat exchanger length and long residence time were employed and all possible chemical reactions were allowed to take place. The results, presented in figures 49, 50, and 51 showed no significant degree of chemical reaction. Figures 52, 53, and 54 are the chemical equilibrium solutions, representing infinite reaction time and indicating significant amounts

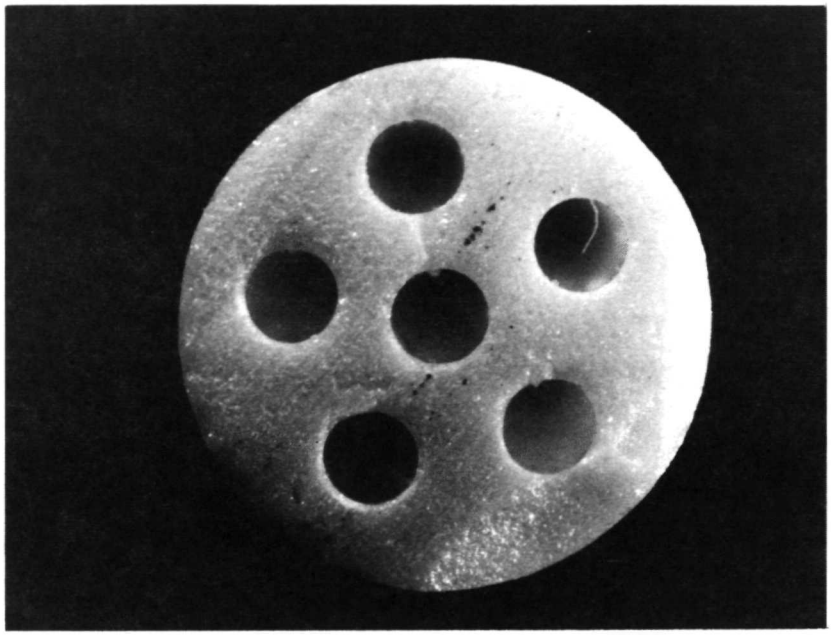

SAMPLE S51-1 20X

Figure 47.- Cross section of the multiple hole ceramic heater.

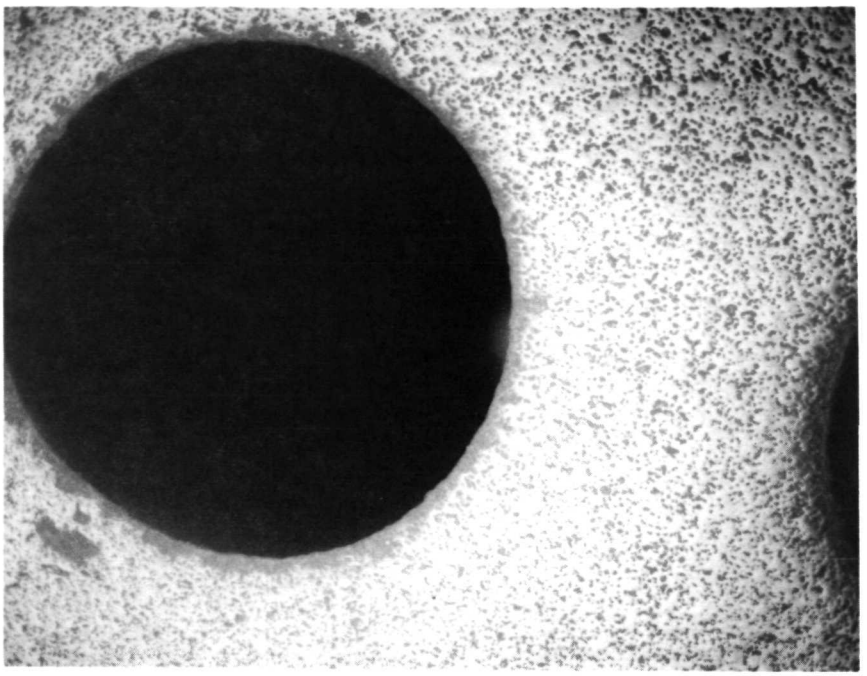

AS RECEIVED 125X

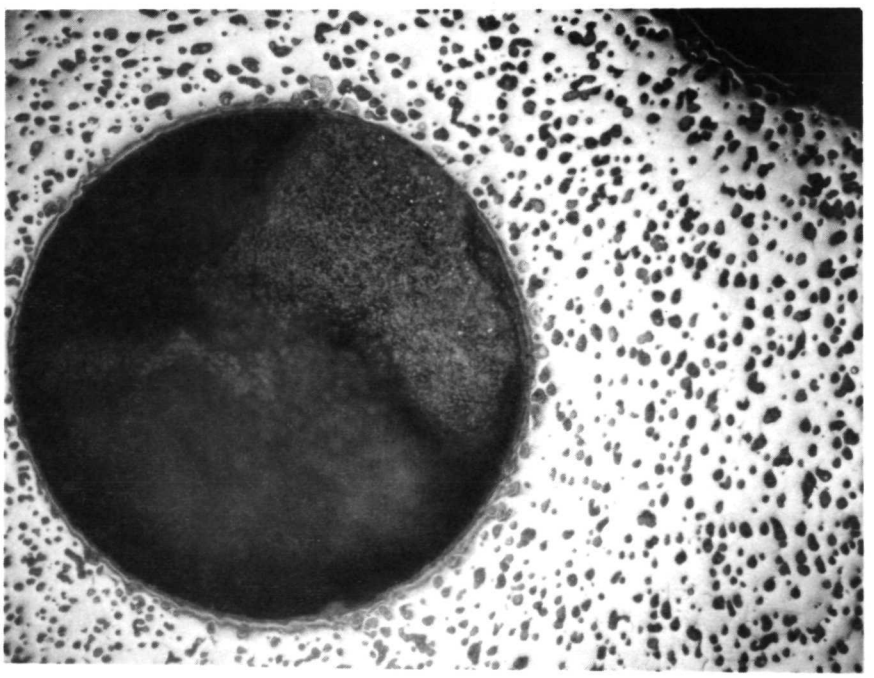

AFTER 38 HOURS OF OPERATION 125X

Figure 48.- Multiple hole ceramic heater sample S51-1.

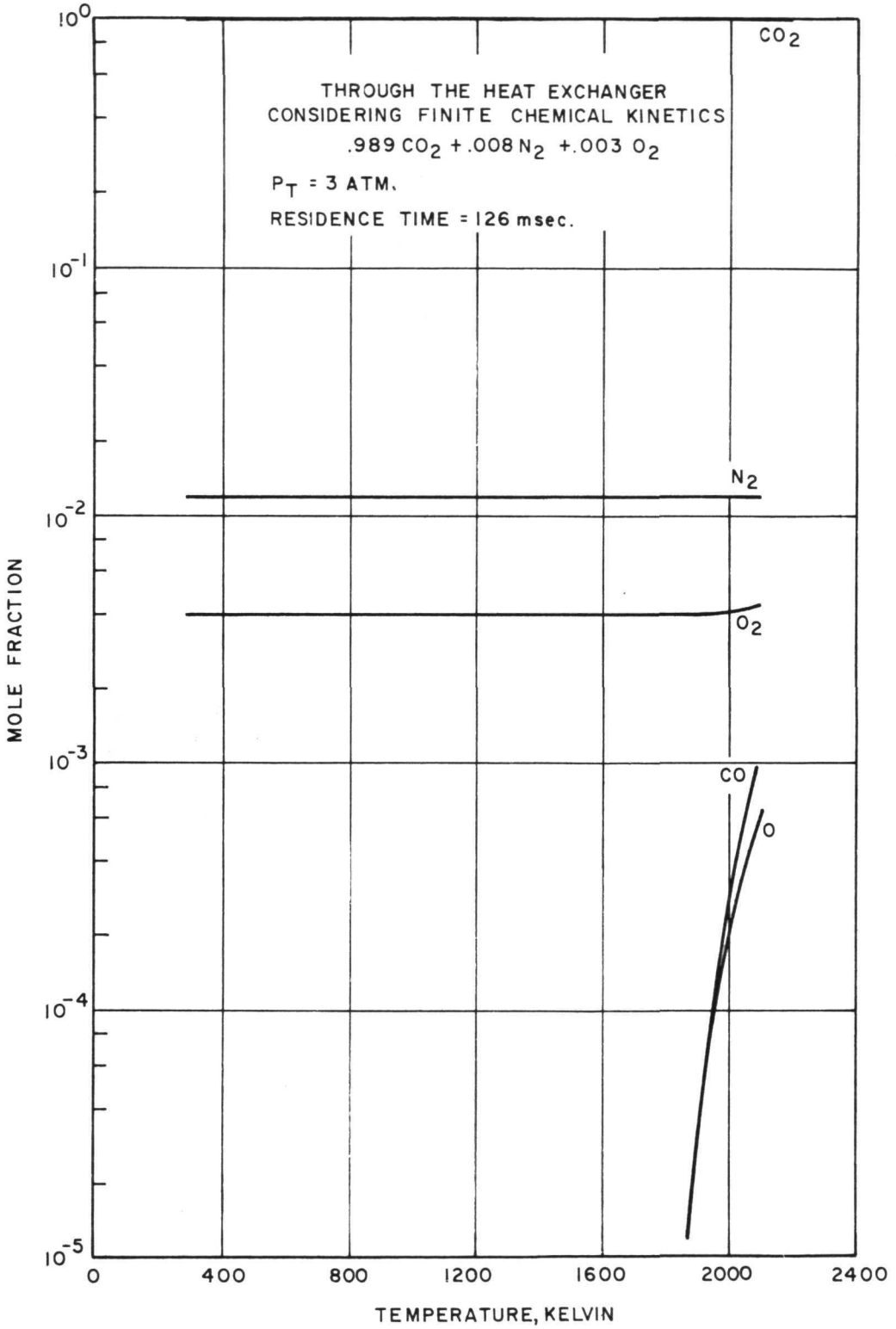

Figure 49. - Chemical species considering finite chemical kinetics.

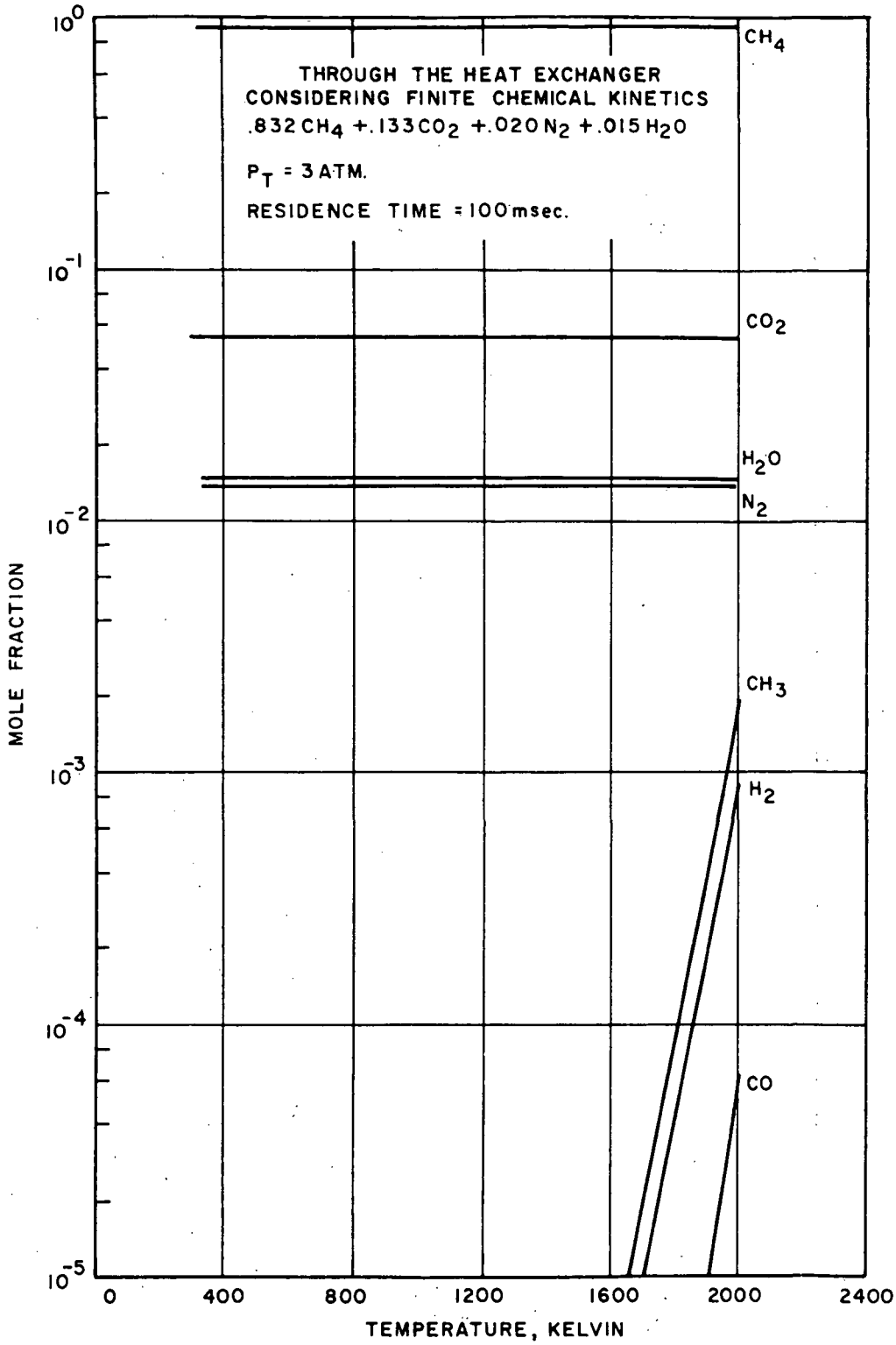

Figure 50. - Chemical species considering finite chemical kinetics.

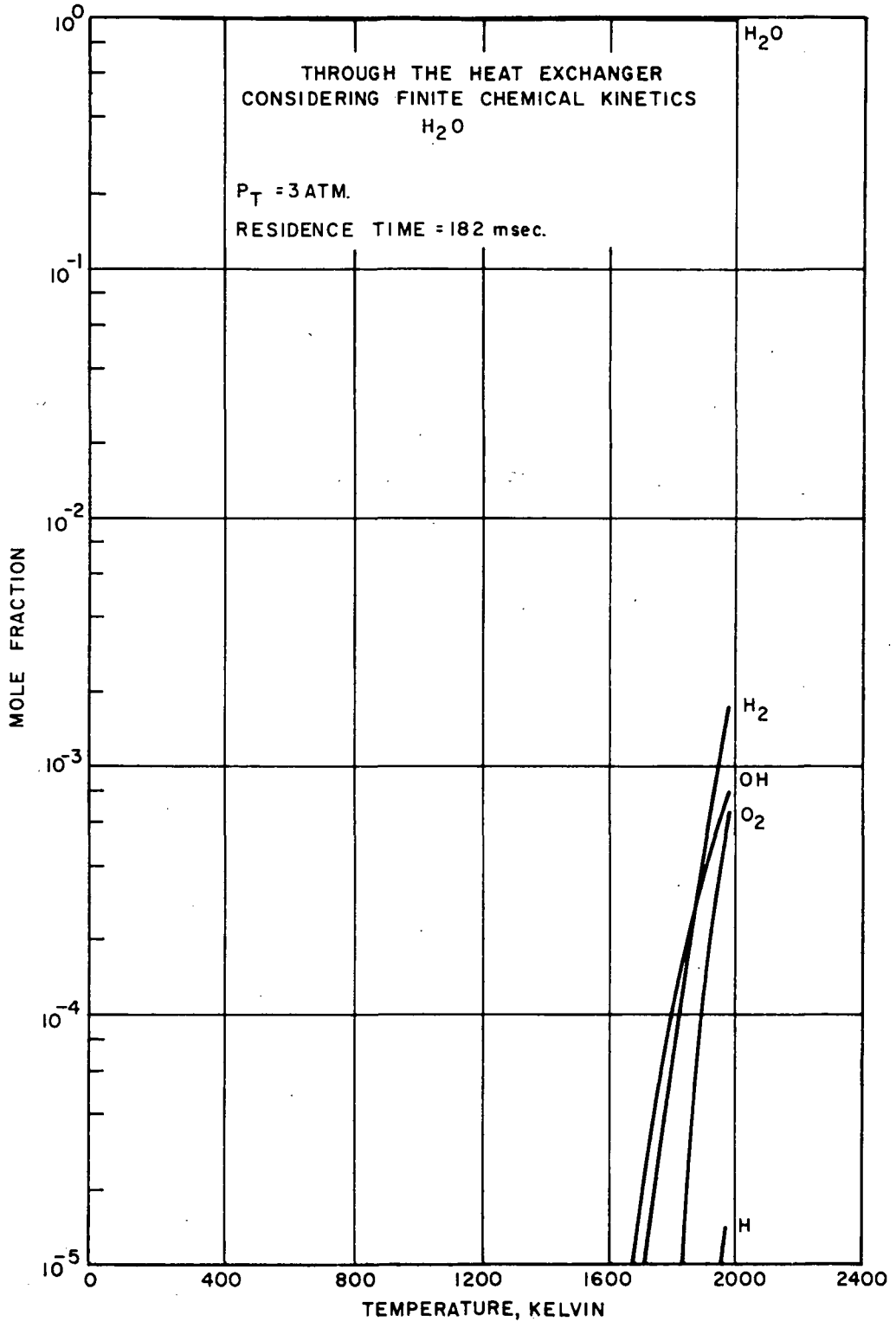

Figure 51. - Chemical species considering finite chemical kinetics.

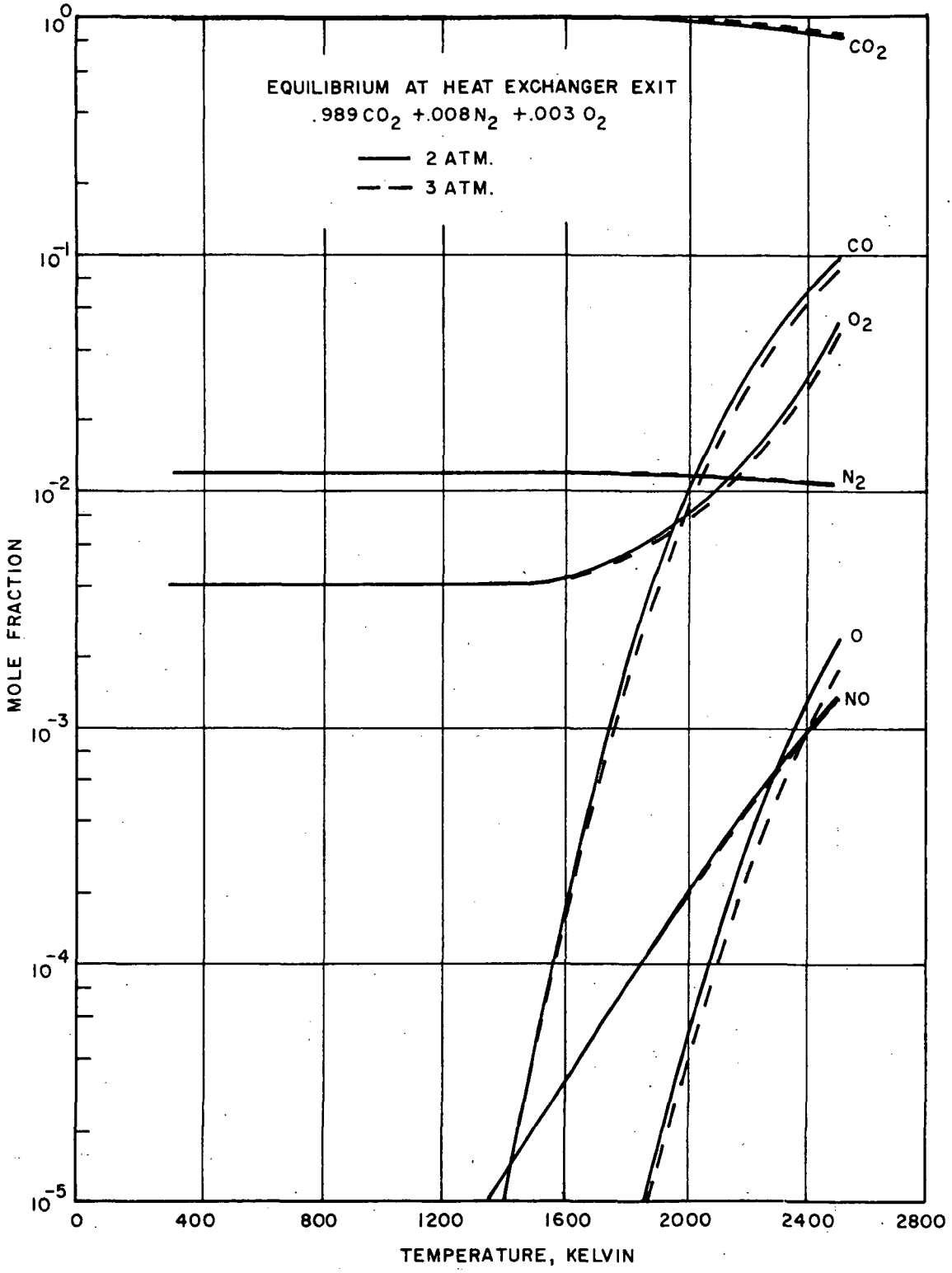

Figure 52. - Chemical species for chemical equilibrium.

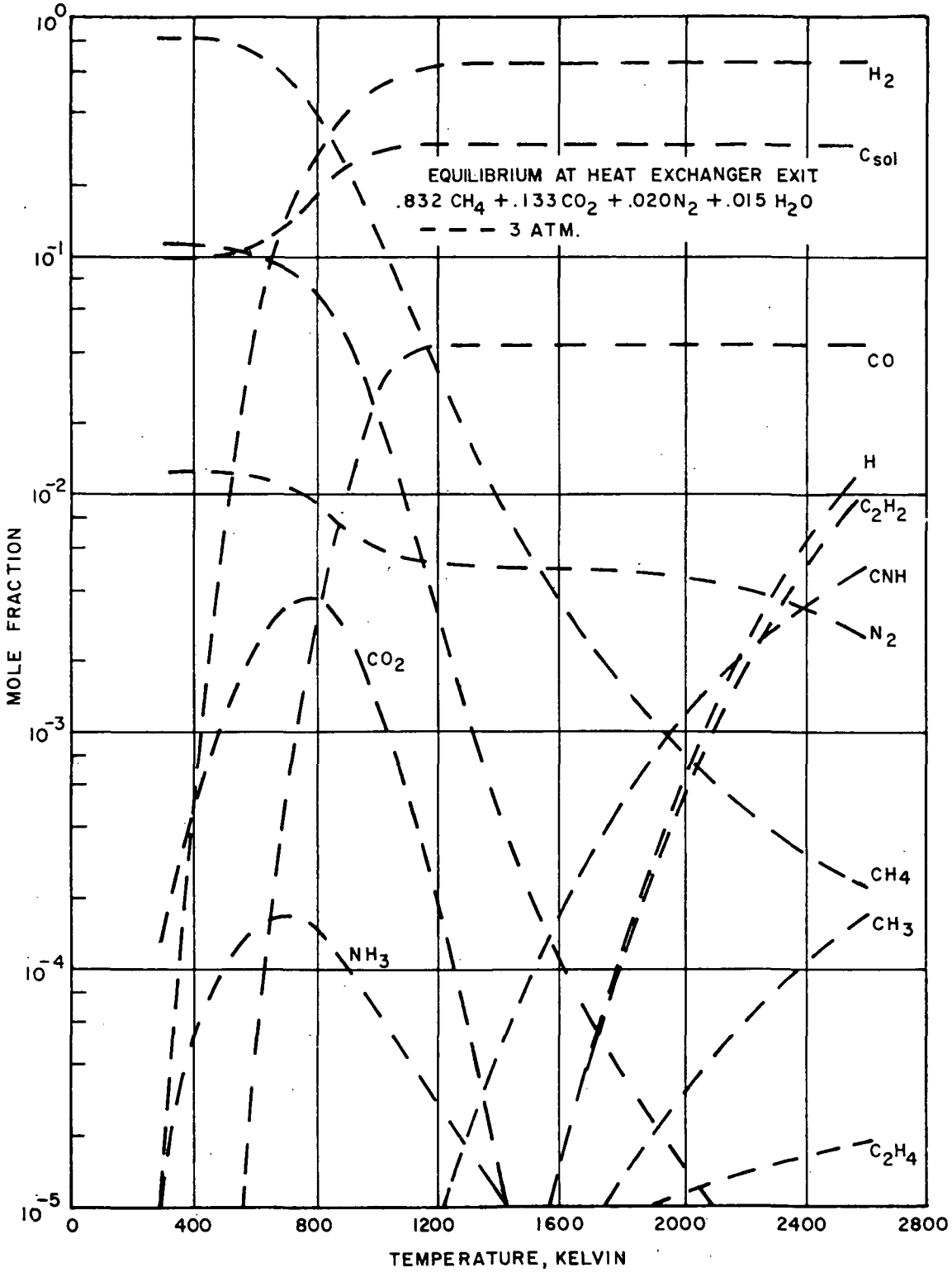

Figure 53. - Chemical species for chemical equilibrium.

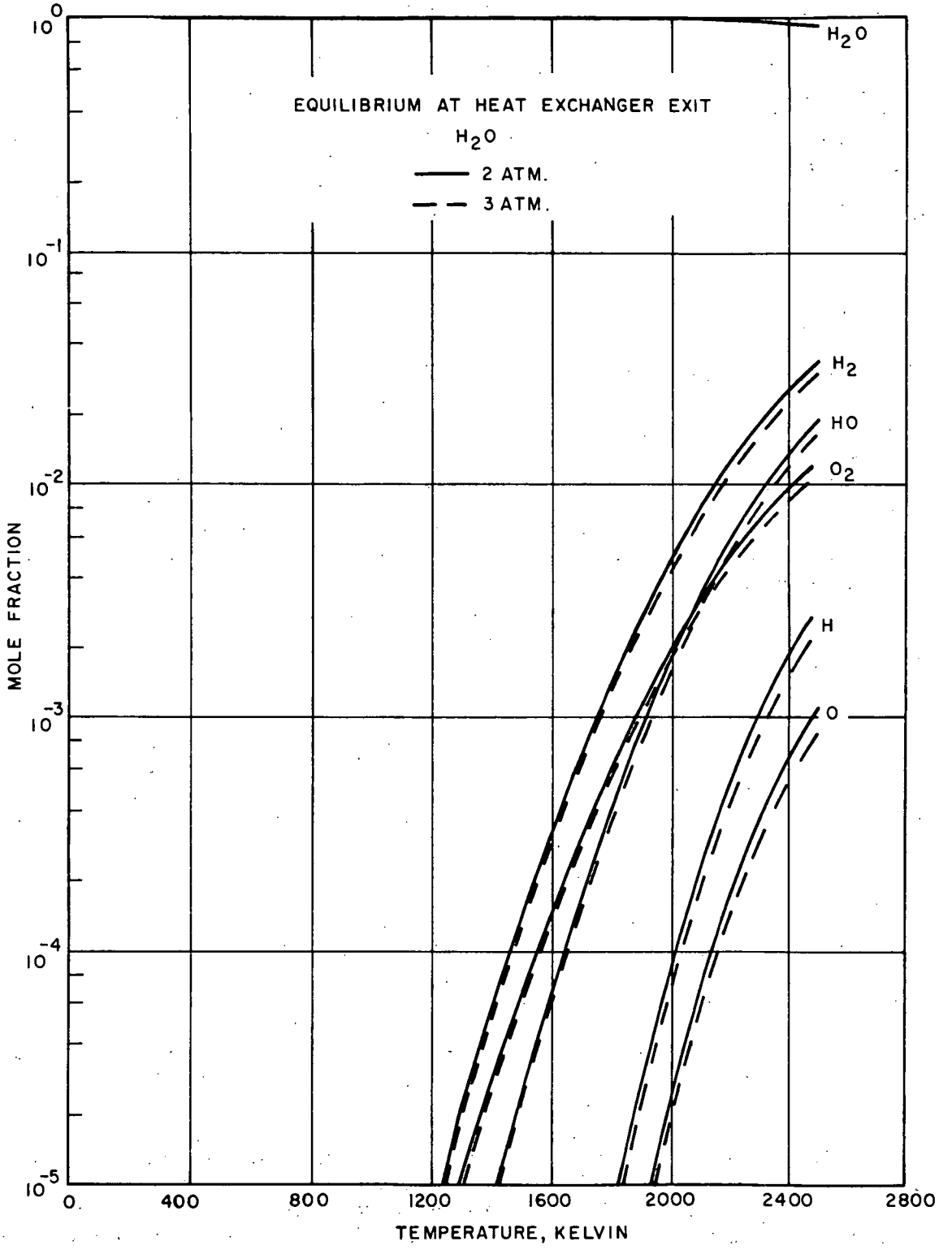

Figure 54. - Chemical species for chemical equilibrium.

of reaction products. These are shown for comparison purposes. In effect, then, resistojet performance calculations can be made from so-called "frozen-frozen cases" and residence time is unimportant.

The performances of 25-and 50-mlb thrustors, individually designed for specific propellants, are shown in figures 55, 56, and 57. Note that the inlet gas temperature for the molecular sieve and Sabatier propellants is 298°K and the H_2O is 417°K so the water is treated as a vapor. For the H_2O case, the evaporator power must be added to represent the true overall power input. The power required for sensible and latent heating of liquid water at 298°K to vapor at 417°K and 3 atmospheres pressure, for example, is given by

$$P_{evap} = \dot{m}\Delta h = 2640\ \dot{m} \qquad (32)$$

where the mass flow rate $\dot{m}$ is in grams per second and the evaporator power is in watts. The methane performance curves have a temperature limit of 1000°K because of solid carbon formation at higher temperature.

The study indicated that no advantage was to be gained by mixing propellants and in some cases a penalty was incurred. Mixing the Sabatier output with the molecular sieve and water recovery outputs would necessitate operation at chember temperatures of no more than about 1000°K to avoid carbon deposition. An overall higher effective specific impulse is realized if the various biopropellant sources are used separately at their respective maximum chamber temperatures (up to about 1000°K for CH_4 and 2000°K for CO_2 and H_2O).

Table XV gives the design parameters and performance goals of the particular resistojet described in the THRUSTOR DESIGN section. The electric power values are considered to be conservative. Actual power consumption will depend on the efficiency of the insulation system used in the final thrustor design. The gas temperatures of 1900°K and 900°K in table XV are based on conservative differences between heater maximum wall temperatures and exit gas temperatures of 100°K for CO_2 and H_2O, and of 50°K for CH_4. That is, heater maximum wall temperatures of 2000°K and 950°K, respectively, are assumed. The 950°K for CH_4 is the limiting temperature to avoid a carbon deposition problem in the thrustor. With the multiple passage, the exit gas temperature will approach the ceramic heater maximum wall temperature within about 70°K in the case of CO_2 and H_2O.

In passing through the colder noble metal nozzle depicted in the figure 17 design, gas temperature will decrease by an estimated 50°K. The decrease in gas temperature is an undesirable effect. It occurs to a greater extent in the concentric tubes type thrustor which has an adverse temperature gradient in the inner-most heating element near the nozzle because of relatively cold gas flow sweeping into passage 2 from passage 1 (see reference 3). The temperature drop at the nozzle inlet in the ceramic heater thrustor of figure 17 is not as significant. With a ceramic nozzle, an alternate to the metal nozzle for the figure 17 design, this temperature drop will be reduced further.

TABLE XV

THRUSTOR DESIGN GOALS

	CO_2	H_2O	CH_4
Thrust, N (25-mlb)	0.11	0.11	0.11
Gas Temperature, °K	1900	1900	900
Chamber pressure, atm	1.4	1.4	1.4
Specific impulse, s	192	270	200
Mass flow, g/s	.059	.042	.057
Electric power, w *	160	192**	104

* Includes thermal losses

** Based on inlet steam at 417°K

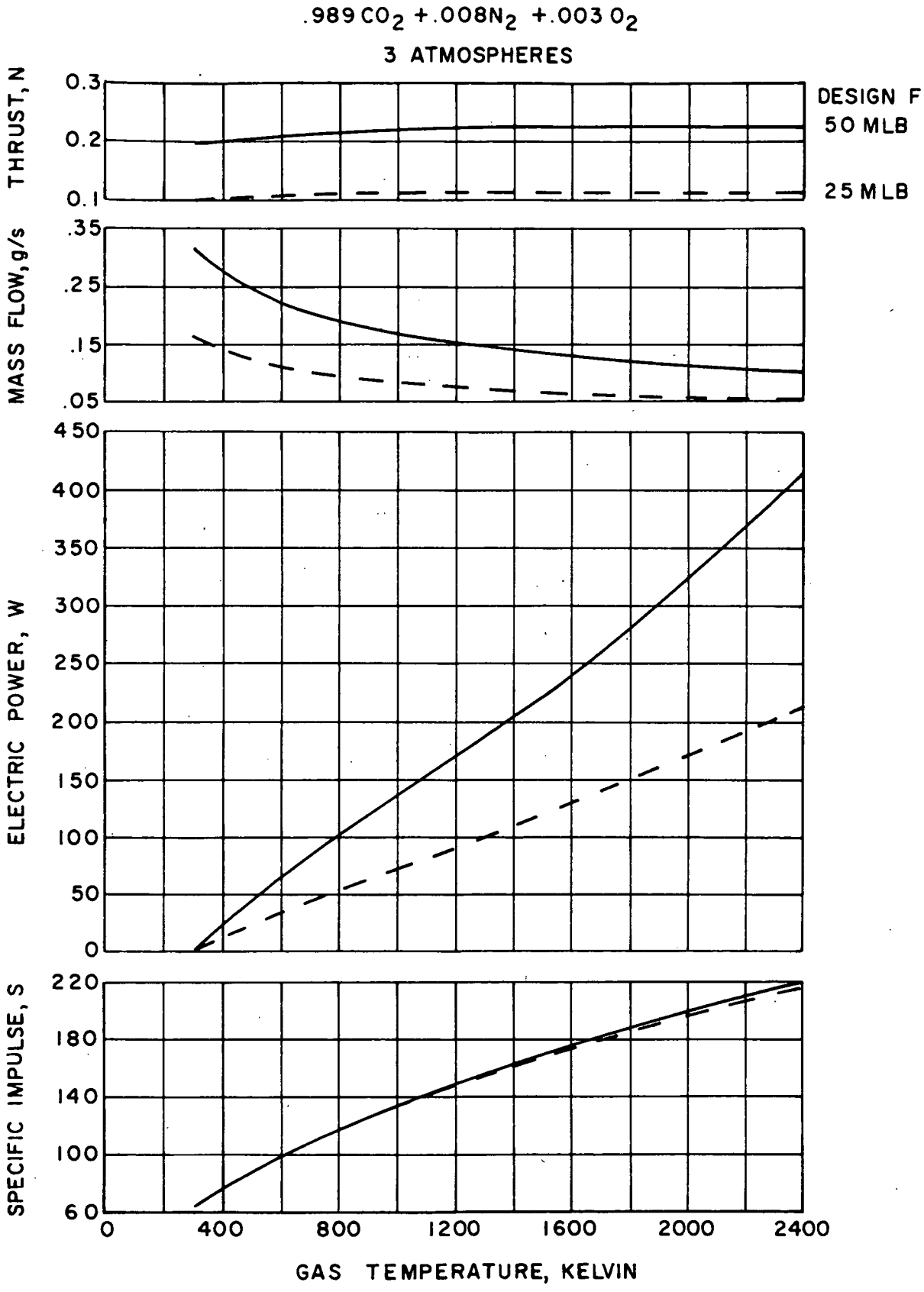

Figure 55. - Predicted performance for biowaste resistojets.

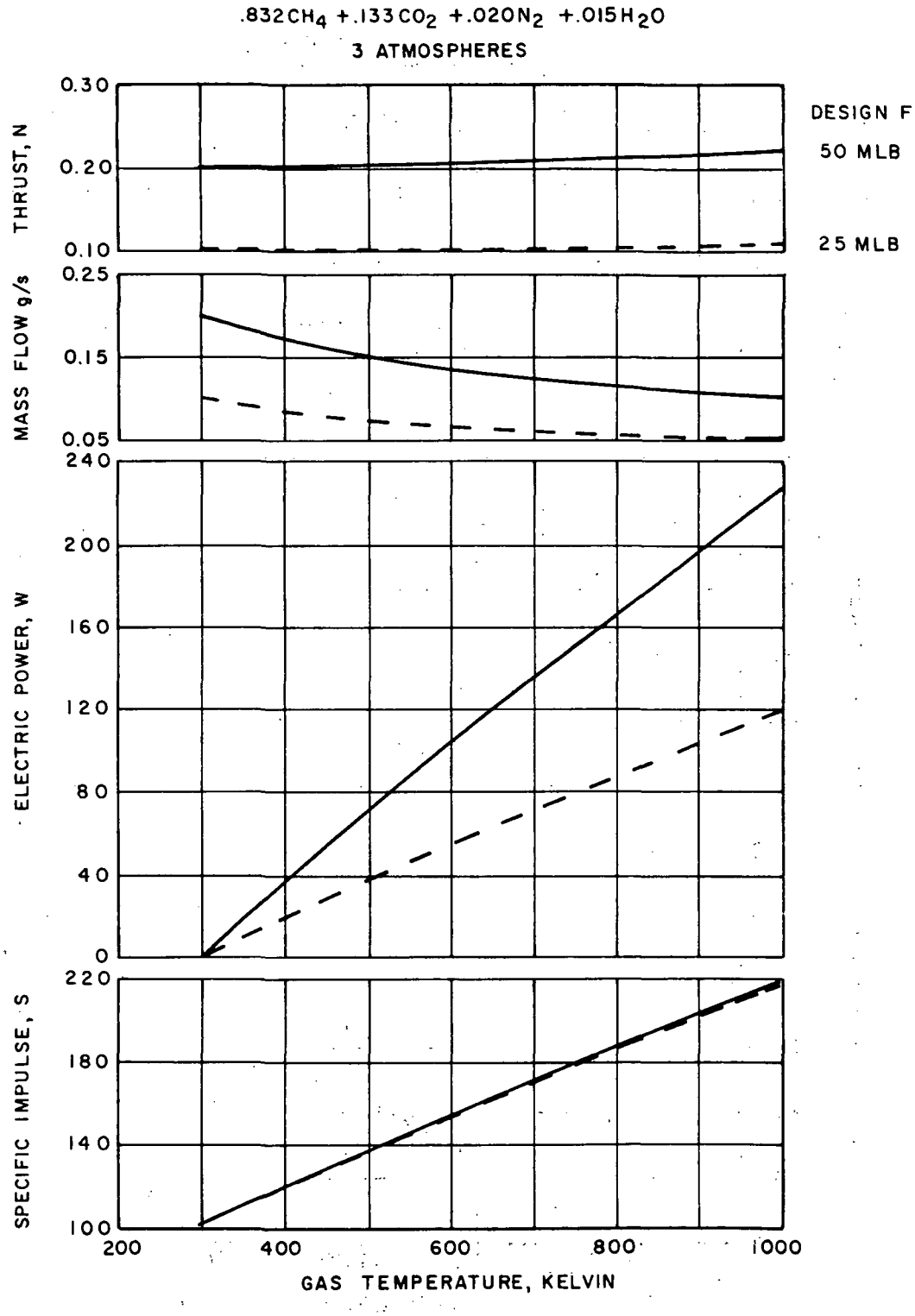

Figure 56. - Predicted performance for biowaste resistojets.

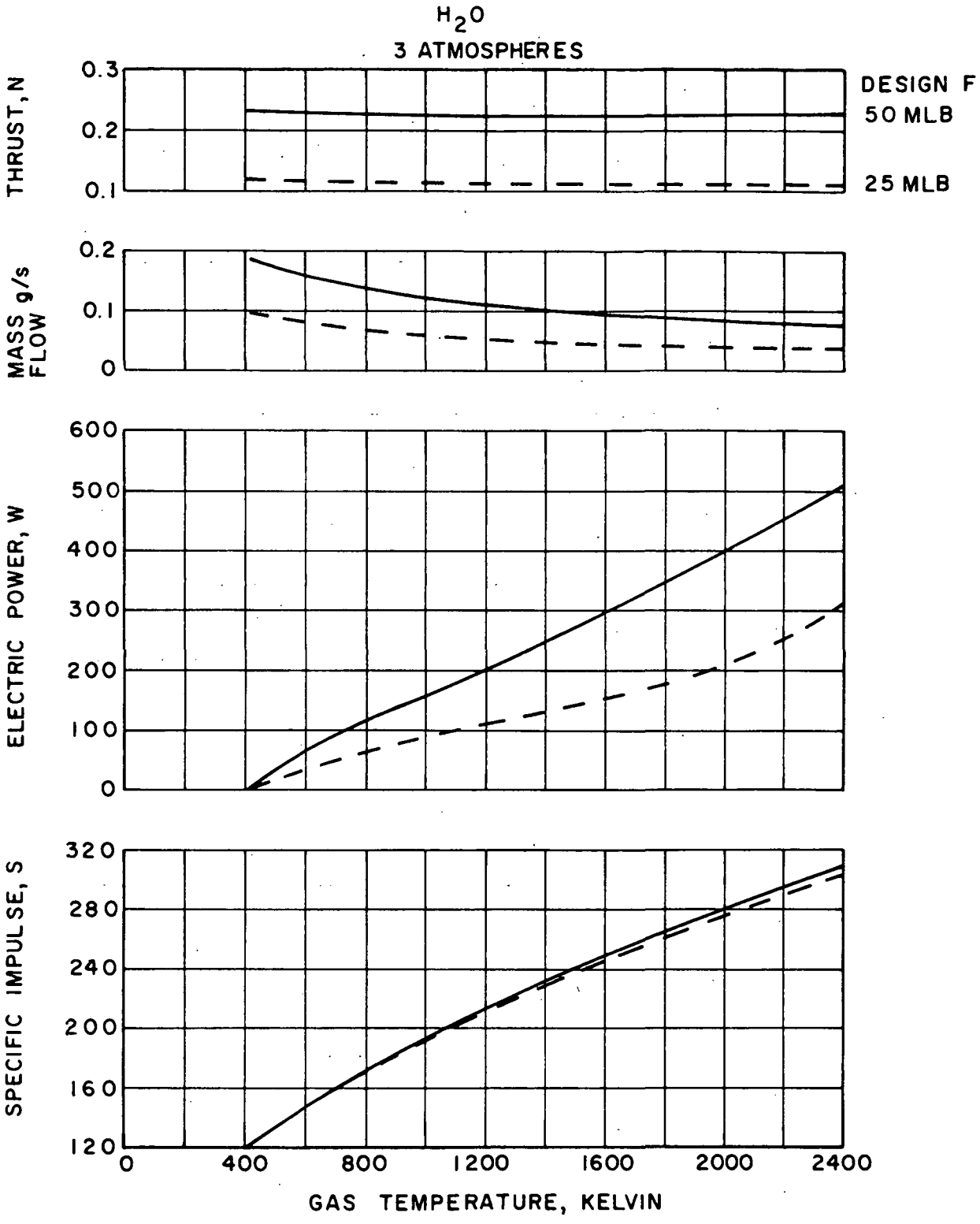

Figure 57. - Predicted performance for biowaste resistojets.

CONCLUSIONS

Contemporary biowaste resistojets have been developed to meet the CMG desaturation and orbit-keeping requirements of the space station. These thrustors utilize noble metal heater technology and offer thrusting performance commensurate with chamber gas temperatures of up to about 1550°K. Certain anomolies occur with variations in the composition of the biopropellants. CO_2 presents a carbonyl corrosion problem for the platinum-rhodium alloys. The addition of a trace of O_2 appears to aggravate the corrosion problem with this alloy. Platinum-iridium alloy is not susceptible to near-term carbonyl corrosion; however, oxidation corrosion persists if a trace of O_2 is contained in the CO_2. Pure platinum lacks mechanical strength. While TD platinum has greatly improved high temperature creep strength, it does not offer sufficient improvement in low temperature yield strength. The result is that a contemporary all-metal resistojet using the TD Pt heater material will suffer a significant compromise in electrical characteristics in order to meet launch vibration environment requirements. If a contemporary resistojet is used on the space station, most likely it will utilize a heater made of Pt-Ir alloy coupled with a requirement that trace amounts of O_2 in the propellant supply be neutralized by minor additions of H_2.

In view of the possible shortcomings of the contemporary all-metal resistojet, one of those being the consideration that supplemental propellant may be required for the space station application, a higher performance thrustor development program is continuing using ceramics as advanced heater materials. Specifically, the advanced (higher specific impulse thrustor) will:

(1) minimize or eliminate the need for supplemental propellant

(2) offer greater growth potential for the Space/Base application.

Zirconia and thoria ceramics have been chosen as heater materials for the advanced concept biowaste resistojet. These are electrically conducting materials once they are preheated to temperatures above 1000°K. They exhibit exceptional resistance to the biopropellants. This has been demonstrated with zirconia by 500 hour tests at temperatures above 1900°K with CO_2, H_2O, Air and a 10^{-5} Torr vacuum. Thoria, too, is expected to have as good, or better, chemical resistance to the biopropellants.

This phase of the advanced biowaste resistojet study program has resulted in a so called "hybrid" design. The advantages of ductile metal parts for a lower temperature regenerator, and of the higher temperature ceramics for the high temperature resistive heater, have been combined into the hybrid resistojet. This advanced biowaste resistojet design offers final stage heater temperature capability of up to about 2000°K, resulting in chamber gas temperatures to about 1900°K. Electrical characteristics are easily adapted to the space station power system with, typically, 120 volts at 1.7 amperes required for a 200 watt power condition.

A multiple passage tubular configuration has been chosen for the ceramic heater in order to meet heat transfer requirement (approach wall temperature to within less than 100°K) in a relative short, rugged heater. The design presented utilizes a ceramic heater element 4.1 mm in diameter having an L/D of only 17. The design is such that the heater element is hydrostatically balanced and free to expand on one end to minimize creep loads. Component materials have been sized mechanically for stress levels and thermally for temperatures compatible with lifetimes of the order of 10^4 hours.

Although a severe gas temperature ratio (exit to inlet) condition existed for the proof of concept test, no apparent instabilities were noted. That is, no major abnormality was noted in the measured parameters (voltage, current, power, resistance, heater temperature and mass flow rate). Final gas temperature was found to closely approach (within 100°K) the heater wall temperature of 2000°K with a 25 mlb thrustor flow rate, indicating that the multiple passage ceramic heater will make an efficient final stage heater for the biowaste resistojet. Pressure loading on the ceramic heater tube due to pressure drop will be compressive and at least an order of magnitude less than the allowable value (based on creep stress and 10,000 hours lifetime) for the biowaste resistojet.

REFERENCES

1. Page, R.J.,; Halbach, C.R.,; Ownby, M.L.; and Short, R.A.: Life Test of Six High Temperature Resistojets. AIAA Paper No. 69-294, presented at the AIAA 7th Electric Propulsion Conference, Williamsburg, Virginia, March 3-5, 1969.

2. Yoshida, R.Y.; Halbach, C.R.; and Hill, C.S.: Life Test Summary and High Vacuum Tests of 10 mlb Resistojets. J. Spacecraft and Rockets, vol. 8, no. 4, April 1971, pp. 414-416.

3. Halbach, C.R.: 10 mlb Biowaste Resistojet Performance, AIAA Paper No. 71-687, presented at the AIAA 7th Propulsion Joint Specialist Conference, Salt Lake City, Utah, June 14-18, 1971.

4. Halbach, C.R.; and Yoshida, R.L.: Development of a Biowaste Resistojet. J. Spacecraft and Rockets, vol. 8, no. 3, March 1971, pp. 273-277.

5. Halbach, C.R.: Technology Development of a Biowaste Resistojet. Seventh Quarterly Report, Marquardt Co. Report S-1009, June 1971.

6. Greco, R.V.; and Bliss, J.R.: Resistojet System Studies Directed to the Space Station/Space Base. Volume I: Station/Base Biowaste Resistojet System Design. NASA CR-111879, McDonnell Douglas Report G2125, April 1971.

7. Anon: Operational Ninety-Day Manned Test of a Regenerative Life Support System. McDonnell Douglas Test Report MDC G2282, NASA CR-111881, May 1971.

8. Leipold, M.H.; and Taylor, J.L. (JPL): Ultra-High-Frequency Oxide Induction Heating Furnace. Review of High Frequency Heating, vol. II, no. 3, pp. 6-7, published by Lepel High Frequency Laboratories, Inc.

9. Sprovle, R.T.: Solid Electrolytes -- New Applications for ZrO_2. Zircoa News Focus, (Available from Zircoa Chemetals Division, P.O. Box 39217, Solon, Ohio 44139).

10. Mitoff, S.P.: Electrical Conduction Mechanisms in Oxides. Section 5 in Progress in Ceramic Science Vol. 4, (edited by J.E. Burke), Pergamon Press, N. Y., 1966, pp. 217-264.

11. Hilsenrath, Joseph; et al: Tables of Thermal Properties of Gases. National Bureau of Standards Circular 564, 1955.

12. Keenan, Joseph H.; Keyes, Frederick G.; Hill, Philip G.; and Moore, Joan G.: Steam Tables. John Wiley & Sons, Inc., 1969.

13. Keenan, Joseph H.; and Kaye, Joseph: Gas Tables. John Wiley & Sons, Inc., 1950.

14. Svehla, Roger A.: Estimated Viscosities and Thermal Conductivities of Gases at High Temperatures. NASA TR-R-132, 1962.

15. Edwards, D.K.; Denny, V.E.; and Mills, A.F.: Transfer Processes. Holt, Rinehart and Winston, Inc., 1970.

16. Kutateladze, S.S.; and Borishanskii, V.M. (Arthur, J.B., trans.): A Concise Encyclopedia of Heat Transfer. Permagon Press, 1966.

17. Fraas, Arthur P.; and Ozisik, M. Necati: Heat Exchanger Design. John Wiley & Sons, Inc., 1965.

18. Reid, Robert C.; and Sherwood, Thomas K.: The Properties of Gases and Liquids. McGraw-Hill, Inc., 1966.

19. Tsederberg, N.V. (Scripta Technica, trans.): Thermal Conductivity of Gases and Liquids. MIT Press, 1965.

20. Page, R.J.; Short, R.A.; and Halbach, C.R.: Evaluation of Zirconia, Thoria and Zirconium Diboride for Advanced Resistojet Use. ARTCOR report. NASA CR-112075, May 1972.

21. Touloukian, Y.S., ed.: Thermophysical Properties of High Temperature Solid Materials. Thermophysical Properties Research Center, Purdue University. The Macmillan Company, 1967.
    Vol. 1 - Elements
    Vol. 2 - Nonferrous Alloys
    Vol. 4 - Oxides and Their Solutions and Mixtures

22. Anon.: Platinum - The Metal, Its Properties and Applications. The International Nickel Company, Inc., 1968.

23. Anon.: Rhodium - The Metal, Its Alloys, Chemical Compounds and Catalytic Properties. The International Nickel Company, Inc., 1966.

24. Anon. ed.: Plenum Press Handbooks of High Temperature Materials. Plenum Press. 1964
    No. 1 - Materials Index (Shaffer, P.T.B.)
    No. 2 - Properties Index (Samsonov, G.V.)
    No. 3 - Thermal Radiative Properties (Wood, W.D.; et al)

25. Campbell, Ivor E.; and Sherwood, Edwin M.: High Temperature Materials and Technology. John Wiley & Sons, Inc., 1967.

26. McMahon, W.R.; and Wilder, D.R.: Hemispherical Spectral Emittance of Selected Rare Earth Oxides. J. Amer. Ceramic Soc., vol. 51, April 1968, pp. 187-192.

27. Richmond, Joseph C.: Effect of Surface Roughness on Emittance of Nonmetals. J. Optical Soc. Amer., vol. 56, no. 2, Feb. 1966, pp. 253-254.

28. Richmond, J.C.: Thermal Radiation Properties of Ceramic Materials. NBS Spec. Publ. No. 303, 1969.

29. Noguchi, Tetsuo; and Kozuka, Takeshi: Temperature and Emissivity Measurement at 0.65 Micron with a Solar Furnace. Solar Energy, vol. 10, no. 3, 1966, pp. 125-131.

30. Siegel, Robert; and Howell, John R.: Thermal Radiation Heat Transfer. McGraw-Hill, Inc., 1972.

31. Hottel, H.C.; and Sarofim, A.F.: Radiative Transfer. McGraw-Hill, Inc., 1967.

32. Sparrow, E.M.; and Cess, R.D.: Radiation Heat Transfer. Brooks/Cole Publishing Company, 1966.

33. Oppenheim, A.K.: Radiation Analysis by the Network Method. Published in: Recent Advances in Heat and Mass Transfer; Hartnett, J.P., ed. McGraw-Hill Book Company, Inc., 1961.

34. Schneider, P.J.: Temperature Response Charts. John Wiley & Sons, Inc., 1963.

35. Myers, Glen E.: Analytical Methods in Conduction Heat Transfer. McGraw-Hill Book Company, 1971.

36. Carslaw, H.S.; and Jaeger, J.C.: Conduction of Heat in Solids. Second ed., Oxford University Press, 1959.

37. Ozisik, M. Necati: Boundary Value Problems of Heat Conduction. International Textbook Company, 1968.

38. Schneider, P.J.: Conduction Heat Transfer. Addison-Wesley Publishing Company, Inc., 1955.

39. Kays, W.M.: Convective Heat and Mass Transfer. McGraw-Hill Book Company, 1966.

40. Bussard, R.W.; and DeLauer, R.D.: Fundamentals of Nuclear Flight. McGraw-Hill Book Company, 1965.

41. Kunkle, John S.; Wilson, Samuel D.; and Cota, Richard A. (editors): Compressed Gas Handbook. NASA SP-3045, 1969.

42. Yavorsky, P.J.: Properties and High Temperature Applications of Zirconium Oxide. Ceramic Age, June 1962.

43. Mazdiyasni, K.S.; Lynch, C.T.; Smith, J.S.: Development of New Ceramic Materials (Zyttrite) by Thermal and Hydrolytic Decomposition of Metal Alcholates. AFML-TR-66-418, Dec. 1966.

44. Mazdiyasni, K.; and Lurch, C.T.: Alkoxy - Based Single and Mixed Phase Refractor Oxide Particulates. C.R. Journees Etud. Solides. Finement Div., 1967 (Pub. 1969) pp. 9-28. Ed. by Ehretsmann, J., Dir. Doc. Fr. (Paris).

45. Halbach, C.R.: 10 Mlb Biowaste Resistojet Performance. Preprint No. 71-687, Presented at AIAA 7th Propulsion Joint Specialist Conference (Salt Lake City), June, 1971.

46. Halbach, C.R.; Page, R.J.; Short, R.A., et al.: Resistojet Thruster Life Tests and High Vacuum Performance. NASA CR-66970, 1970.

47. Zima, G.E.: Vaporization of Advanced Power Plant Metals Under Vacuum and Forced Convection Conditions. Rept. UCRL-14274. Lawrence Radiation Laboratory, University of California, June 24, 1965.

48. Kingery, W.D.: Factors Affecting Thermal Stress Resistance of Ceramic Materials. J. Am. Ceram. Soc., vol. 38, 1955, pp. 3.

49. Carter, R.E.: Glower Lamp and Process. U.S. Patent No. 3,429,832, Feb. 25, 1969.

50. Schroeder. T.F.; et al.: Oxygen-Deficient Zirconia and Thoria: Their Thermal Shock Resistance and Equilibrium Oxygen Pressure. North American Rockwell Corp., Rocketdyne Division Report R-7525 (AD 671 690), 24 June, 1968.

51. Elyutin, V.P.; et al.: Reaction of ZrO_2 with Carbon. Izv. Vyssh-Ucheb. Zaved. Chern. Met. 1970, 13 (1), 1970, pp. 5-8. (Russian).

52. Imai, H. and Hosaka, S.: Reaction of Pressed Mixtures. Zairyo, 17 (177), 1968, pp. 531-5. (Japan).

53. Bunikov, D.D. and Kharitonov, F. Va.: Resistance of Calcium Oxide Stabilized Zirconia Ceramics Against High Temperature Stream. Epitanya E 21 (10), 1969, pp. 375-7. (Hung.).

54. Weast, R.C. Editor.: Handbook of Chemistry and Physics. 52nd Edition, The Chemical Rubber Co., 1971.

55. Campbell, I.E.; and Sherwood, E.M.: High Temperature Materials and Technology. Chap. 8, John Wiley, 1967.

56. Larssen, Per D.: Abstracts of Articles on Ceramic-To-Metal and Ceramic-To-Ceramic Seals With Emphasis on Joining With Noble Metals, The Active Metal Process, and The Hydride Process. ARTCOR Bulletin J-117-1, October, 1971.

57. Bower, Warren K.: Letter to R.J. Page at ARTCOR. Battelle Columbus Laboratories, March 16, 1972.

58. Pisciotta, A. Jr.; Eusanio, E.N., at al: Resistojet Control System Analysis: Vol. II of Definition of a Resistojet Control System for the Manned Orbital Research Laboratory. Final Report. NASA CR - 66601, 1968.

59. Page, R.J.: Biowaste Propellants Performance and Power Goals-Space Station/Base. ARTCOR Technical Bulletin, no. 16, Advanced Rocket Technology, Irvine, Ca., Oct. 1970.

60. Halbach, Carl R.; Arthur, Paul D.; and Page, Russell J.: Evaluation of Advanced Component Concepts for an Integrated Environmental Control / Life Support - Resistojet Control System. NASA CR-112104, July 1972.

APPENDIX

ANALYSIS OF THREE-WAY RADIATIVE ENERGY INTERCHANGE BETWEEN THE BALLAST RESISTOR HEATER COIL, THE ALUMINA COIL SUPPORT INSULATOR, AND THE REGENERATOR

The thermal subsystem for this particular phase of the problem consisted of an electrical resistance heated Pt-20 Rh wire coil, an electrically-insulating alumina heater coil support element, and a coiled Pt-20 Rh regenerator tube supported by a metallic cylinder. This thermal subsystem is illustrated in figure A-1. Figure A-1(a) shows the physical arrangement of the elements comprising this thermal subsystem.

Since the space between elements is evacuated in this particular region of the thrustor, and since there is little or no good thermal contact between elements, it was considered valid to base the heat transfer analysis for this subsystem on radiative transfer only. The problem, in simplified form, is defined as one involving radiative transfer in an enclosure between three diffuse - gray surfaces, each isothermal. This definition of the problem, which neglects axial variations in temperature of the elements, is consistent with the one-dimensional radial heat flow model assumed for the initial analysis of the complete thrustor. The use of the diffuse - gray simplification is standard practice where the radiative properties of the materials permit.

In the computation of the temperatures and heat fluxes in the thermal subsystem, the problem was first transformed into that of an equivalent linear electrical network (reference A-1) which was then solved by the computational methods of linear electrical network analysis. Figure A-1(b) shows the analogous electric circuit diagram used to represent the three-surface radiation network subsystem for analysis purposes. For that type of analysis, table A-I shows the relationships used to relate the analogous electrical parameters to the actual thermal radiation parameters.

Using these relationships, a set of simultaneous linear equations were written, in terms of the thermal equivalents of the electrical network voltages, currents and resistances, in order to solve for the thermal parameter by using an electrical circuit analysis technique. That technique is basically one of requiring that the algebraic sum of all currents into every node (surface) shall be zero, where current is equal to voltage difference divided by resistance. The thermal equations are actually linear in T_i^4.

If the three isothermal surfaces of the specified thermal subsystem are designated by

surface 1 = ballast resistor heater coil

surface 2 = alumina coil support insulator

surface 3 = regenerator tube coil and support cylinder

TABLE A-I

THERMAL RADIATION PARAMETERS AND ELECTRICAL CIRCUIT ANALOGS

Thermal Parameter	Symbol	Units	Analogous Electrical Circuit Parameter
Hemispherical emissive power of a black body source i	$E_i = \left(\sigma T_i^4\right)$	W/m^2	Voltage of source i
Surface i radiosity (also called: leaving flux density, radiancy, and radiant emittance)	W_i	W/m^2	Voltage at surface node i
Surface i net heat flux	Q_i	W	Net current from voltage source i to surface node i
Net heat flux between surface i and surface j	Q_{ij}	W	Net current from surface node i to surface node j
Surface i characteristic resistance	$R_i = \left(\frac{1-\varepsilon_i}{\varepsilon_i A_i}\right)$	m^{-2}	Resistance between voltage source i and node i
Surface i - surface j shape factor resistance	$R_{ij} = \left(\frac{1}{A_i F_{ij}}\right)$	m^{-2}	Direct resistance between surface node i and surface node j

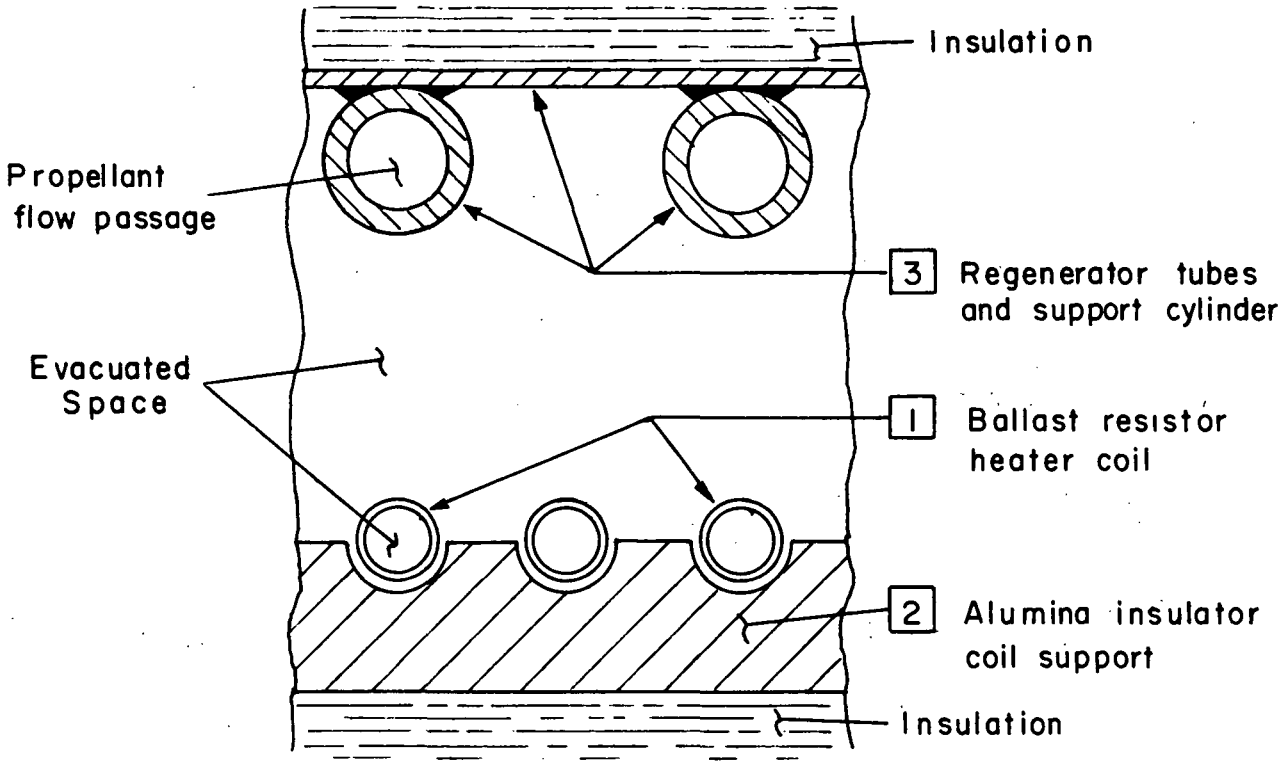

(a) Physical arrangement of elements of subsystem.

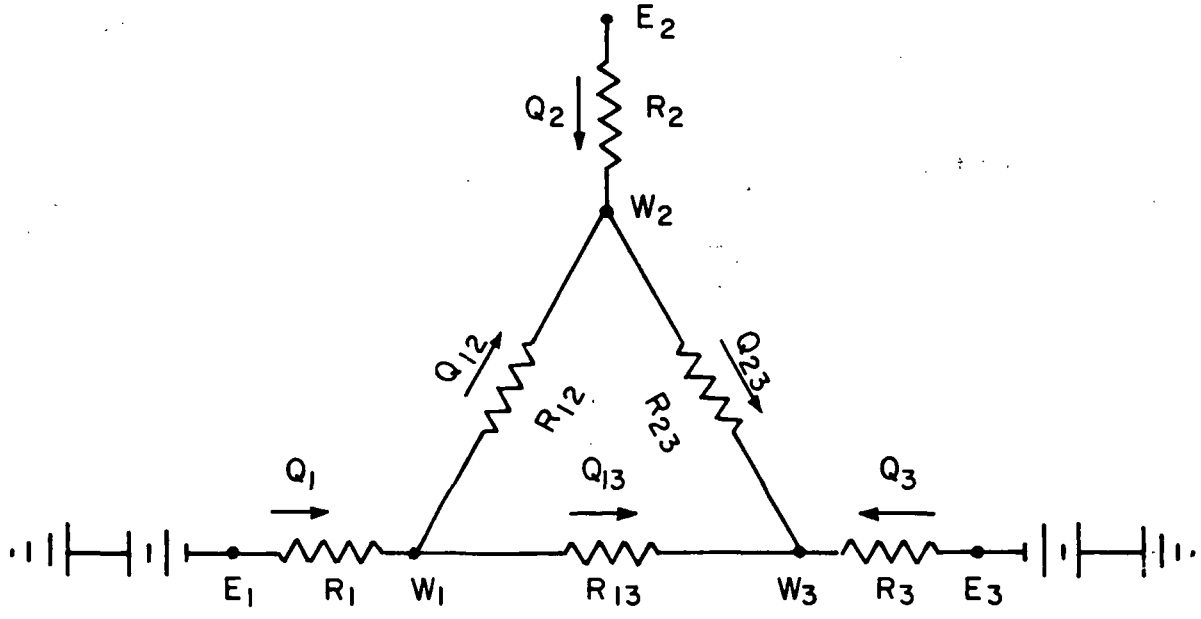

(b) Electric circuit representation of radiant interchange within subsystem.

Figure A-1.- Three-surface thermal subsystem as idealized for analysis.

then the applicable set of simultaneous linear equations are

$$Q_1 + Q_{21} + Q_{31} = Q_1 - Q_{12} - Q_{13} = 0 \tag{A1}$$

$$Q_2 + Q_{12} + Q_{32} = Q_2 + Q_{12} - Q_{23} = 0 \tag{A2}$$

$$Q_3 + Q_{13} + Q_{23} = 0 \tag{A3}$$

For the simplified thermal system, the alumina coil support insulator is considered to be radiatively adiabatic; that is, it floats thermally and is not connected to either a source or a sink. Mathematically, this is expressed by

$$Q_2 = 0 \tag{A4}$$

When this condition is substituted in the set of simultaneous equations, it results in

$$Q_{12} = Q_{23} \tag{A5}$$

$$Q_1 = Q_{13} + Q_{12} \tag{A6}$$

$$Q_3 = -Q_1 \tag{A7}$$

These equations are expressed in terms of heat fluxes Q_i and Q_{ij}, the thermal equivalent of electrical currents. Making use of the fundamental electrical circuit relationship

$$I = \frac{E}{R}$$

we can rewrite the heat fluxes as

$$Q_1 = \frac{E_1 - W_1}{R_1} = \frac{(\sigma T_1^4 - W_1)}{\left(\frac{1 - \varepsilon_1}{\varepsilon_1 A_1}\right)} \tag{A8}$$

$$Q_3 = \frac{E_3 - W_3}{R_3} = \frac{(\sigma T_3^4 - W_3)}{\left(\frac{1 - \varepsilon_3}{\varepsilon_3 A_3}\right)} \tag{A9}$$

$$Q_{12} = (W_1 - W_2)\ (A_1 F_{12}) \tag{A10}$$

$$Q_{23} = (W_2 - W_3)\ (A_2\ F_{23}) \tag{A11}$$

$$Q_{13} = (W_1 - W_3)\ (A_1\ F_{13}) \tag{A12}$$

where

A_i = area of i th surface

F_{ij} = configuration shape factor for surface i relative to surface j

ε_i = hemispheric emissivity of surface i

σ = 5.6697×10^{-8} W/m^2 $^oK^4$ (Stefan-Boltzmann constant)

and the other symbols are as defined in table A-I.

Substituting the above expressions for the heat fluxes into the set of reduced simultaneous equations, we have the following three independent relationships

$$(W_1 - W_2)\ (A_1\ F_{12}) = (W_2 - W_3)\ (A_2\ F_{23}) \tag{A13}$$

$$\frac{(\sigma T_1^{\,4} - W_1)}{\left(\frac{1 - \varepsilon_1}{\varepsilon_1\ A_1}\right)} = (W_1 - W_3)\ (A_1\ F_{13}) + (W_1 - W_2)\ (A_1\ F_{12}) \tag{A14}$$

$$\frac{(\sigma T_3^{\,4} - W_3)}{\left(\frac{1 - \varepsilon_3}{\varepsilon_3\ A_3}\right)} = -\frac{(\sigma T_1^{\,4} - W_1)}{\left(\frac{1 - \varepsilon_1}{\varepsilon_1\ A_1}\right)} \tag{A15}$$

plus the fourth relationship

$$W_2 = E_2 = \sigma T_2^{\,4} \tag{A16}$$

In these four equations there are 14 variables: W_1, W_2, W_3, A_1, A_2, A_3, F_{12}, F_{13}, F_{23}, T_1, T_2, T_3, ε_1, ε_3. Two more independent relationships are provided by the fact that the emissivities of the ballast resistor coil, ε_1, and the regenerator tube wall, ε_3, are known functions of the Pt-20 Rh material temperatures, as shown in figure A-2. That is,

$$\varepsilon_1 = f\ (T_1) \tag{A17}$$

$$\varepsilon_3 = f\ (T_3) \tag{A18}$$

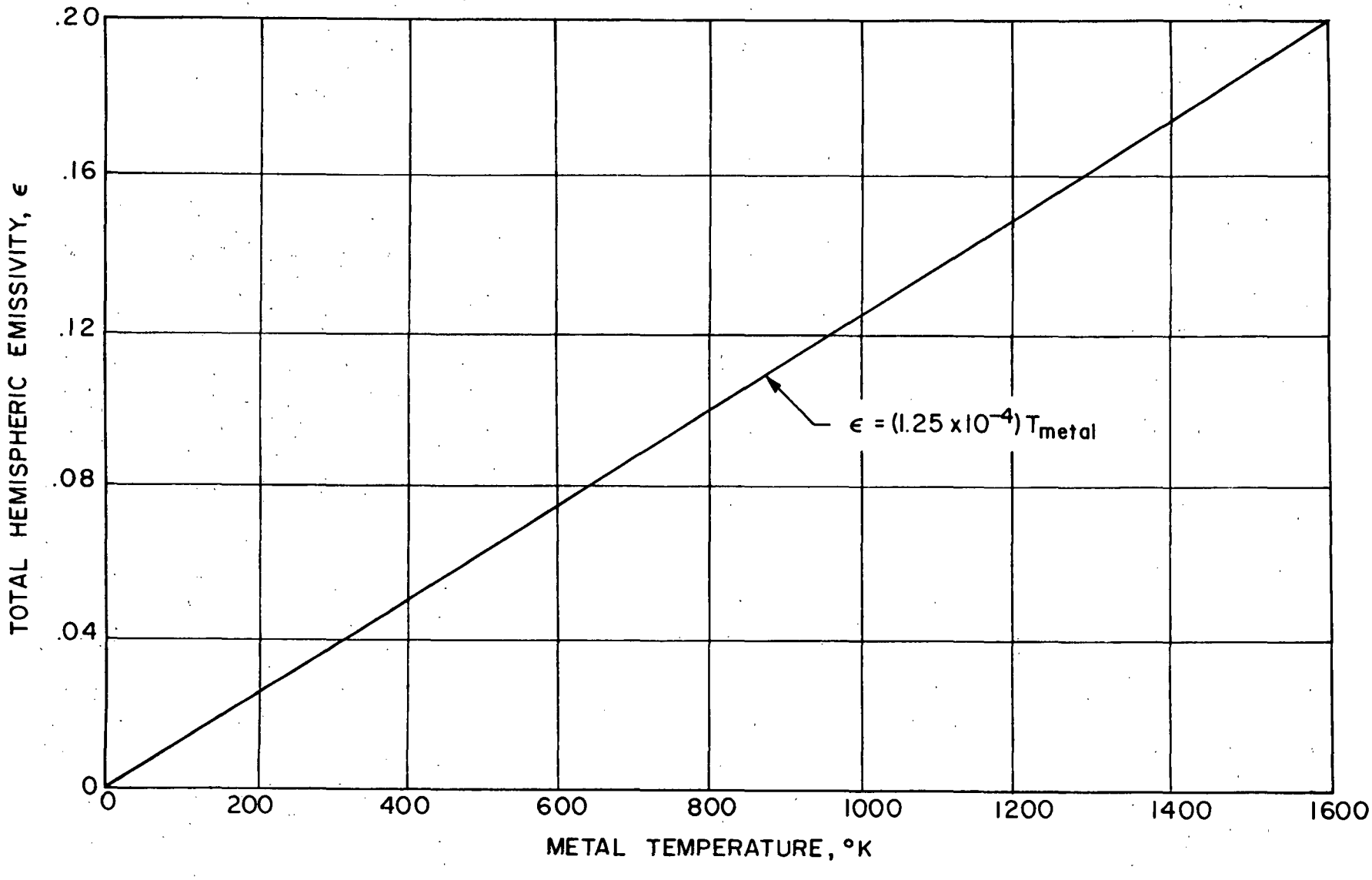

Figure A-2.- Total hemispheric emissivity of Pt-20 Rh alloy.

The regenerator wall temperature T_3 was taken as approximately equal to the intermediate gas temperature T_{T_4}, which was treated as an independent variable, or parameter, throughout the thrustor thermal analysis; it was assigned a series of values between 700 and 1000°K. In prior calculations, the surface areas of the insulator, A_2, and the regenerator, A_3, were computed as functions of T_{T_4} (=T_3) (see figure A-3), as was the power input to the ballast resistor (=radiated heat flux). Therefore, we have three more independent relationships:

$$A_2 = f\ (T_3) \tag{A19}$$

$$A_3 = f\ (T_3) \tag{A20}$$

$$\frac{(\sigma T_1^{\ 4} - W_1)}{\left(\frac{1 - \varepsilon_1}{\varepsilon_1 A_1}\right)} = f\ (T_3) = Q_1 \tag{A21}$$

The values of those terms which are unique functions of T_3 are listed in table A-II.

The configuration factors F_{ij} were evaluated by analyzing the geometry of the subsystem, and were found to be approximately

$$F_{12} = 0.60$$

$$F_{13} = 0.40$$

$$F_{23} = 0.98$$

The Pt-20 Rh ballast resistor wire temperature T_1 was fixed at 1180°K, a temperature selected to ensure an adequate operational life for the thrustor, based on available test data on Pt-20 Rh material.

In this analysis, then, there were 9 independent equations relating the 14 variables. A total of 5 of the variables had been evaluated, 4 of them being constants (T_1, F_{12}, F_{13}, F_{23}) and 1 of them being a parameter, T_3, assigned a series of values. For the specified thermal subsystem, this provided enough information to solve for all of the unknowns in terms of the parameter T_3, using iterative techniques. The principal unknowns of interest were the ballast resistor wire heater surface area, A_1, and the alumina coil support insulator temperature, T_2. The radiosities W_1, W_2, and W_3 were useful intermediate values used for computing the other unknowns, but they have no physical significance themselves.

The principal results of this one phase of the analysis are presented as plots of A_1 and T_2 as functions of the independent variable T_3 in figures 9 and 10 in the Thermal Analysis section of the report, along with the results of other phases of the analysis.

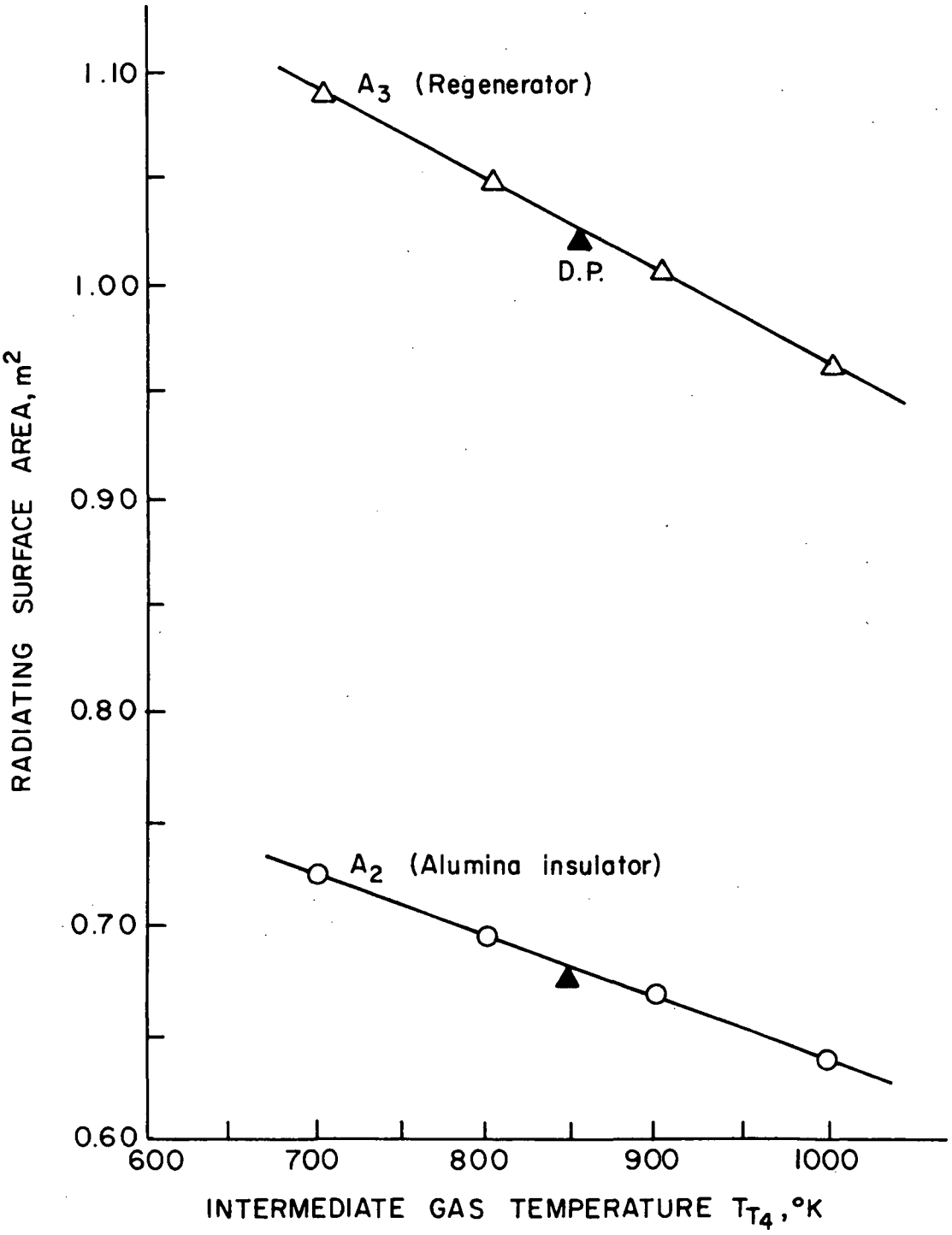

Figure A-3.- Radiating surface areas of regenerator and alumina insulator coil support as a function of intermediate gas temperature.

TABLE A-II

VARIABLES UNIQUELY DEFINED BY
REGENERATOR WALL TEMPERATURE T_3

Symbol	Variable	Value at Design Point ($T_3 = T_{T4} = 850°K$)
A_2	Aluminia insulator radiating surface area	0.68 m^2
A_3	Regenerator radiating surface area	1.03 m^2
ε_3	Regenerator radiating surface total hemispheric emissivity	0.11
Q_1	Power input to ballast resistor (= radiated heat flux)	39.1 W

APPENDIX REFERENCES

A-1 Openheim, A.K.: Radiation Analysis by the Network Method. Published in: Recent Advances in Heat and Mass Transfer, Hartnett, J.P., ed. McGraw-Hill Book Company, Inc., 1961.